PERFORMANCE OF FLEXURE-CONTROLLED REINFORCED CONCRETE STRUCTURAL WALLS UNDER SEQUENTIAL FIRE-EARTHQUAKE LOADS

A Dissertation

by

SHUNA NI

Submitted to the Office of Graduate and Professional Studies of
Texas A&M University
in partial fulfillment of the requirements for the degree of

DOCTOR OF PHILOSOPHY

Chair of Committee,	Anna C. Birely
Committee Members,	Luciana R. Barroso
	Joseph M. Bracci
	Anastasia H. Muliana
Head of Department,	Robin L. Autenrieth

August 2018

Major Subject: Civil Engineering

ABSTRACT

The performance of reinforced concrete (RC) structural walls under individual hazards has been well studied. However, little is known regarding the behavior of RC structural walls under sequential hazards. The research presented here seeks to address the performance of RC structural walls under sequential fire-earthquake loads (both post-earthquake fire and post-fire earthquake).

Longer burn times of post-earthquake fire and initial seismic damage can have significant structural impacts on RC structures which are usually considered to have superior performance in a fire. An 8-inch wall with characteristics representative of typical construction in seismic regions was utilized as the basis of the simulations. The wall with non-uniform layout of reinforcement provides a complex deformed shape under fire. Individual typical earthquake damage states were introduced to the wall to assess impact on fire resistance. The fire resistance of a wall was discussed according to thermal-insulation and load-bearing criteria in codes. The results show that crack does not impact the fundamental response of a wall under fire while cover loss decreases its load-bearing capacity significantly. Moreover, the location of cover loss has remarkable impact on the deformed shape of a wall and its load-bearing fire resistance. While the thermal-insulation capacity decreases below code requirements, the load-bearing fire resistance of earthquake-damaged walls is still acceptable.

Another potential but infrequently studied hazard is the post-fire earthquake scenario. The impact of fire damage on the earthquake behavior of RC walls is not well understood, which leads to some safety concerns in earthquake after fire or aftershocks after post-earthquake fire. A simulation procedure combining SAFIR and OpenSees is proposed and validated for the PFE analysis of RC structural walls. Based on the validated the simulation procedure, a parametric

study on the PFE performance of RC walls was conducted. Results indicate that fire damage decreases the load-bearing capacity and stiffness of RC walls under reversed-cyclic loads while fire damage decreases the deformation capacity in most cases. Severe fire exposure may shift damage from the boundary element to the web. Wall characteristics which significantly impact the residual wall response quantities are wall thickness, boundary element length, and axial load ratio. In addition, a framework for simplified nonlinear modeling was proposed for the PFE performance of RC walls. The models are defined by modification factors that account for the change in wall response relative to that of a wall without fire damage. Modification factors, established from the results of the parametric study, are a function of fire damage indices that account for the effect of fire on the material properties of steel and concrete. Results indicate that the model is generally able to predict the response of a fire-damaged wall.

ACKNOWLEDGEMENTS

I would like to thank my Ph.D. adviser and mentor, Dr. Anna Birely, for her continuous encouragement as well as technical and financial support during my Ph.D. career. I would also like to thank my committee member, Dr. Luciana Barroso, Dr. Joseph Bracci, and Dr. Anastasia Muliana, for their guidance and support throughout the course of this research.

Thanks also go to my friends and colleagues and the department faculty and staff for making my time at Texas A&M University a great experience. I want to extend my gratitude to the Texas A&M University faculty research initiation grant for providing financial support to my Ph.D. research. I also acknowledge the high performance computing resources provided by Texas A&M University (https://hprc.tamu.edu)

Finally, thanks to my parents for their encouragement and support.

CONTRIBUTORS AND FUNDING SOURCES

Contributors

This work was supervised by a dissertation committee consisting of Professor Anna Birely, Professors Lucianna Barroso and Joseph Bracci of the Zachry Department of Civil Engineering and Professor Anastasia Muliana of the Department of Mechanical Engineering.

All work for the dissertation was completed by the student, under the advisement of Anna Birely of the Zachry Department of Civil Engineering

Funding Sources

Graduate study was supported by Texas A&M University faculty research initiation grant. Portions of this research were conducted with the high performance research computing resources provided by Texas A&M University (https://hprc.tamu.edu).

TABLE OF CONTENTS

LIST OF FIGURES

LIST OF TABLES

CHAPTER 1

INTRODUCTION

Reinforced concrete (RC) structural walls are common in multistory buildings, serving important functions as lateral-load resisting elements and as fire walls. Although the performance of RC structural walls under individual fire or earthquake has been studied, little is known regarding the performance of RC structural walls under sequential hazards (both post-earthquake fire (PEF) and post-fire earthquake (PFE)).

RC walls enjoy an excellent reputation for fire resistance. An RC wall is usually able to limit the spread of fire and carry the imposed loads for the duration of the fire. However, this may not hold true when a post-earthquake fire affects an earthquake-damaged wall that has cracked, lost concrete cover, and/or experienced core crushing with rebar buckling at its boundary element. The safety concerns arising from this issue have not been studied.

Well-designed RC walls typically provide good earthquake performance: those with aspect ratios less than two being shear-controlled, and those with aspect ratios greater than two being flexure-controlled. In earthquakes, flexure-controlled walls are characterized by excellent ductility and good energy dissipation capacity, provided that they have not previously been damaged, e.g. by fire. An investigation into the earthquake performance of fire-damaged flexure-controlled RC walls is therefore necessary for a realistic appraisal of the safety of RC walled buildings that may experience post-fire earthquakes.

This dissertation aims to address the need for understanding of the behavior of RC flexure-controlled walls under sequential fire and earthquake loads. The methodology is numerical analysis using Abaqus/Standard for PEF and a simulation procedure based on OpenSees and

SAFIR for PFE. Results are used to identify whether the structural damage to a wall due to the first hazard (fire or earthquake) significantly influences its resistance to the second hazard (earthquake or fire). The critical situations in which the impact of seismic damage or fire damage is significant are identified. For the post-fire earthquake performance of RC walls, a parameter study is carried out to identify the impact of wall characteristics (wall geometry, reinforcement and axial load) on the post-fire earthquake performance of RC structural walls. Data from the parametric study is used to develop a framework for simplified nonlinear modeling of RC walls.

1.1. Background and Motivation

To ensure occupants' safety, the design of a structure should allow adequate time for evacuation in the event of an earthquake or fire, and also take into account the safety of any emergency-services personnel who may be required to enter during or after such events. However, most previous research on the behavior of structures confronting such hazards has been limited to either fire alone, or earthquakes alone. Accordingly, the present study aims to enhance the engineering community's understanding of the behavior of structures under sequential fire-earthquake loads, including both post-earthquake fires and post-fire earthquakes.

Post-earthquake fire in urban regions can be particularly destructive due to i) the breakage of utility lines increasing the likelihood of fire ignition; ii) damage to passive and active fire-defense systems in a structure and iii) delay or elimination of firefighting resources due to blocked roads, hindered communication systems, disability of water supply system and limited available response teams (Fradkin, 2005; Lew et al., 1971; Yane and Scawthorn, 1993; Todd et al., 1994; Wilkinson et al., 2013; Sekizawa and Sasaki, 2014). Destructive post-earthquake fires have led to significant widespread damage to infrastructure and final losses in the regions

predominantly of wood construction (Scawthorn, 1996). RC structures generally provide sufficient fire resistance due to the non-combustibility and low thermal conductivity of concrete (Bailey, 2002). Therefore, post-earthquake fire in concrete buildings will not result in significant widespread damage to the extent of fire spread seen in wood buildings. However, the potential for loss at the individual structure level still exists, on account of increased likelihood of fire ignition, increased burning periods, and potential reduction of fire resistance due to seismic damage.

Seismic damage of RC structures includes cracks, loss of concrete cover, core crushing, buckling or rupture of reinforcing steel, residual deformation and degradation of material properties. The negative impact of seismic damage on the fire resistance of RC structural components has been demonstrated by a number of experimental tests and numerical analysis (Sharma et al., 2012; Shah et al., 2014; Behnam et al., 2013; Behnam and Ronagh, 2012, 2013 & 2014; Mostafaei and Kabeyasawa, 2010; Wen et al., 2016; Wu and Xiong, 2012). However, those studies are limited to the post-earthquake fire resistance of RC columns and moment frames. Studies on the post-earthquake fire resistance of RC structural walls are absent from the literature. On account of the important roles of RC walls in suppressing the spread of fire and maintaining the structural adequacy of a building under fire, the significance and mechanism of the impact of earthquake damage on the fire resistance of RC walls should be determined; additionally, research is necessary to determine the critical earthquake damage which will significantly influence the fire resistance of RC walls.

A large earthquake may not only cause destructive post-earthquake fires but may also be followed by aftershocks. In such an event, an RC structure which has survived in a post-earthquake fire may be at risk for significant damage or collapse in subsequent earthquakes. This leads to another safety concern, the post-fire earthquake performance of RC structures. Post-fire

earthquake scenarios may also arise in the event of a major fire preceding a future earthquake. Consequently, resilient design and evaluation of existing infrastructure necessitates an understanding of structural performance under such hazards.

Fire following earthquake may significantly degrade the material properties (Nassif, 2006; Chang et al. 2006; Harada, 1961; Lee et al., 2008; Neves et al., 1996; Kirby et al., 1985) of RC structural components such that the structural integrity is compromised for earthquakes. Previous research has focused on the post-fire earthquake performance of RC columns (Cheng et al., 2010; Lie et al., 1986, 1988; Bénichou et al., 2013; Mostafaei et al., 2009), beams (EI-Hawary et al., 1996 and 1997), moment frames (Xiao and Meng, 2005; Mo et al., 2004) and walls (Xiao et al., 2004; Liu, 2010; Chi et al., 2014; Muller et al., 2012). For the post-fire seismic performance of RC structural walls, the previous research is limited to walls that failed in shear under reversed-cyclic lateral loads or the performance of fire-damaged walls under out-of-plane reversed-cyclic loads. The post-fire earthquake behavior of RC structural walls with flexure-controlled response has not been studied. The key role of flexure-controlled RC walls as lateral resisting components make them of particular importance in considering the post-fire earthquake performance of mid- or high-rise buildings; therefore, the post-fire earthquake performance of flexure-controlled walls should be evaluated comprehensively.

Numerical analysis is indispensable in the evaluation of the post-fire earthquake performance of flexure-controlled walls, given the high cost of wall tests under sequential fire-earthquake loads. An effective and efficient simulation procedure is needed to capture the response to both fire and earthquake loads. A full understanding of the post-fire earthquake performance of flexure-controlled RC walls also requires a comprehensive parametric study to identify critical situations in which the impact of fire damage is significant, the damage patterns

of fire-damaged walls, and the impact of wall characteristics on the earthquake performance of fire-damaged walls. Moreover, simplified modeling tools should be developed to assist engineers in capturing the effects of fire within the context of models and software commonly used for seismic analysis.

1.2. Research Objectives

The primary objectives of the research presented in this dissertation are to advance the understanding of flexure-controlled RC walls subjected to sequential earthquake-fire hazards. Specific objectives are to

1) Investigate the effect of the first hazard (fire or earthquake) on the resistance of RC structural walls to the second hazard (earthquake or fire);
2) Identify the critical situations in which the resistance of an RC wall to the first hazard is significantly compromised by the second hazard;
3) Identify how wall characteristics (wall geometry, reinforcement ratio and axial loads) influence the PFE performance of RC structural walls;
4) Propose a simplified model for the evaluation of post-fire earthquake response of RC structural walls.

1.3. Outline of Document

This dissertation explores the performance of flexure-controlled RC structural walls to sequential fire and earthquake hazards. An evaluation of post-earthquake fire (PEF) performance is presented first (Chapter 2), followed by an evaluation of the post-fire earthquake (PFE) (Chapter 3-5).

Chapter 2 presents an investigation into the impact of physical seismic damage on the fire resistance of RC walls, using thermal-mechanical analysis in Abaqus/Standard. Models were validated using published experimental data of sixteen RC walls tested under fire. The behavior of an undamaged wall was assessed relative to the behavior of segments of walls typically explored in previous research. Damage states (crack, cover loss, core crush and rebar buckle), representative of damage observed following earthquakes and in laboratory tests, are introduced to the wall to assess impact on fire resistance. The fire resistance was discussed based on two criteria, thermal-insulation criterion and load-bearing criterion. The effect of lateral restraint on the post-earthquake fire performance of RC walls is also discussed.

Chapter 3 presents the development and validation of a simulation procedure for the post-fire seismic performance of flexure-controlled RC structural walls. The simulation procedure utilizes SAFIR for heat transfer and OpenSees for seismic analysis. Development focuses on the appropriate adjustment of residual material properties for incorporation into seismic analysis. The simulation procedure is verified by test data of RC walls under sequential fire-earthquake loads.

Chapter 4 presents a parametric study of the post-fire earthquake response of RC walls. Twenty-one walls are subjected to 25 fire scenarios, followed by reversed-cyclic loads to simulate the post-fire earthquakes. The response quantities (stiffness, strength, deformation capacity and failure modes) of the fire-damaged walls are compared to those of the undamaged wall. Wall characteristics considered in this study include wall geometry, reinforcement ratios and axial loads.

Chapter 5 presents the development of a simplified modeling approach for the post-fire seismic performance of flexure-controlled RC structural walls with boundary elements. The models are defined by modification factors that account for the change in wall response (stiffness, strength and deformation capacity) relative to that of a wall without fire damage. Those

modification factors are the functions of fire damage indices that account for the effect of fire on the material properties of steel and concrete.

Chapter 6 presents summaries and conclusions of this dissertation and identifies future research needs.

CHAPTER 2

IMPACT OF PHYSICAL SEISMIC DAMAGE ON THE FIRE RESISTANCE OF REINFORCED CONCRETE WALLS*

Numerical simulations are conducted to investigate the impact of physical seismic damage on the fire resistance of reinforced concrete (RC) structural walls. A wall with characteristics representative of typical construction in seismic regions is utilized as the basis of the simulations. A two-story wall is considered, with lateral restraint at all floors and at the top only to simulate loss of restraint from floor slabs. The behavior of an undamaged wall is assessed relative to the behavior of slices of walls typically explored in simulation studies. The non-uniform layout of reinforcement is shown to provide a complex deformed shape. Individual damage states, representative of damage observed following earthquakes and in laboratory tests, are introduced to the wall to assess impact on fire resistance. Cracking is shown to have a greater impact on the thermal-insulation fire resistance than on the load-bearing fire resistance. Concrete loss (cover loss or core crushing) in the boundary elements and web is shown to result in the possibility of increased out-of-plane deformations and decreased load-bearing fire resistance. Lateral restraint at the floors provides significant support that minimizes the effects of damage on the load-bearing fire resistance. While the fire resistance is reduced by damage in the wall studied, fire resistance times are not of concern; however additional studies would be warranted for thin walls and walls with large axial load ratios.

---

*Ni, S. and Birely, A.C., Impact of Physical Seismic Damage on the Performance of Reinforced Concrete Wall, Journal of Construction and Building Materials, 182 (10) (2018) 469-482; reprinted with permission of publisher.

2.1. Introduction

Historically, the greatest losses due to fire following earthquakes have been due to the spread of fires from one structure to the next. Consequently, significant research, summarized by Lee and Davidson (2010), has focused on understanding, modeling, and preventing the spread of fires. In modeling fire spread, emphasis is placed on sources of ignition and how fire moves from one structure to another. In such models, reinforced concrete (RC) buildings are generally assumed to be noncombustible and act as barriers to the spread of fire.

While post-earthquake fire in concrete buildings will not result in widespread damage to infrastructure and financial losses to the extent of fire spread seen in wood buildings in some previous earthquakes (Lee et al., 2008), the potential for loss at the individual structure level still exists. A number of recent experimental tests and numerical simulations (Wen et al., 2016; Ronagh and Behnam, 2012 & 2013; Shah et al., 2016; Mostafaei and Kabeyasawa, 2010; Shah et al., 2017; Behnam et al., 2013) have demonstrated that seismic damage in RC structures can significantly reduce the fire resistance. These losses are of particular importance given that fires are more likely to start and to burn for extended periods of time following an earthquake. If the seismic damage prior to the fire allows for a more rapid spread of the fire within the building, such losses to building contents may be even larger. If the structural integrity of the structure is compromised due to the combination of seismic and fire damage, irreparable damage/deformations may occur that render the building unrepairable.

A detailed review of PEF provided by Mousavi et al. (2008) includes a detailed history, mitigation strategies, and a two-step method for evaluation of building performance: 1) seismic analysis and post-processing to determine effects on characteristics that may impact fire resistance,

and 2) thermal and/or thermal-mechanical analysis to assess fire resistance. Mousavi et al. (2008) identified PEF research needs, including experimental and analytical studies to inform development of guidelines for assessing PEF performance of structures.

The PEF performance of RC structures has been studied experimentally, although tests are typically terminated prior to failure. Shah et al. (2017) tested four RC frames with and without ductile detailing. Each frame was subjected to reverse-cyclic loads followed by a compartment fire. Wider cracks and concrete spalling occurred in the frame with non-ductile detailing, leading to higher internal temperatures. Neither frame collapsed during the fire test. Meacham and Chen et al. (2013, 2015 & 2016) conducted a series of full-scale experiments on a 5-story RC building to investigate seismic performance of non-structural building systems and PEF performance of the building. The specimen was subjected to 13 ground motions on a shake table, followed by six fire tests on an upper story, with the tests primarily focused on the behavior of the non-structural components.

Due to the challenges and expense of conducting experimental studies of RC structures under sequential earthquake-fire loads, numerical analysis is an efficient method for investigating PEF performance. Wen et al. (2016) used finite element models to analyze the fire performance of RC columns with concrete cover damaged. Results indicated that fire resistance decreases as the length of the damaged concrete region increased. Behnam et al. (2012 & 2013) conducted sequential pushover-fire analysis of single-story and multi-story RC frames. The negative impacts of concrete cover loss, residual deformation, section damage and material degradation were taken into account. It was found that the fire resistance would decrease when significant seismic damage was present. Behnam and Ronagh (2013) analyzed three-story frames with a natural fire curve.

Mostafaei and Kabeyasawa (2010) studied a six-story RC structure with seismic damage to columns; walls were included in the model, but damage to walls was not included. The effects of material degradation and heat penetration were found to significantly decrease the fire resistance of the structure, with cracking identified as the main contributor to reduced fire resistance.

This study is focused on investigating the post-earthquake fire resistance of RC structural walls to assess if there is a need to consider such a risk, and if so, what seismic damage(s) are most critical. RC walls are critical lateral load resisting elements that are found in both steel and concrete buildings and may also serve as load bearing walls and as fire barriers. Consequently, understanding wall behavior may be critical to assessing the PEF performance of many buildings. The objective of the study is to identify the impact of physical characteristics of damage and boundary conditions on seismic resistance. The methodology follows the outline provided by Mousavi et al. (2010), with the first stage of modeling seismic response replaced by prescribed damage. Uncoupled thermal-mechanical analysis is conducted in Abaqus/Standard using a standard fire curve. Prescribed damage, defined based on the worst-case possible damage observed following earthquakes or in seismic tests, allows for identifying the most-critical damage modes and the possible extent of seismic damage on the fire resistance. Standard fire curves, while not realistic of a long-duration post-earthquake fire, allow for a comparison to wall behavior reported in the literature.

2.2. Overview of Wall Characteristics and Behavior

2.2.1. Seismic Characteristics & Behavior

In this paper, post-earthquake fire is considered for planar RC walls that serve as axial and lateral load resisting members. The wall studied is representative of typical characteristics of walls on the west coast of the United States, summarized by Birely (2012). Figure 2-1 shows the geometry and reinforcement of the wall used in this study. Longitudinal reinforcement is concentrated in boundary elements at the edge of the wall, with hoops and cross-ties providing confinement to improve ductility during seismic loading.

Figure 2-2 illustrates typical damage in RC walls. Flexural cracks form at the boundary regions. Shear cracking occurs in the web of the wall. Damage beyond cracking is concentrated in the "toe" of the wall, which is the lower region of the boundary element, and may include loss of cover, bar buckling or fracture, and crushing of the confined core (Birely, 2012; Pugh, 2012, Kam and Pampanin, 2011; Dazio et al. 2009; Berg and Stratta, 1964; Doğangűn, 2004). In walls that have a mixed shear-flexure response or a shear dominated response, crushing of the web concrete may occur. The amount and extent of damage is dependent on many wall characteristics, including the reinforcement ratio, shear demand, and axial load. Much research, both experimental and simulation, has been conducted on the seismic performance of walls and is not summarized here; a comprehensive summary, including relationships between wall characteristics, seismic demands, and probability of damage, is provided by Birely (2012).

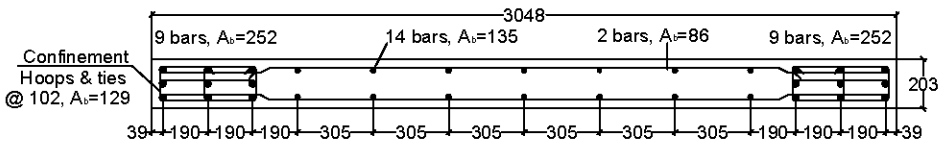

Figure 2-1 Typical planar wall characteristics: unit, mm; Ab, cross-section area of one steel bar.

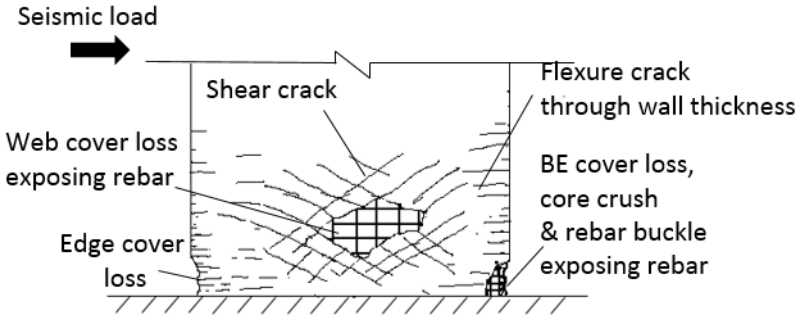

Figure 2-2 Typical seismic damage to walls.

2.2.2. Fire Characteristics & Behavior

When a wall is subjected to a fire, the heat transfer between the fire and wall is mainly by thermal radiation and heat convection which are the boundary condition of the heat transfer analysis (Bergman et al., 2011), shown in Figure 2-3. The thermal radiation is mainly controlled by the emissivity of the wall surface. The heat convection is mainly controlled by the film coefficient of the air flow. Thermal convection is accompanied by thermal conduction in most cases. However, energy transferred in conduction between fire and the wall is much smaller than that in the other two ways. The heat transfer from the fire exposed side of a wall to the unexposed side is by heat conduction, which is controlled by the thermal conductivity coefficient of concrete.

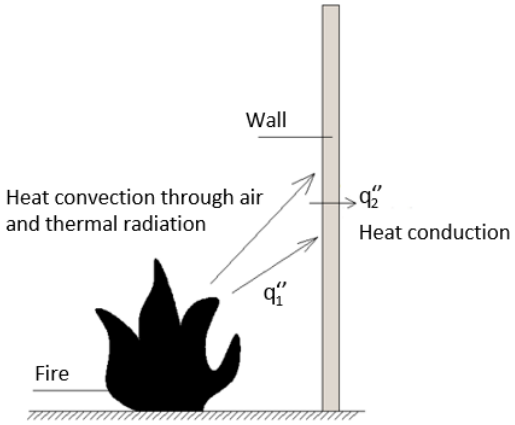

Figure 2-3 Heat transfer between fire and wall.

A number of experimental studies (Crozier and Sanjayan, 2000; Ngo et al., 2013; Lee et al., 2013; Kumar and Kodur, 2017) have determined that the fire resistance of walls is impacted by the wall thickness, slenderness ratio (height to thickness), reinforcement layout (single or double layers; centered or off-center), and axial load ratio and location of application (concentric or eccentric). Lee et al. (2013) observed that axial extension of the walls occurred initially, with an eventual contraction occurring prior to failure; axial extension was more rapid in thinner walls and the contraction occurred earlier in walls with higher axial loads. Kumar and Kodur (2017) describe the out-of-plane deformation history, in which the wall initially bows away from the fire exposed side, with reverse bowing occurring after sufficient strength and stiffness degradation occurs.

In establishing fire resistance of walls, experimental tests and numerical simulations often consider simplified boundary conditions. In multi-story buildings, wall deformations will be restrained by floor slabs and the loads from the stories above. Tests by Mueller et al. (2014 & 2015) demonstrate the importance of considering the impact of boundary conditions on the response of walls. Further, experimental tests and numerical simulations are often of walls with

uniform reinforcement distributions and do not account for the unique web and boundary regions in walls designed for seismic resistance. Muller et al. tests 2014& 2015) included slices of walls with reinforcement representative of boundary regions; however, these tests were conducted for slices isolated from the web.

The fire resistance of the walls is considered based on the deformation limits of ISO 834 (2012) and thermal-insulation criterion of EN1992-1-2 (2004). ISO 834 defines failure under axial load as axial contraction greater than h/100, where h is the initial height or when the rate of axial contraction exceeds 3h/1000 per minute. The EN1992-1-2 insulation fire resistance (Criterion "I"), is the ability to maintain temperature below a specific threshold on an unexposed side and is assumed to be satisfied when the average temperature rise on the full unexposed surface is limited to 140 ^{o}C and the maximum temperature rise on the same surface is limited to 180 ^{o}C.

2.3. Overview of Numerical Model

Abaqus/Standard (2016) was used to conduct finite element modeling in this study. Models consisted of uncoupled thermal-mechanical analysis of the walls, with the thermal analysis conducted prior to the mechanical analysis; this has been demonstrated to provide valid results while reducing the computational time, and is consistent with the recommendations of Mousavi et al. (2008) for PEF analysis of structures.

For heat transfer analysis, concrete was modeled with 8-node linear heat transfer brick elements (DC3D8) and reinforcement was modeled with 2-node heat transfer link elements (DC1D2). Tie connections were used to capture heat transfer between the concrete and steel. Thermal properties were selected in accordance with EN 1992-1-2 (2004). Specific heat assumed

a 3% moisture content. The initial temperature was 20°C. The fire-exposed side of the wall was modeled with an emissivity level of 0.7 and a convection coefficient of 25W/m^{2o}C as specified by EN 1991-1-2 (2002) and EN 1992-1-2 (2004). Unexposed sides were modeled with a convection coefficient of 9W/m^{2o}C (EN 1992-1-2, 2004).

For mechanical analysis, concrete was modeled using 8-node linear brick elements (C3D8R) with reduced integration and default hourglass control. Reinforcing bars were modeled using 2-node linear 3-D truss elements (T3D2). Reinforcement was embedded in the concrete with the assumption of perfect bond. The concrete model is concrete damaged plasticity. The uniaxial compressive stress-strain curve at elevated temperature is based on the recommendation of EN 1992-1-2 (2004) and tension softening behavior is based on the recommendations of CEB-FIB (fib Model Code 2010, 2013), shown in Figure 2-4a and Figure 2-4b. The impact of temperature on the mechanical properties (compressive strength, peak compressive strain, crushing strain and tensile strength) and thermal expansion models are according to EN 1992-1-2 (2004), with siliceous concrete assumed, shown in Figure 2-5a and Figure 2-5b. The EN 1992-1-2 concrete model implicitly incorporates transient creep strain (Gernay, 2011). Steel is modeled as an elastic-perfectly-plastic material, shown in Figure 2-4c. The yield strength and elastic modulus vary with temperature as recommended by EN 1992-1-2 (2004), shown in Figure 2-5c. The mechanical analysis does not account for thermal induced cracking or spalling of the concrete.

The mesh of models in the heat transfer analysis is consistent with that for the mechanical analysis. A minimum of four elements were used along the wall thickness to alleviate the hourglass problem due to the reduced integration of the element type C3D8R. The mesh was developed such that the aspect ratio of individual elements did not exceed 3.

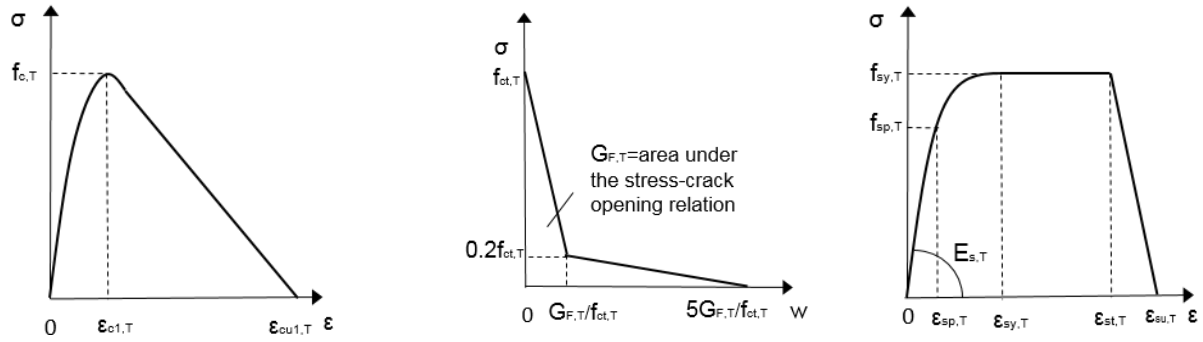

(a) Concrete in compression (b) Concrete in tension (c) steel

Figure 2-4 Stress-strain curves of materials (EN 1992-1-2, 2004; fib Model Code 2010, 2013).

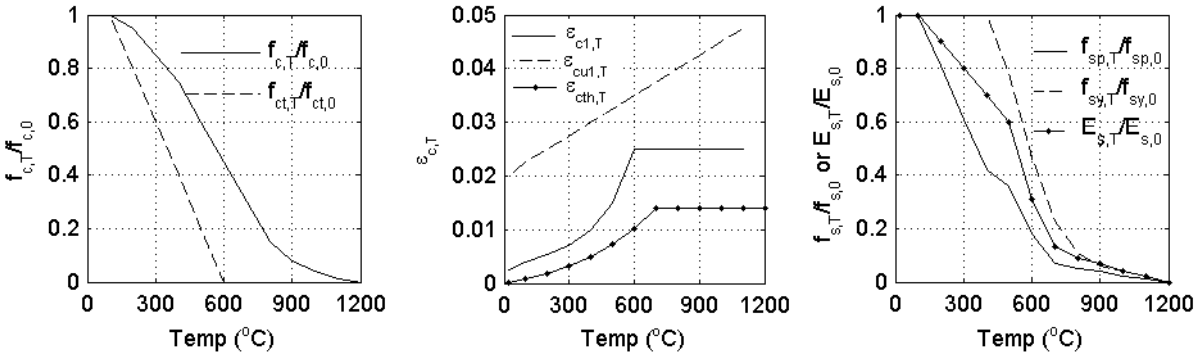

(a) Concrete strength (b) Concrete strain (c) Steel

Figure 2-5 Concrete and steel mechanical properties at elevated temperature (EN 1992-1-2, 2004).

2.3.1. Validation using Experimental Data

The numerical models were validated using experimental results of fifteen tests by Crozier and Sanjayan (2000). The dimensions and concrete type for the fifteen test specimens are summarized in Table 2-1. Walls with a length of 1200 mm and a height of 3600 mm were simply supported and heated below the walls with the AS1530.4 Australian fire temperature versus time curve (AS1530.4, 1997). Walls were tested with and without in-plane loads. Most specimens failed due to extensive deflection. Specimens IL150-66$_1$, IL150-52$_1$, IL150-66$_2$ and IL150-52$_2$ failed due

to fracturing into two pieces. During the fire test, spalling of concrete only occurred to the specimen L150-66_1.

Walls were modeled as described above, with thermal boundary conditions and fire curve described in the tests. Due to the symmetry of the specimens, a quarter of a wall was modeled with symmetrical boundary conditions. The coarse aggregate used in the test is basalt which is sub-siliceous in nature. The thermal expansion nature of basalt falls between siliceous aggregate and calcareous aggregate. Therefore, both thermal expansion models in EN 1992-1-2 (2004) were used for the validation, with the results considered to bound the response for the concrete used in the experiments. The wall model is subjected to 20^{o}C initial temperature; the bottom surface of the wall model is exposed to fire with film coefficient 25W/m^2 ^{o}C and emissivity 0.7. Since the top face of the wall is covered by ceramic-fiber insulation blankets, the thermal boundary condition for the unexposed surface is subject to insulated thermal boundary conditions. Mechanical loads were applied to simulate the mechanical loads in the fire tests.

Table 2-1 Test specimen properties (Crozier and Sanjayan, 2000).

Specimen	t_w (mm)	H/t_w	f_{cm}(MPa)
IL75-70	75	48	79
IL75-48	75	48	53
L75-70	75	48	79
L75-48	75	48	54
IL100-70	100	36	76
IL100-48	100	36	51
L100-70	100	36	76
L100-48	100	36	52
IL150-66_1	150	24	77
IL150-52_1	150	24	67
IL150-66_2	150	24	83
IL150-52_2	150	24	70
L150-66_1	150	24	77
L150-52_1	150	24	64
L150-66_2	150	24	83
L150-52_2	150	24	71

Note: t_w is wall thickness, H/t_w is the ratio of wall height to wall thickness, f_{cm} is the compressive strength of concrete on the day of fire testing

Figure 2-6 provides a comparison of the experimental and numerical temperature distribution of the specimens IL150-66_2 and L150-52_2. IL150-66_2 is the 150mm thickness specimen with 28-day concrete compressive strength of 66 MPa and two layers of reinforcement which was subjected combined inplane and lateral load; L150-52_2 is the 150 mm thickness specimen with 28-day concrete compressive strength of 52 MPa and two layers of reinforcement which was subjected lateral load only. The numerical results agree well with the experimental results, which indicates that the heat transfer analysis with well-defined properties of concrete and steel can predict the temperature distribution of the shear walls well. The discrepancies between the simulation and experiments are a result of i) minor differences in the furnace temperature from the intended fire temperatures-time curve, ii) a lack of reported environmental temperature at test

which may have varied from the initial temperature of 20°C assumed for the simulation models, and iii) the difference of concrete thermal properties in the tests from the model in EN 1992-1-2 (2004). Table 2-2 provides a comparison of the experimental and numerical temperatures for all the 150mm thickness specimens.

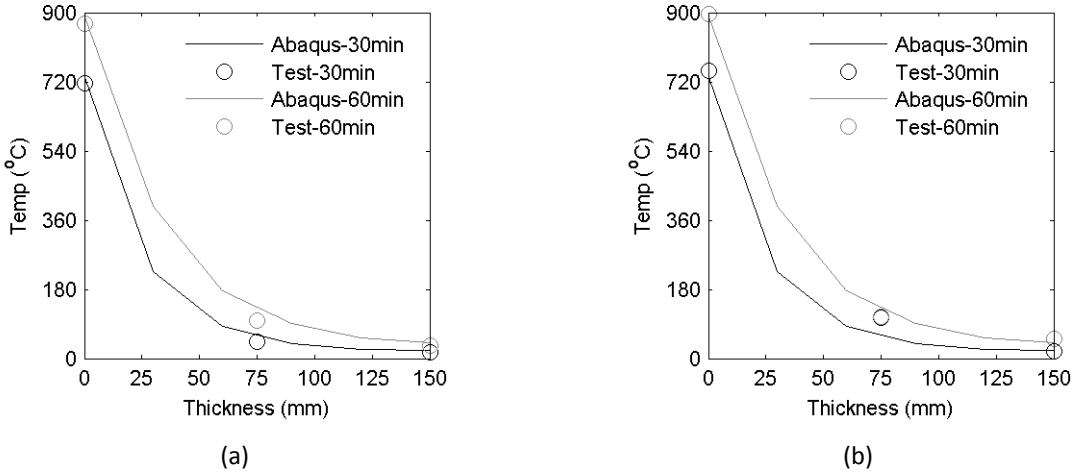

Figure 2-6 Comparison of experimental and numerical temperature for Crozier and Sanjayan (2000) wall tests, (a) IL150-66$_2$ and (b) L150-52$_2$.

The mechanical analysis of a wall under fire stops at the point when the deflection rate of the wall in the out-of-plane direction become extremely large (fracture failure pattern) or when the deflection of the wall in the out-of-plane direction is extensive (extensive deflection failure pattern), which is consistent with the failure criteria of the walls in the tests. Figure 2-7 provides the comparison of the experimental and numerical deflection vs time for IL150-66$_2$ and L150-52$_2$. The experimental deflection curves fall between the two simulated deflections, which is also true for the numerical results of most other walls. In the analysis, wall specimen IL150-66$_2$ undergoes fracture failure pattern while wall specimen L150-52$_2$ undergoes extensive deflection failure

pattern, consistent with the observation from the tests. The experimental and numerical mechanical results of walls under fire are summarized in Table 2-3. In Table 2-3, the numerical results are the average values from the analysis based on siliceous and calcareous thermal expansion models. The experimental deformation data of Specimen IL150-52_1 was treated as a spurious result; therefore no mechanical response of this specimen was simulated.

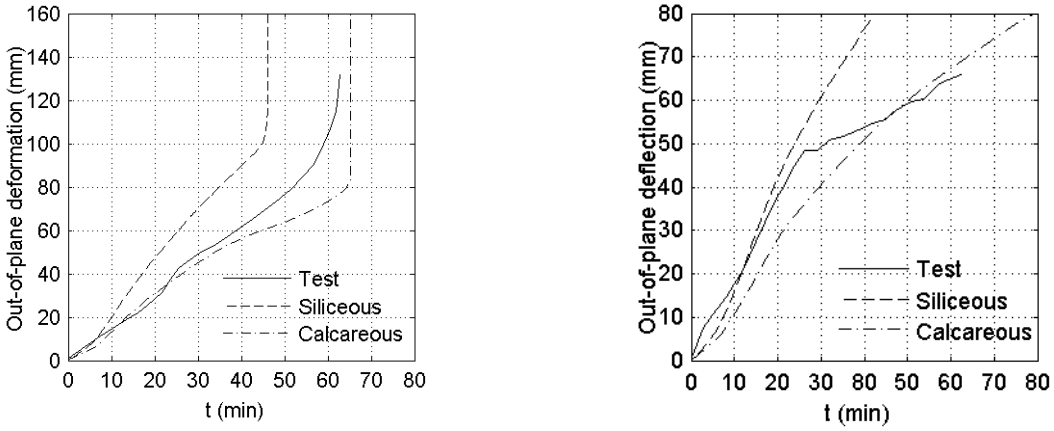

(a) (b)

Figure 2-7 Comparison of experimental and numerical mechanical behavior for Crozier and Sanjayan (2000) wall tests, (a) IL150-66_2 and (b) L150-52_2.

Table 2-2 Comparison of experimental and numerical thermal results for Crozier and Sanjayan (2000) wall tests.

Specimens	Time (min)	Temperature (°C)								
		Exposed surface			Mid-thickness			Unexposed face		
		Test	Abaqus	Error	Test	Abaqus	Error	Test	Abaqus	Error
IL150-66$_1$	30	789	739	6%	52	53	3%	14	22	55%
	60	895	891	0%	101	118	17%	33	41	25%
IL150-52$_1$	30	790	739	6%	100	53	47%	20	22	9%
	60	901	891	1%	101	118	17%	33	41	25%
IL150-66$_2$	30	717	739	3%	43	55	27%	16	22	36%
	60	872	891	2%	98	119	22%	35	41	18%
L150-66$_2$	30	756	739	2%	50	55	9%	24	22	9%
	60	897	891	1%	102	119	17%	48	41	14%
L150-52$_2$	30	750	739	1%	107	55	49%	18	22	21%
	60	897	891	1%	110	119	9%	52	41	21%
IL150-52$_2$	30	717	739	3%	82	55	33%	35	22	38%
	60	862	891	3%	109	119	10%	58	41	29%
AVG.				3%			22%			25%
STDEV.				2%			15%			13%

Table 2-3 Comparison of experimental and numerical mechanical results for Crozier and Sanjayan (2000) wall tests.

Specimen	Fail mode		Deflection at fire exposure limit			Collapse time (mins)		
	Test	Abaqus	Test (mm)	Abaqus (mm)	Error (%)	Test (min)	Abaqus (mins)	Error (%)
IL75-70	Deflection	Deflection	150	173	15	---	---	---
IL75-48	Deflection	Deflection	124	144	17	---	---	---
L75-70	Deflection	Deflection	167	173	4	---	---	---
L75-48	Deflection	Deflection	170	176	4	---	---	---
IL100-70	Deflection	Deflection	166	166	0	---	---	---
IL100-48	Deflection	Deflection	220	188	15	---	---	---
L100-70	Deflection	Deflection	162	152	6	---	---	---
L100-48	Deflection	Deflection	142	140	2	---	---	---
$L150\text{-}66_1$	Deflection	Deflection	60	67	12	---	---	---
$L150\text{-}52_1$	Deflection	Deflection	73	66	10	---	---	---
$L150\text{-}66_2$	Deflection	Deflection	54	84	57	---	---	---
$L150\text{-}52_2$	Deflection	Deflection	66	84	28	---	---	---
$IL150\text{-}66_1$	Collapse	Collapse	---	---	---	65	54.715	16
$IL150\text{-}66_2$	Collapse	Collapse	---	---	---	62	55.67	10
$IL150\text{-}52_2$	Collapse	Collapse	---	---	---	62	68.635	11
AVG.					14			12
STDEV.					16			3

2.4. Fire Resistance of Undamaged Reference Walls

2.4.1. Overview

For investigation of the influence of seismic damage on the fire resistance of walls, a reference wall with typical seismic characteristics (Birely, 2012) was designed. The cross-section of the wall is shown in Figure 2-1. The compressive strength of concrete in the reference wall is 35 MPa with 3% moisture content; therefore the wall is not prone to spalling under fire conditions (Hertz, 2003). The yield strength of reinforcement of the wall is 414 MPa. The bottom two stories were modeled, with a story height of 3.05m. The axial load applied to the wall is 10 percentage of the gross capacity (2135kN), which is the most common axial load ratio in RC walls of real buildings or in wall specimens of tests (Birely, 2012; Pugh, 2012). Although a fire can occur in any floor of a building, only the bottom story is exposed to fire in this study as the most extreme seismic damage (loss of cover, bar buckling, crushing) in walls is most commonly restricted to this location (Birely, 2012; Pugh, 2012, Kam and Pampanin, 2011; Dazio et al. 2009; Berg and Stratta, 1964; Doğangűn, 2004). ASTM E119 (ASTM E119-18, 2018) fire curve was used to heat walls. The boundary condition at the base of the wall is fixed. Two boundary conditions are considered above the base. The first restrains out-of-plane deformation at the top of the second floor only. The second restrains out-of-plane deformation at the top of the first and second floors. Although neither of these boundary conditions are representative of realistic boundary conditions (i.e. restraint provided by floor slabs, that in turn may be affected by seismic and fire damage), they are considered to bound the conditions that would be provided for a wall within a structure. Figure 2-8 illustrates the boundary conditions and the location of the fire. Fire resistance of a wall is evaluated based on the thermal-insulation criterion (Criterion I in EN 1992-1-2, 2004) and the

load-bearing criterion (Criterion R in EN 1992-1-2, 2004). The evaluation of the load-bearing criterion is implemented based on the recommendation of ISO 834 (2012) about the deformation limit and the deformation rate limit of components under compression which has been discussed in Section 2.2.2.

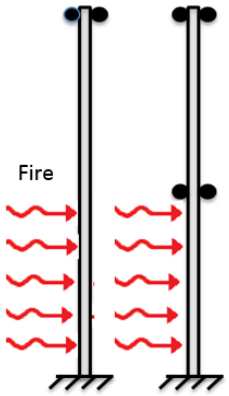

Figure 2-8 Mechanical and thermal boundary conditions.

2.4.2. Thermal-insulation Fire Resistance

The thermal-insulation fire resistance is determined using the thermal-insulation criterion in EN 1992-1-2 (2004) by measuring the average and maximum temperature on the unexposed surface of the wall, shown in Figure 2-9 for the reference wall. The average temperature history in Figure 2-9 is the average history of all node temperature at the unexposed side while the maximum temperature history in Figure 2-9 is the maximum envelope history of all node temperature at the unexposed side. The average temperature limit of 140 ^{o}C controls and is reached at 409 minutes. The maximum temperature limit of 180 ^{o}C is reached at 415 minutes. Both durations are greater than the four hour (240 minute) minimum resistance required by ACI 216.1-14 (2014).

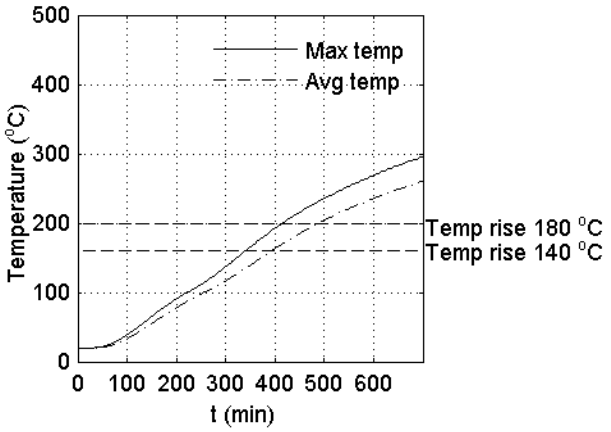

Figure 2-9 Maximum and average temperature history on the unexposed side.

2.4.3. Impact of Reinforcement Layout on Mechanical Response

Most studies (experimental and numerical) of wall behavior under fire are of walls or wall segments that have uniform distribution of reinforcement (Crozier and Sanjayan, 2000; Ngo et al., 2013; Lee et. al, 2013) and there is limited research on the response of walls with confined cross-sections and out-of-plane support (Mueller and Kurama, 2015; Muller et al., 2014). As characteristics of planar walls designed for seismic resistance have both confined and unconfined regions of the cross-section, coupled with the different damage characteristics that will occur in these two regions, it is necessary to understand the response of a full undamaged wall compared to the wall segments typically investigated.

Two segments, the boundary element and an identical length segment of web, were compared to the reference wall with out-of-plane restraint at the top of the second floor. Figure 2-10 shows the cross-sections of the two segments. The axial load was adjusted such that the segments had the same axial stress ($0.1f'_{c,0}$) as the full wall. The boundary segment is confined and contains a higher percentage of reinforcement. The longitudinal reinforcement ratio is 2.44% for the B.E. segment and 0.58% for the web segment.

Figure 2- 10 Boundary element (left) and web (right) cross-sections.

Figure 2-11a shows the axial deformation of the two segments and the full wall. Initially all three have axial shortening due to the applied axial load, with elongation similar over the first fifteen minutes, after which the amount of elongation varies. The web has the smallest axial elongation. The axial deformation is greater in the full wall than it is in either of the segments. Ultimately, the wall begins to reverse direction, with the amount of elongation decreasing prior to failure. No such reversal occurs for the wall segments, however, the analyses were terminated prior to failure.

Figure 2-11b shows the out-of-plane deformation over time for the segments and the full wall, measured at mid-height; a positive value indicates deformation towards the fire. The wall bows towards the fire as a result of the thermal gradient and P-delta effect. The out-of-plane deformation is larger in the boundary element segment than in the web segment. The boundary element deformation increases throughout the fire duration, whereas the web begins to reverse direction after 500 minutes due to more severe fire-induced axial eccentricity, consistent with the findings of previous studies (Mueller and Kurama, 2015; Muller et al., 2014). Comparison to the full wall is best illustrated by the deformed shape. Figure 2-12 shows the out-of-plane deformed shape of each segment and the equivalent location in the full wall at 240 minutes and shortly before failure (637 minutes). The deformed shape is consistent for both segments, with the boundary element deformation larger. For the full wall, the deformed shape is different in the web and boundary regions. The deformed shape of the web in the full wall is the same as the web segment,

but is significantly larger. The deformed shape of the boundary element in the full wall is different from the boundary segment, with the bottom moving away from the fire. The movement of the bottom of the boundary element away from the fire begins early in the fire duration and continues until shortly before failure.

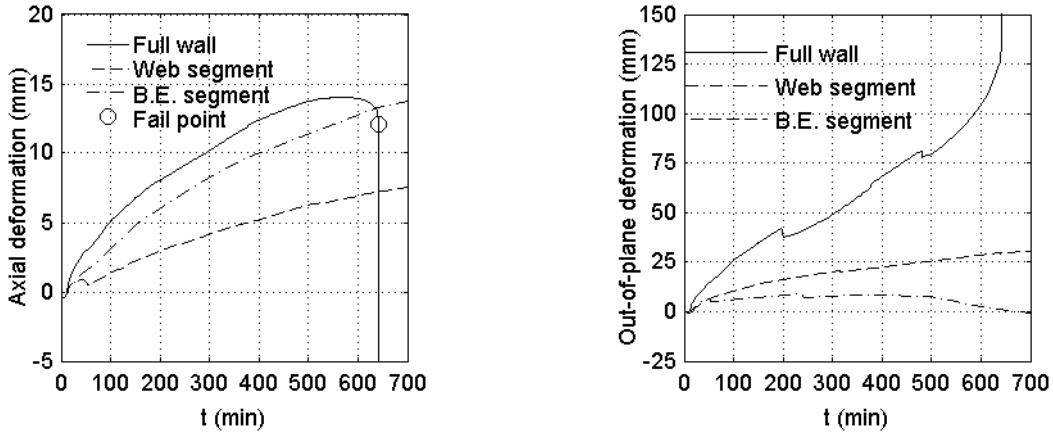

(a) (b)

Figure 2-11 Deformation of the boundary element segment and the web segment under fire, (a) axial deformation and (b) out-of-plane deformation.

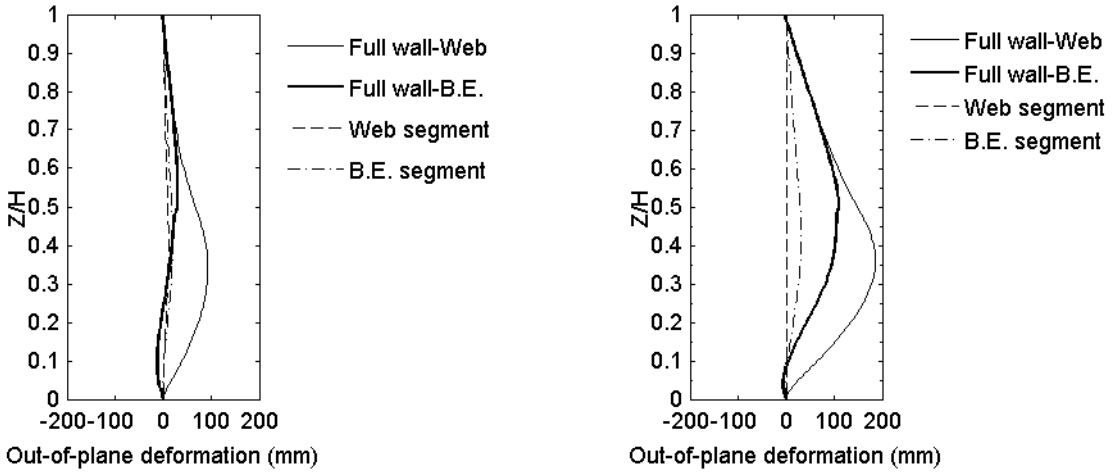

(a) (b)

Figure 2-12 Deformed shape comparison of the reference wall and wall segments at (a) 240 and (b) 637 mins (failure of full wall), "B.E." means boundary element.

2.4.4. Impact of Lateral Restraint on Mechanical Response

To investigate the impact of lateral restraint, the two mechanical boundary conditions shown in Figure 2-8 were modeled for the reference wall. Figure 2-13 shows the axial deformation (positive = axial expansion) and out-of-plane deformation (positive = towards fire) measured at one-half the unbraced length from the bottom of the wall. For fire duration up to approximately 60 minutes, the behavior is nearly identical for the two walls. At longer times, the wall with restraints at both floors sees a decrease in the rate of out-of-plane deformation. The wall with restraints at the top only continues at roughly the same rate. Both walls have a gradual drop in the rate of the axial deformation. At approximately 520 minutes, the wall with top restraint only reaches its peak axial expansion, with failure occurring at 637 minutes. In contrast, the wall with restraint at each floor has smaller out-of-plane deformation at 637 minutes and had not reached a peak axial expansion at termination of the analysis (note the analysis was terminated at 700 minutes, but the wall had not lost load bearing capacity). It should be noted that the load-bearing fire resistance of both walls exceeds the thermal-insulation fire resistance and exceeds the minimum four hours required by ACI 216.1-14 (2014).

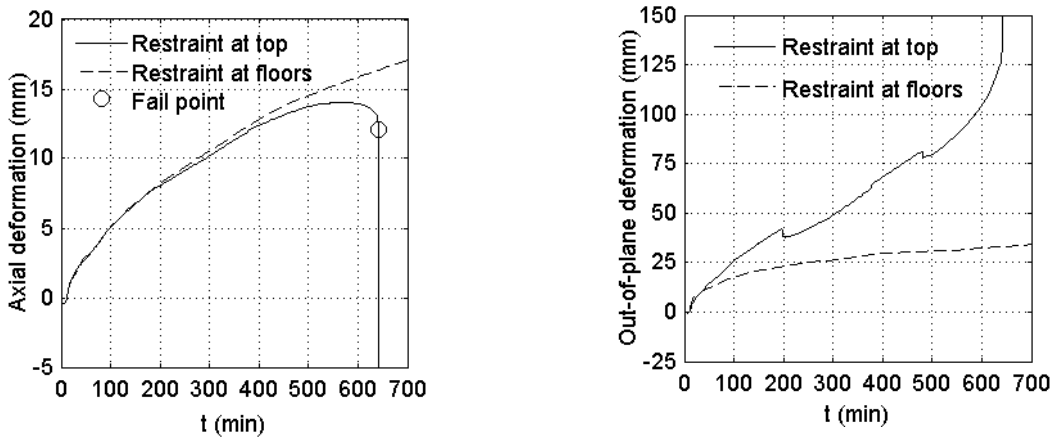

(a) (b)

Figure 2-13 Influence of lateral restraint on the deformation of walls under fire, (a) axial deformation and (b) out-of-plane deformation.

2.5. Influence of Seismic Damage on Fire Resistance

Seismic damage to RC walls include cracks, loss of cover, buckling or rupture of reinforcement, residual deformation, and degradation of material properties. The prediction of damage and the subsequent effect on fire resistance is a complex undertaking. As the interaction of earthquake and fire demands on a wall is not well known, a simplified approach is taken in this paper in which it is assumed that the physical damage to the concrete is the largest contributor to the decrease in fire resistance of walls due to earthquake damage. Figure 2-14 shows the manner in which the physical damage was added to the walls. Details of the damage and the influence on the fire resistance are discussed in the following sections, with a boundary condition of out-of-plane restraint at the top of second floor only used to consider the worst case scenario. A numerical summary is provided in Table 2-4. Load-bearing resistances are based on ISO834 criteria for deformation and deformation rates. The load-bearing resistance of the walls analyzed in this section is controlled by the deformation rate in the axial direction; therefore only the load-bearing resistance based on deformation rate is provided in Table 2-4. Discussion of each damage type's

influence is followed by a section to discuss the impact of lateral restraint at every floor of damaged walls.

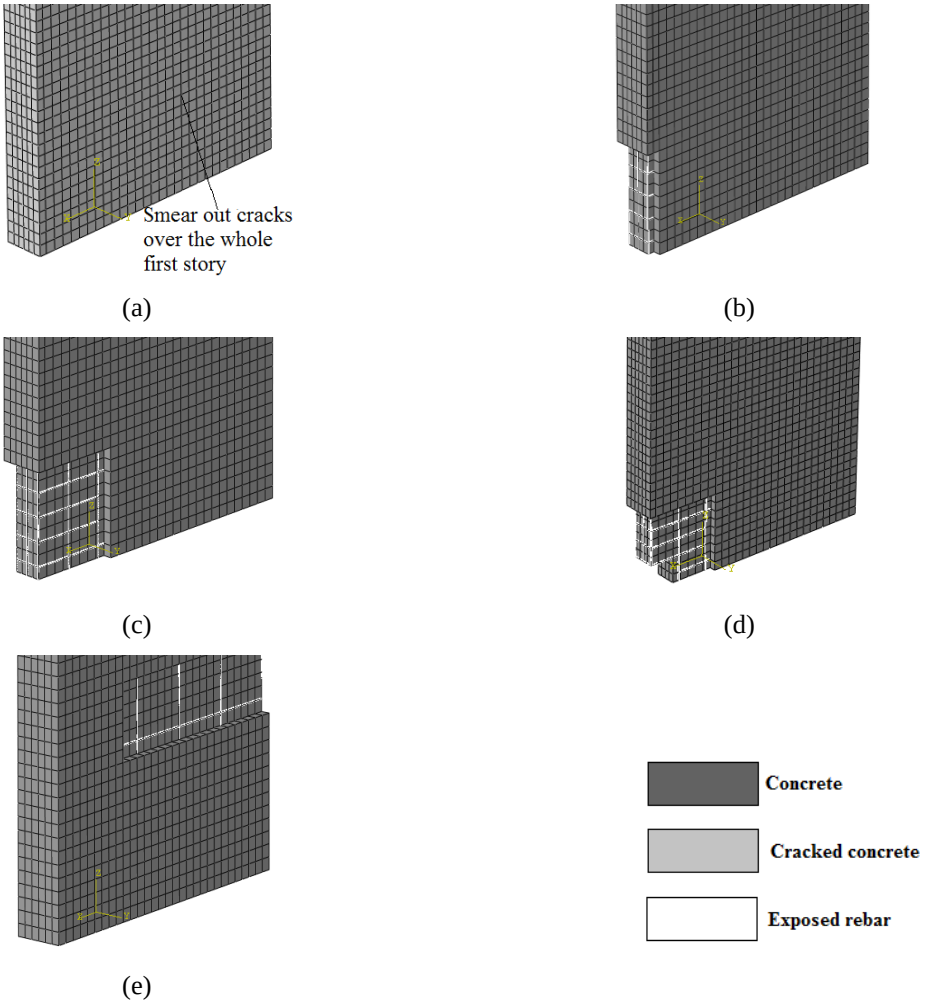

Figure 2-14 Modelling of seismic damage to walls in Abaqus, (a) crack, (b) boundary element edge cover loss, (c) full B.E. cover loss, (d) full B.E. cover loss & core crushed and (e) web cover loss.

Table 2-4 Fire resistance of walls based on thermal-insulation and load-bearing criteria.

	Thermal-insulation criterion				Load-bearing criterion	
Damage type	Max T (min)	Avg T (min)	FR_I (min)	D_I/UD_I (%)	FR_R (min)	D_R/UD_R (%)
Undamaged	415	409	409		637	
cracked	351	338	338	83	569	89
Edge cover loss	186	407	186	45	385	60
Full BE cover loss	138	389	138	34	285	45
Full BE cover loss & core crushed	-	-	-	-	250	39
Web cover loss	184	377	184	45	438	69

Note: Max T is the fire resistance based on the maximum temperature rise; Ave T is the fire resistance based on the average temperature rise ; FRI is the minor one of the two fire resistance values based on Max T and Ave T, according to Criterion "I" (EN 1992-1-2, 2002); FRR is the fire resistance based on Criterion "R" (EN 1991-1-2, 2002); DI/UDI is the thermal-insulation fire resistance of damaged wall to undamaged wall; DR/UDR is the load-bearing fire resistance ratio of damaged wall to undamaged wall.

2.5.1. Cracking

The influence of cracking on the thermal resistance of RC structures is affected by crack characteristics (depth, width and location). Figure 2-15 illustrates the potential orientation of fire relative to cracks. In a beam (a), the direction of heat propagation is parallel to cracks that form along a partial depth of the beam. The literature provides a number of studies on the influence of this type of cracks on the fire resistance. Ervine et al. (2012) indicate that cracks may decrease the heat propagation, with the degree of change influenced by the moisture content of concrete (Vejmelková, 2008), concrete composition (Shen et al., 2017) and width of cracks (Ervine et al., 2012). In a wall (b), the direction of heat propagation is perpendicular to cracks that form through the thickness of the wall. The impact of this crack type on the rate of gas flow has been studied experimentally (Hutchinson and Wang, 2010), demonstrating that the gas flow increases with increased crack width. In a fire, the increased gas flow will allow the unexposed side to increase

temperature faster and the interior faces of the crack will be subjected to increased temperature (Ba et al., 2016), allowing for increased temperature between cracks. At the same time, cracks may allow for the escape of steam (Hertz, 2003), decreasing the likelihood of concrete spalling. The complex interaction of the gas flow and escape of steam in cracked walls subjected to fire requires an in-depth investigate to fully understand. Absent this, it is conservatively assumed that heat propagation through the wall will be increased by the presence of cracks. To simulate this increased heat propagation in a simplified manner in the existing model, the heat propagation is introduced to the model by increasing thermal conductivity by 10% and decreasing the specific heat by 10%. These values do not reflect physical changes in these material properties, but instead are intended to capture the possible overall effect of the cracks increasing the heat propagation through the wall; this is analogous to using stiffness modifiers to account for cracked concrete in mechanical models of structures subject to lateral loads. Cracks are assumed to occur only in the first story.

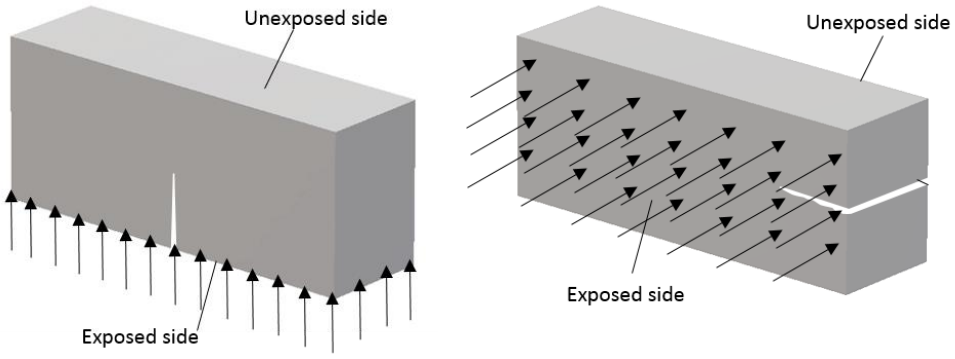

(a) (b)

Figure 2-15 Orientation of heat flow relative to cracks for (a) beams and (b) walls.

Table 2-4 provides a summary of the reduction of fire resistance due to cracking. The cracks result in an almost 10% reduction in the load-bearing fire resistance. Considering the

thermal-insulation criterion of fire resistance, the wall with cracks has lower fire resistance (338 minutes from 409 minutes) on the average temperature rise.

Figure 2-16 shows the influence of cracking on the deformation of the wall as a function of time. For the cracked model, the characteristic shape of the deformation versus time curves and the deformed shape of the wall, shown in Figure 2-16 and Figure 2-17, remain unchanged. In the cracked walls, the reversal of axial deformation direction occurs slightly sooner, accompanied by a decrease in load bearing capacity.

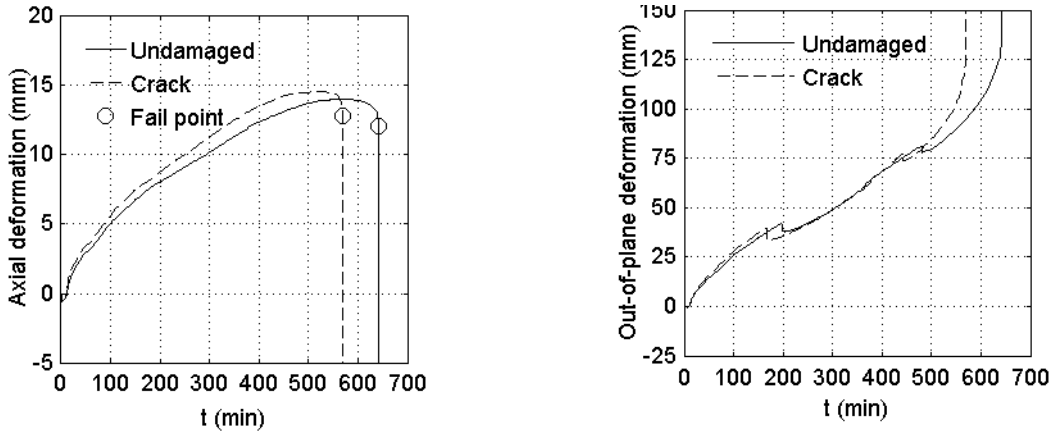

(a) (b)

Figure 2-16 (a) Axial and (b) out-of-plane deformation of cracked walls under fire.

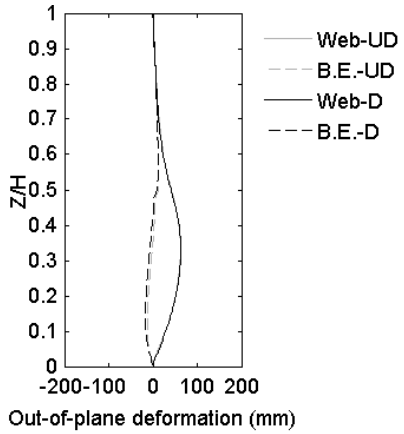

Figure 2-17 Deformed shape of cracked walls at 240 min (UD = undamaged; D = damaged).

2.5.2. Boundary Element Damage

Following cracking, the damage most common in walls is loss of cover in the boundary element. To simulate cover loss, concrete elements were removed; a detailed discuss of this and other methods to account for cover loss are provided by Ni and Birely (2014). Two levels of cover loss were considered in the boundary element: loss of cover at the edge of the wall only (end cover and first 76 mm along the length) and loss of cover along the full boundary element length (457 mm). Both cover loss damages are 457 mm in height; in a preliminary study the length of the cover damage was shown to influence the response significantly more than the height of the damage (Ni and Birely, 2014). Additionally, loss of cover and loss of the confined core was considered, in which rebar and concrete were removed from the first 191 mm of the length of the boundary region, as shown in Figure 2-14b-d.

The reduction of fire resistance due to boundary element damage is summarized in Table 2-4. For both levels of cover loss, the thermal-insulation criterion is controlled by the maximum temperature, rather than the average as is the case for the undamaged wall. The thermal-insulation fire resistance is reduced to 45 percent and 34 percent of the undamaged wall for edge and full B.E. cover loss, respectively. In both cases, the thermal-insulation criterion controls the overall fire resistance, although the load bearing fire resistance is reduced by a great percentage, 40 percent and 55 percent, respectively. Thermal-insulation fire resistance is not considered for the wall with core crushing as the integrity criterion is no longer considered to hold.

Figure 2-18 shows the axial and out-of-plane deformation for the walls with boundary element damage. Axial deformation of the walls with cover damage is similar to that of the undamaged wall until shortly before failure of the walls, but unlike the undamaged wall, have a

sudden reversal in axial deformation. The wall with core crushing damage has the smallest axial expansion, plateauing at approximately 6 mm leading up to failure. The out-of-plane deformation in the damaged walls deviates from that of the undamaged walls at earlier times than the axial deformation does. The out-of-plane deformation in Figure 2-18b shows the deformation at midheight in the web. The deformation of the walls with damaged boundary elements are best illustrated in Figure 2-19, which shows the deformed shape over the full height in both the boundary element and in the web. The deformed shape at the web (solid lines) is similar regardless of damage, with the magnitude of the maximum displacement unaffected in the case of edge cover loss (Figure 2-19a) and larger than the undamaged wall for larger amounts of concrete loss (Figure 2-19b and 19c). The deformed shape at the boundary element (dashed lines) is affected by the severity of the concrete loss. In the wall with end cover loss (Figure 2-19a), the difference is very minor, with slightly larger deformations away from the fire above the damaged region. In the case of larger concrete loss (Figure 2-19b and c), the damage region has reduction in rotational resistance, allowing the boundary region above the damage to move towards the fire, similar to the behavior observed in walls with hinged supports (Crozier and Sanjayan, 2000).

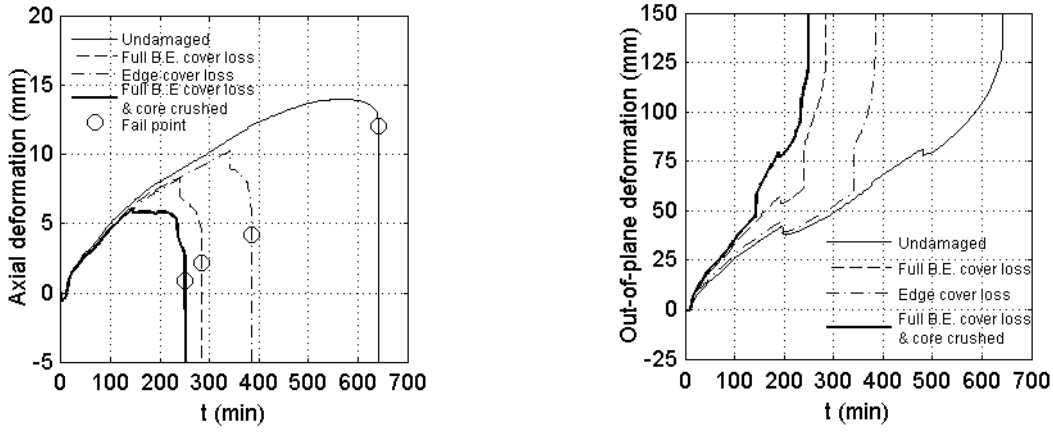

(a) (b)

Figure 2-18 (a) Axial and (b) out-of-plane deformation of walls with boundary element damage under fire.

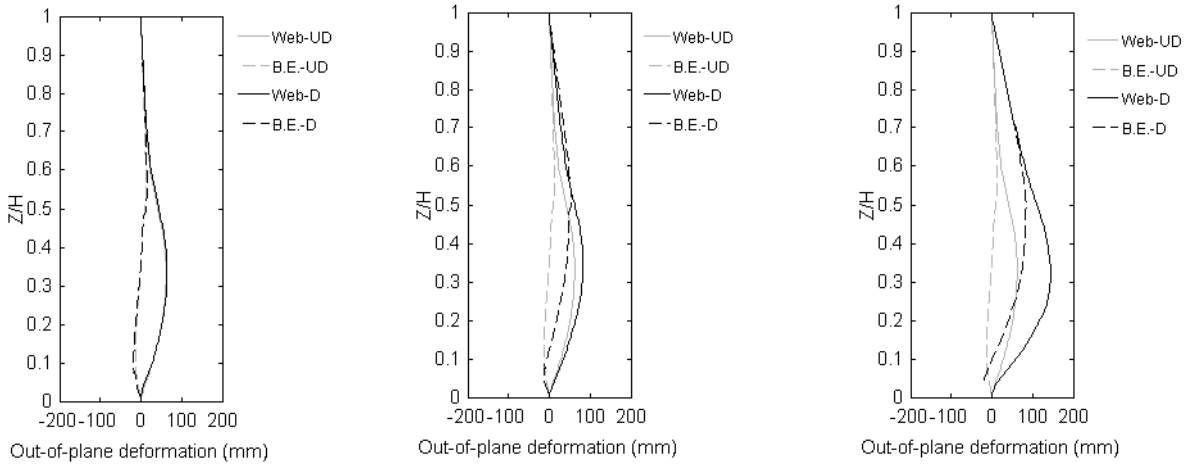

(a) (b) (c)

Figure 2-19 Deformed shape of walls with boundary element damage at 240 min (a) edge cover loss, (b) full B.E. cover loss, and (c) B.E. cover loss plus core crushing.

2.5.3. Web Damage

Although cracking and boundary element concrete damage account for the majority of observed damages in planar walls designed with modern codes, the occurrence of web cover damage can occur in walls. Given the complex deformation of the undamaged walls under fire, it is worth considering the influence of damage to the web concrete. Web cover damage is modeled

as shown in Figure 2-14e, with the damage located above the base as is consistent with observed web damage (Birely, 2012); concrete elements are removed as was done for the loss of cover in the boundary element.

The reduction of the thermal-insulation fire resistance is similar to that of edge cover loss, with the maximum temperature controlling and reducing the fire resistance from 409 to 184 minutes (45 percent). This controls over the load-bearing resistance, which decreases to 438 minutes (69 percent of that of the undamaged wall).

Figure 2-20 shows the axial and out-of-plane deformation of the wall with web damage. Unlike for the boundary element damage, the axial deformation of the web damaged wall is significantly different from that of the undamaged wall. The smaller axial expansion is accompanied by larger out-of-plane deformation. Figure 2-21 shows the deformed shape of the undamaged and damaged wall at the web and boundary element. The deformed shape of the web (solid lines) is impacted by the web damage. In the undamaged walls, the full height of the wall moves towards the fire, but in the damaged wall, only the region above the damage moves towards the fire, resulting in larger magnitude deformations. The deformed shape of the boundary element is mostly not affected by the web damage, but the deformation is more towards fire.

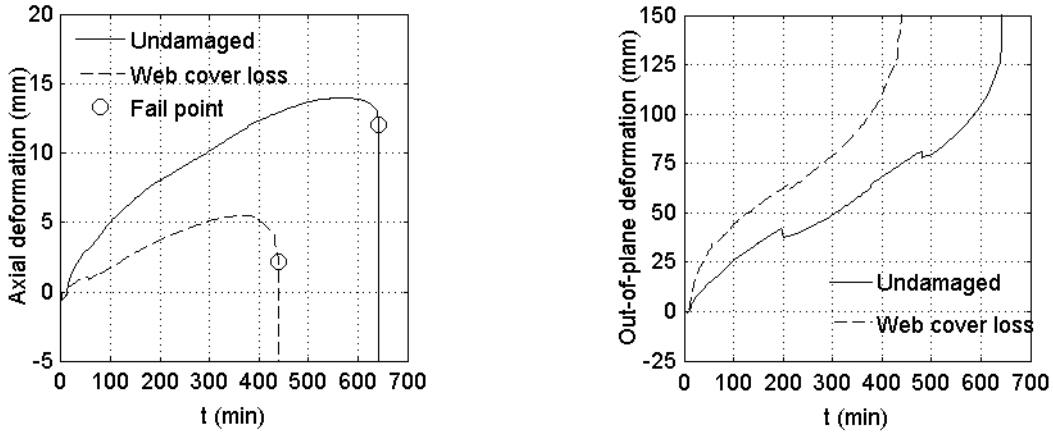

(a) (b)

Figure 2-20 (a) Axial and (b) out-of-plane deformation of walls with web damage under fire.

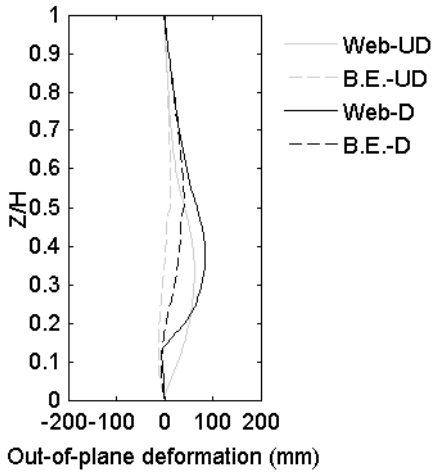

Figure 2-21 Deformed shape of walls with web cover at 240 min.

2.5.4. Impact of Lateral Restraint on Mechanical Response

The previous sections evaluated the impact of damage on the response of walls with roller support at the top only. As shown for the undamaged wall, including restraint at the top of the first floor can significantly improve the load-bearing fire resistance. To consider this effect on the behavior of damaged walls, the wall with the most severe damage (boundary element cover loss with core crushing) is modeled with restraint at the first and second floors.

The thermal-insulation fire resistance is unaffected by the mechanical boundary conditions. The axial and out-of-plane deformations are shown in Figure 2- 22. With the restraint at the first floor, the undamaged and damaged walls are able to sustain load for 700 minutes, at which point the analysis was terminated. The deformed shape at 240 minutes is shown in Figure 2- 23. As with the wall without first floor restraint, the damaged region has reduced rotational restraint, but the region above the damage deforms away from the fire as in the undamaged wall. The differences in response of the damaged wall with and without lateral restraint at the first floor illustrate the complex interaction of the wall with adjacent components, and with it, the need to consider realistic boundary conditions to fully assess the impact of damage on the load-bearing fire resistance of walls.

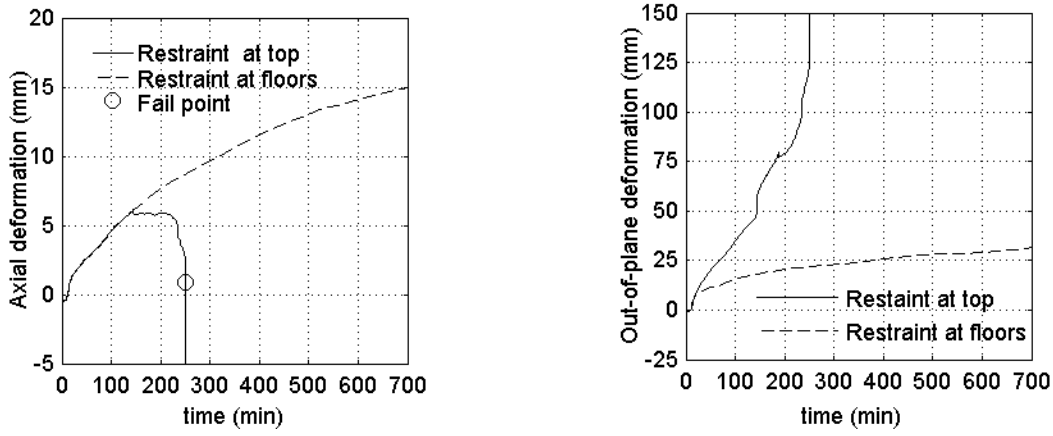

(a) (b)

Figure 2- 22 (a) Axial and (b) out-of-plane deformation of walls with roller supports at floors.

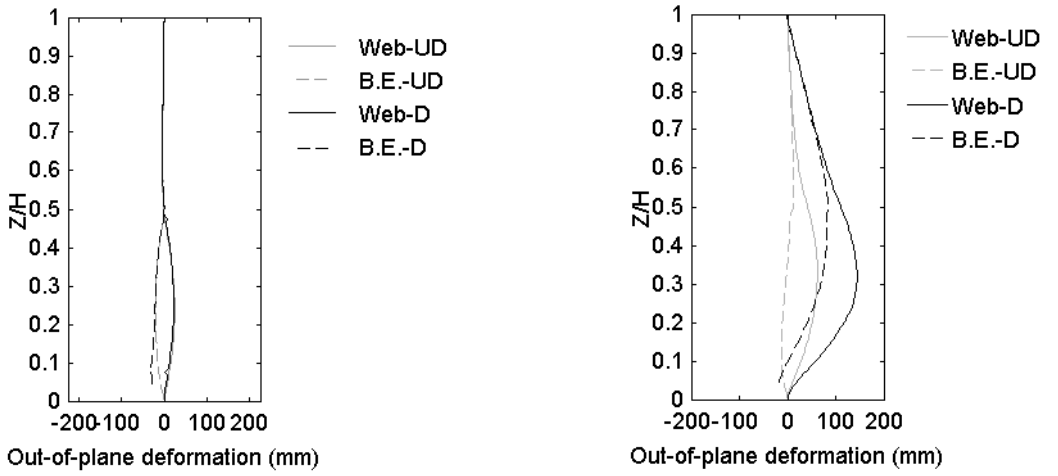

Figure 2- 23 Deformed shape comparison of wall with boundary element cover loss with core crushing (a) with roller support at floors (b) wall with roller support at top.

2.6. Conclusions

Finite element models were developed to investigate the impact of physical seismic damage on the fire resistance of RC walls. The bottom two-stories of the walls were modeled, with fire applied to one-side of the first floor and lateral restraints were provided at the top of the second floor. Models were run with and without lateral restraint at the top of the first floor, thereby providing bounds of the restraint that would be provided by the floor slab. Baseline models without seismic damage were developed to establish. Wall cross-sections with confined boundary elements were shown to have a more complex shape than walls with a uniform distribution of reinforcement.

Damage patterns evaluated consisted of cracks, loss of cover in the boundary element, core concrete crushing, and loss of cover in the web. Damage was prescribed as the most severe observed following past earthquakes and laboratory tests.

The effect of seismic cracks were modeled by modifying thermal properties to allow for a more rapid transfer of heat through the wall. The assumed level of cracking decreased the thermal-insulation fire resistance by a greater extent than the load-bearing fire resistance.

When seismic damage consists of cover loss, the decrease of load-bearing resistance become more significant with increasing dimension of cover loss along wall length. The load-bearing fire resistance of the wall with full BE cover loss decreases to less than half the fire resistance of the undamaged wall. Although the presence of the core crush at boundary element decreases the load-bearing resistance further, the decrease is limited, compared to the negative effect of full BE cover loss. Moreover, the location of cover loss has a significant impact on the deformed shape of the wall and the load-bearing fire resistance. The loss of concrete cover at the web decreases the rotational stiffness at the damage region, making the behavior of that region under fire similar to a hinge. The studies of this paper mainly focus on the potential negative effect of individual earthquake damage on the fire resistance of a RC wall. The investigation of the fire resistance of a RC wall with several types of seismic damage is necessary in the future. Additionally, the load-bearing fire resistance may be further impacted by residual deformations and mechanical damage caused by an earthquake.

Although the load-bearing capacity of the earthquake damaged walls studied in this paper decreases, it is important to note that this is for the most extensive damage possible following an earthquake and when subject to the ASTM E119 fire curve which represents temperatures larger than would occur during a long-duration fire in a post-fire earthquake scenario. Under these extreme conditions, the load-bearing fire resistance is still quite large for most damage types (exceeding 4 hours for the worst damage), indicating that post-earthquake fire is not a multi-hazard

risk for many wall designs/damage combinations. However, further research may be warranted for thinner walls and walls with higher axial load ratio, with consideration for natural fire characteristics and realistic boundary necessary.

CHAPTER 3

SIMULATION PROCEDURE FOR THE POST-FIRE SEISMIC ANALYSIS OF REINFORCED CONCRETE STRUCTURAL WALLS*

The impact of fire induced structural damage on the lateral load resistance of RC structures, particularly RC structural walls, is not well understood, but may be critical in the event of sequential fire-earthquake hazards. A simple verified simulation procedure for the post-fire seismic analysis of RC structural walls is necessary to advance the understanding of the post-fire seismic performance of RC structural walls. However, individual software programs which can do well in both thermal analysis and seismic analysis are not currently available. In this paper, a simulation procedure combining SAFIR and OpenSees is proposed for the post-fire seismic analysis of RC structural walls. The thermal analysis of a wall section is conducted in SAFIR while the seismic analysis of the fire-damaged wall is conducted in OpenSees based on the temperature data from SAFIR. The simulation method is verified by test data of RC walls under sequential fire-earthquake loads. The comparison of the numerical and experimental data demonstrated the capabilities of the simulation procedure to capture temperature distribution, stiffness and strength of flexure-controlled RC structural walls.

---

*Ni., S. and Birely, A.C, Simulation procedure for the post-fire seismic analysis of reinforced concrete structural walls, Fire Safety Journal, 95 (2018) 101-1112; reprinted with permission of publisher.

3.1. Introduction

While it is fortunate that the occurrence of failure of buildings under sequential fire-earthquake loads has not yet occurred, the potential for this sequential hazard to occur necessitates an understanding of structural performance for use in hazard mitigation. Such an event may result either from a significant fire occurring not long before an earthquake or as the result of a fire igniting as a result of an earthquake followed by a strong aftershock. While possible, the likelihood of these events is low and thus little research has been directed in the area. The ability to study these hazards is benefited by the availability of accurate yet efficient analysis tools. This paper presents a simulation method to do just this, focusing on the modeling of reinforced concrete (RC) structural walls under sequential fire-earthquake loads. RC walls are an important component to study due to their prominent role as both fire barriers and lateral load resisting systems.

Although not studied extensively, some valuable experimental research has been conducted on the seismic behavior of structural components previously exposed to fire loads. Xiao et al. (2005) tested the post-fire performance of three high-performance concrete frames under reversed-cyclic loads. The fire transformed a strong-column-weak-beam frame into a strong-beam-weak-column one. Fifteen walls were tested under fire and then subject to reversed-cyclic loads by Liu (2010) and it was concluded that fire damage decreases the lateral-load bearing capacity, stiffness and energy dissipation of structural walls. Compared to the decrease of lateral-load bearing capacity, the decrease of stiffness is much more severe. The decrease of stiffness and energy dissipation of fire-damaged walls has also been observed in the tests by Xiao et al. (2004). In addition to the performance of fire-damaged RC structural walls under reversed-cyclic lateral loading, two fire-damaged RC structural walls have been tested under cyclic out-of-plane loading

to determine the axial-flexural capacity of RC structural walls immediately after heating and after cooling down (Mueller and Kurama, 2017).

Since it is expensive to test RC structural members under sequential earthquake-fire loads, numerical investigation into this topic is indispensable. Franssen and Kodur (2001) applied SAFIR to determine the residual load-bearing capacity of RC beams and columns and found that the axial restraint has a positive influence on the load-bearing capacity of fire-damaged simply supported RC beam and that the degradation of material, rather than the residual deformation, has more influence on the residual load-bearing capacity of RC columns under eccentric axial load. Mostafaei et al. (2009) used VecTor3 (ElMohandes and Vecchio, 2013) to analyze the performance of RC columns under monotonic lateral load and found that the lateral load-bearing capacity and ductility of RC column decreases noticeably due to fire exposure. Mo et al. (2004) developed a computer program to investigate the influence of fire damage on the dynamic performance of fire-damage RC frames. Results show that the number of plastic hinge increases in the fire stories and is somewhat greater than the case with axial force. All of the numerical analysis mentioned above has indicated the negative effect of fire exposure on the mechanical performance of RC structures. However, more experimental validation of those simulation methods are required. Besides, none of those methods have demonstrated the ability of the numerical methods in analyzing the post-fire performance of RC structures under quasi-static cyclic loading.

For post-fire seismic performance of RC structural walls under quasi-static cyclic loads, a simulation procedure based on SAFIR (Franssen, 2011) and OpenSees (Mazzoni et al., 2006) is proposed in this paper. Different from the simulation methods mentioned above which use

individual software programs, this simulation method combines the features of two different software programs, specifically thermal analysis in SAFIR and seismic analysis in OpenSees.

3.2. Existing Software Programs for the Post-fire Seismic Analysis of RC Structural Members

The post-fire seismic analysis of RC structural members requires two steps: thermal analysis and seismic analysis. The thermal analysis captures the temperature distribution of RC structural members during the heating-cooling cycle. The temperature is used to establish the modified mechanical material properties of the concrete. These modified properties are then used in the seismic analysis. The seismic analysis captures the mechanical response of the fire-damaged RC structural members under the reversed-cyclic loads. It is difficult for individual software programs to do well in both thermal analysis and seismic analysis, but there are some software programs which excel at one or the other. Two programs are considered in this paper, SAFIR for thermal analysis and OpenSees for seismic analysis. The strengths of each are highlighted in Section 3.3.1 and 3.3.2. The use of SAFIR for thermal analysis could be replaced by the use of experimental data or other software programs capable of conducting the necessary thermal analysis.

3.2.1. SAFIR

SAFIR is a computer program developed at University of Liège. SAFIR can be used to study the behavior of one, two and three-dimensional structures subject to fire. Beam and columns can be modeled using line elements while slabs and walls can be simulated by planar elements. The material models for concrete and steel are based on those in EN 1992-1-2 (2004). SAFIR is

able to conduct thermal analysis and structural analysis of a structure exposed to fire. The capacity of SAFIR in thermal-mechanical analysis has been demonstrated extensively (Lopes et al., 2012; Dimia et al., 2011; Cachim and Franssen, 2009; Lim et al., 2004), including modeling mechanical behavior due to thermal loadings. While SAFIR is a powerful tool for monotonic loading of RC components, the material models of SAFIR were not developed with the intent of use for cyclic analysis. Thus the mechanical analysis in SAFIR is not suitable for the studies of RC structures under reversed-cyclic loads. To demonstrate this, the reversed-cyclic analysis of specimen WSH4 (Dazio et al., 2009) was performed in SAFIR. Figure 3-1a shows the base shear vs drift hysteresis for the wall. The model is unable to capture unloading of the experimental test, showing a pinched response instead of the larger energy dissipation and residual drifts. Additionally, the strength is under-predicted and shows a strength degradation not seen in the experimental test. Most critically, the failure (crushing of concrete and buckling of longitudinal rebar) is not captured by the numerical analysis in SAFIR.

3.2.2. OpenSees

OpenSees (The Open System for Earthquake Engineering Simulation) (Mazzoni et al., 2006) is an open-source software framework developed at the University of California-Berkeley to analyze the non-linear response of structural frames subjected to seismic excitations. OpenSees can successfully model the stiffness, strength, and hysteretic behavior of flexure-controlled RC walls with force-based beam column elements using the modeling recommendations of Pugh et al. (Pugh et al., 2015). In such a model, fiber-sections are used to define the section at each integration point. The uniaxial material models that define the fiber section are regularized through the use of

material-dependent relationships to reduce the mesh dependency of the fiber-section models. This allows for accurate simulation of the flexural deterioration of softening wall sections (Pugh et al., 2015).

In the material regularization, the crushing strain of unconfined concrete is modified to be

$$\varepsilon_{20u}=\frac{G_{fc}}{0.6f_c^{'}L_{IP}}-\frac{0.8f_c^{'}}{E_c}+\varepsilon_0 \qquad \text{Eq. 3-1}$$

where f_c' is the compressive strength of the concrete; E_c is the elastic modulus of unconfined concrete; ε_0 is the peak compressive strain of unconfined concrete; G_{fc} is the fracture energy of unconfined concrete in compression; and L_{IP} is the integration point length.

For confined concrete, the crushing strain of confined concrete is modified to be

$$\varepsilon_{20c}=\frac{G_{fcc}}{0.6f_{cc}^{'}L_{IP}}-\frac{0.8f_{cc}^{'}}{E_{cc}}+\varepsilon_{0c} \qquad \text{Eq. 3-2}$$

where $f_{cc}^{'}$ is the compressive strength of confined concrete; E_{cc} is the elastic modulus of confined concrete; ε_{0c} is the peak compressive strain of confined concrete; G_{fcc} is the fracture energy of the confined concrete in compression. Table 3-1 summarizes recommended relationships between G_{fc} and $f_c^{'}$ and between G_{fc} and G_{fcc} (Pugh et al., 2015).

The fracture strain ε_u of steel is modified to be

$$\varepsilon_u=\varepsilon_y+\frac{G_s}{(f_u-f_y)L_{IP}} \qquad \text{Eq. 3-3}$$

where G_s is the post-yield energy; f_y is the yield strength; f_u is the ultimate strength; ε_y is the yield strain of steel. Figure 3-1b shows the OpenSees results for specimen WSH4 under reversed-cyclic loads using force-based beam-column elements. Overall, the OpenSees model does a better job than SAFIR of capturing the strength, energy dissipation and failure of the wall.

Researchers in Edinburgh have added the capacity for analysis of structures in fire (Usmani et al., 2012), however, the thermal commands currently available are challenging for executing the heat transfer analysis through the thickness of the walls. To enable post-fire seismic analysis of a RC walls, it is necessary to combine OpenSees with another software that enables thermal analysis.

Table 3-1 Material energy/ Regularization Recommendations (Pugh et al., 2015)

Material	Force-based element
Concrete (Compression, unconfined)	$G_{fc}=2f_c^{'}(N/mm)$
Concrete (Compression, confined)	$G_{fcc}=1.70G_{fc}$

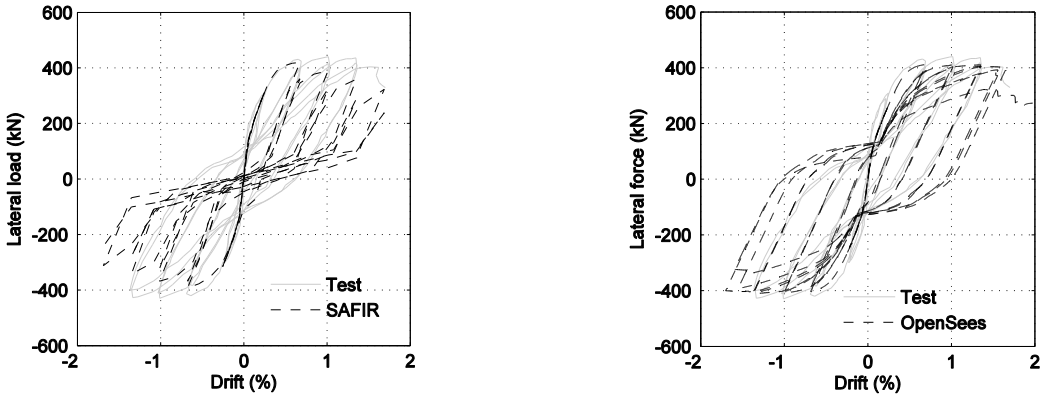

(a) SAFIR (b) OpenSees

Figure 3-1 Numerical lateral load-drift response of specimen WSH4 (Dazio et al., 2009).

3.3. Overview of Simulation Procedure

A simulation procedure combining the thermal analysis in SAFIR and the seismic analysis in OpenSees is proposed and validated for the post-fire seismic analysis of RC structural walls. This method has a high efficiency in analyzing the post-fire seismic behavior of RC walls with flexural failure. User-defined codes in MATLAB (R2013a) were written to enable data exchange

between SAFIR and OpenSees and to post-process simulation results. The main steps of the simulation procedure are as follows:

Step 1: Read the input data, including i) wall characteristic information (wall height, wall length, wall thickness, layout of reinforcement, material properties); ii) load information (thermal boundary condition, fire duration, axial load, load/displacement-control history); and iii) modeling information (number of integration points along a wall element, number of fibers along wall thickness, number of fibers along wall length, shear model).

Step 2: Divide the section of a wall into reinforcing-steel fibers, confined concrete fibers and unconfined concrete fibers, shown in Figure 3-2.

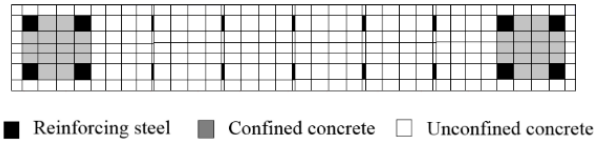

Figure 3-2 Fiber section.

Step 3: Write input files for the thermal analysis in SAFIR according to the input data and run the thermal analysis using SAFIR; each surface of a wall can has a different thermal boundary condition (exposed to fire, exposed to room temperature, or insulated).

Step 4: Determine the maximum temperature of each concrete or steel fiber during the heating-cooling cycle, according to the output data of the thermal analysis in SAFIR. If strains from the thermal analysis are deemed to be significant and included in the cyclic analysis, these values should be extracted.

Step 5: Write input files for the seismic analysis in OpenSees and run the seismic analysis. This requires the following substeps: 1) Generate material models for each fiber in a wall section, including i) calculate the residual material properties of each fiber according to its maximum temperature and recovery time; ii) calculate the confining effect in the wall boundary region; iii) regularize the material properties according to the number of integration points to avoid the mesh dependence in the seismic analysis if the section of a wall is a softening one. 2) Generate fiber sections. 3) Generate linear shear model to simulate the shear deformation of a wall under reversed-cyclic loads, according to the average residual material properties of a wall section. 4) Generate wall models using force-based beam-column elements. 5) Generate other input data for the OpenSees input file (loading history, record commands et al.).

Step 6: Post-process the output data from OpenSees to get the load-drift curves of the wall under reversed-cyclic loads and other critical wall responses quantities.

The flow chart for the interaction between SAFIR and OpenSees is shown in Figure 3-3. Recommendations for the material properties and validation of the proposed procedure are provided in the following sections.

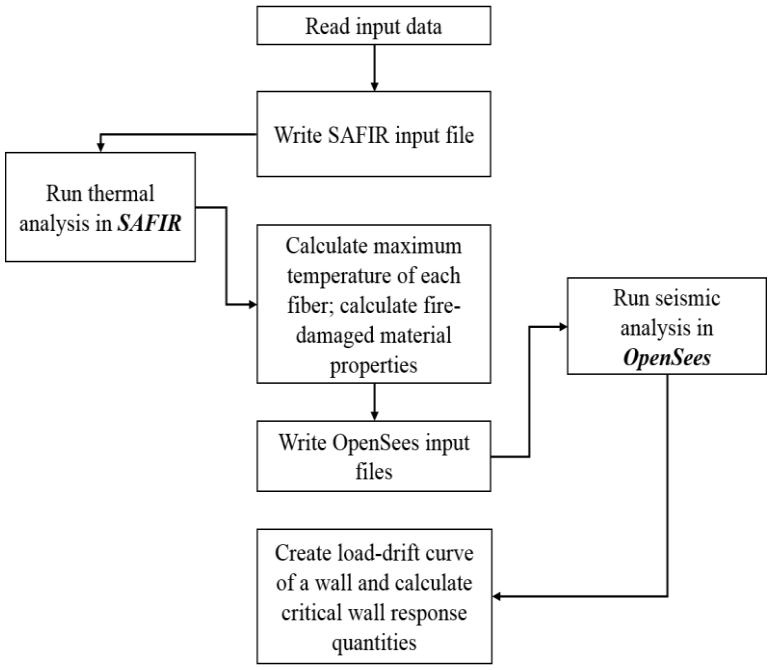

Figure 3-3 Simulation procedure for the post-fire seismic analysis of reinforced concrete structural walls.

3.4. Constitutive Models of Concrete and Reinforcing Steel

Reasonable constitutive models of concrete and reinforcing steel should be selected for the seismic analysis of fire-damaged RC structural walls. The following sections provide an overview of the basic concrete and steel models used, how confined material properties are calculated, and the method used for regularizing the material properties for use in the OpenSees mechanical models.

3.4.1. Basic Models for Fire-damaged Concrete and Reinforcing Steel

The concrete model in the SAFIR thermal analysis is selected as SILICON_ETC or CALCON_ETC (Gernay and Franssen, 2012). SILICON_ETC is the material model for siliceous aggregate concrete. CALCON_ETC is the material model for carbonate aggregate concrete. The

steel model in the SAFIR thermal analysis is selected as STEELEC2EN (Gernay and Franssen, 2012). The thermal properties of the concrete and steel material models (conductivity and specific heat) are based on the material models in EN1992-1-2 (2004). These material models can be replaced by other concrete or steel models in SAFIR (or equivalent models in other software programs that might be used for thermal analysis). It is worth mentioning that concrete models in SAFIR do not consider the difference of concrete thermal conductivity during the heating and cooling phases.

The material models selected for use in the OpenSees models are Concrete01 and Steel02. Since these do not consider the variation of material properties with temperature, the input material properties (shown in Figure 3-4) must be modified for the fire-damaged concrete and steel after fire exposure. Models for the compressive strength $f'_{c,r}$, peak compressive strain $\varepsilon_{0,r}$, crushing strain $\varepsilon_{20c,r}$ and elastic modulus $E_{c,r}$ of fire-damaged concrete are based on the recommendations proposed by Chang et al. (2006). Figure 3-5 shows the variation of fire-damaged concrete properties as a function of temperature. The crushing strain $\varepsilon_{20u,r}$ is the strain corresponding to the stress of $0.2f'_{c,r}$ at the descending branch. Models for the yield strength $f_{y,r}$, elastic modulus $E_{s,r}$ and ultimate strength $f_{u,r}$ of fire-damaged reinforcing steel are based on the research of Tao et al. (2013). Figure 3-6 shows the variation of fire-damage steel properties as a function of temperature. The temperature mentioned in these material models is the maximum temperature the material has experienced during the full heating-cooling cycle. After fire exposure, rehydration of concrete may result in recovery of strength and stiffness if fire exposure does not exceed 500°C. No recovery will occur for reinforcing steel. The recovery of concrete strength and stiffness here are based on the test data by Harada (1961) and are shown in Figure 3-**7**.

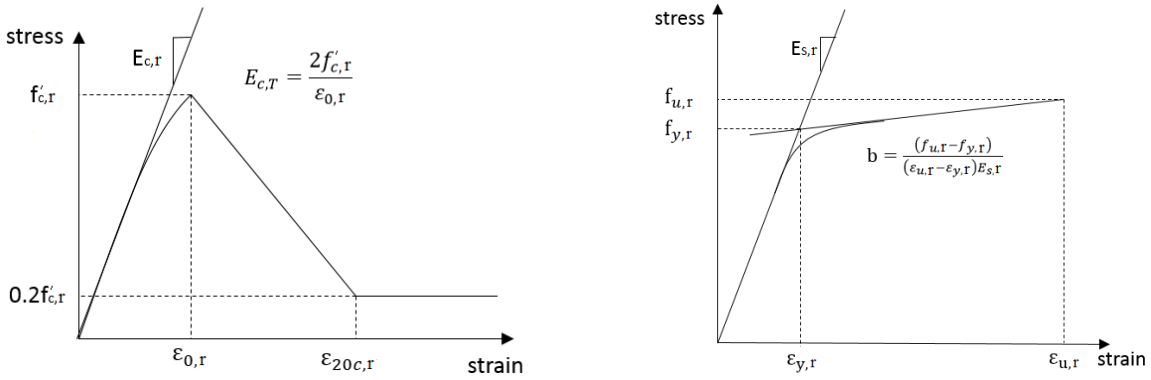

(a) Concrete (b) Steel

Figure 3-4 Stress and strain curves (Mazzoni et al., 2006).

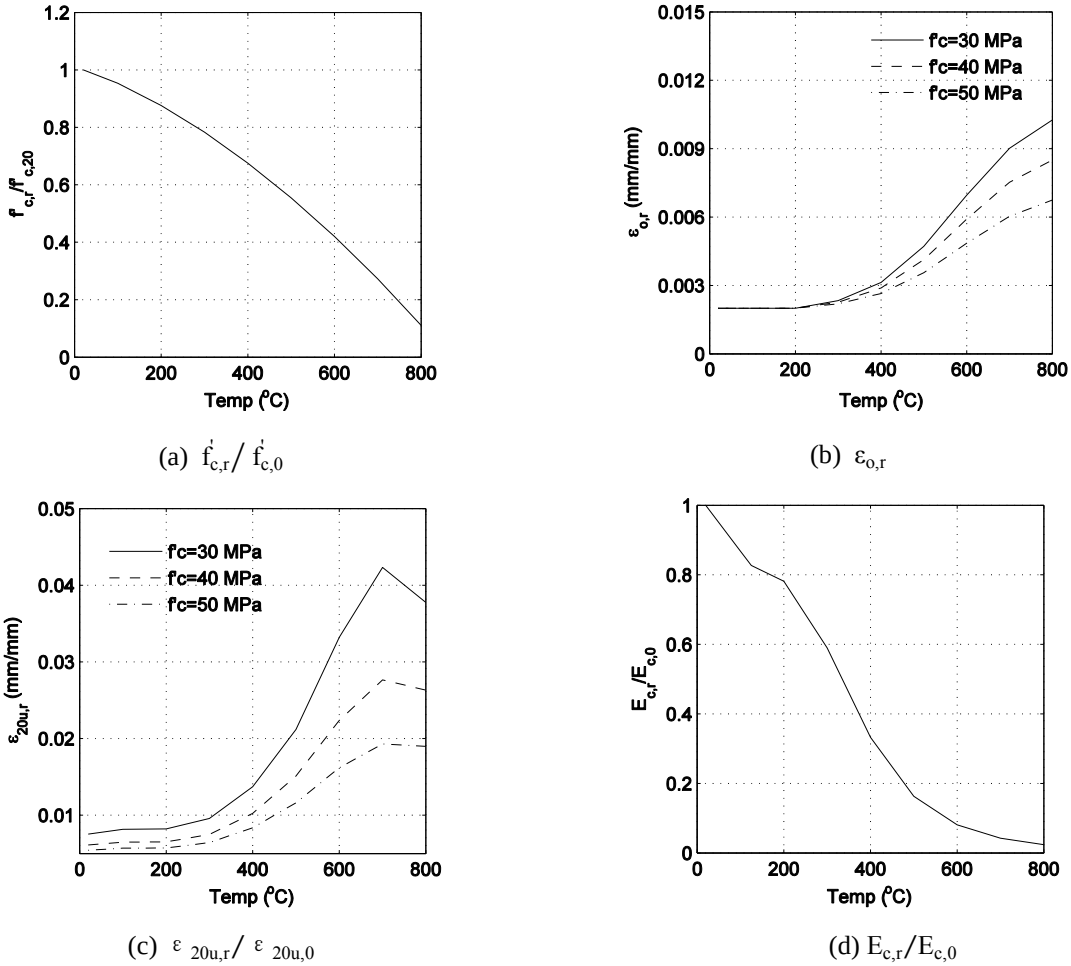

(a) $f'_{c,r}/f'_{c,0}$ (b) $\varepsilon_{o,r}$

(c) $\varepsilon_{20u,r}/\varepsilon_{20u,0}$ (d) $E_{c,r}/E_{c,0}$

Figure 3-5 Variation in concrete properties with temperature (Change et al., 2006).

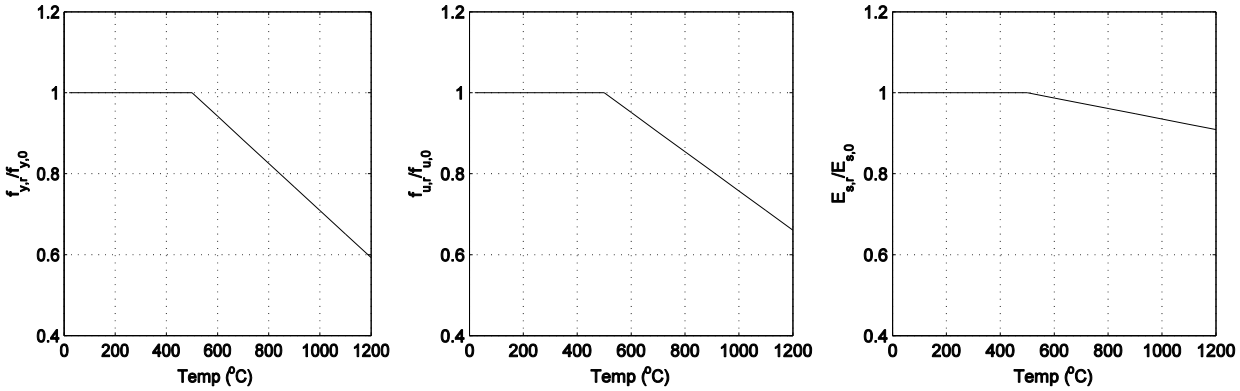

(a) $f_{y,r}/f_{y,0}$ (b) $f_{u,r}/f_{u,0}$ (c) $E_{s,r}/E_{s,0}$

Figure 3-6 Variation in reinforcement properties with temperature (Tao et al., 2013).

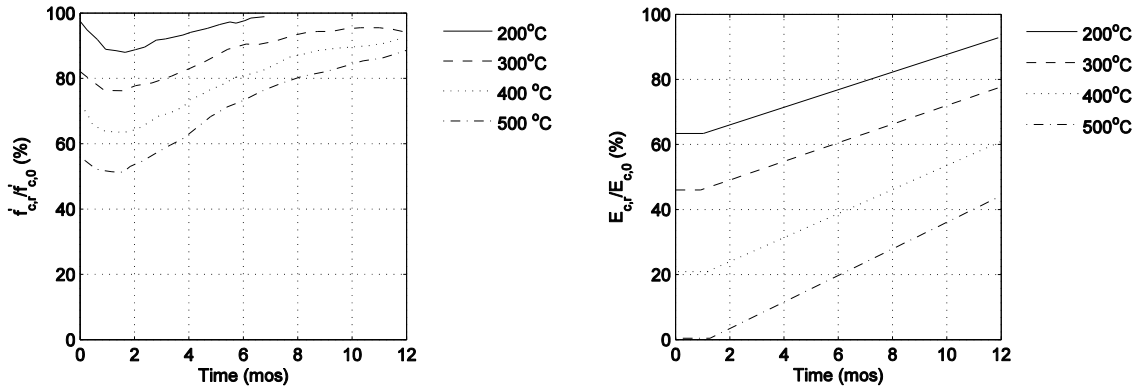

(a) Concrete strength in compression (b) Young's modulus of concrete

Figure 3-7 Natural recovery of the compressive strength and young's modulus of a normal weight concrete heated at various temperatures (Harada, 1961).

The stress-strain curves of Concrete01 are different from those of the fire-damaged Chang concrete model (Chang et al., 2006), even though the variation of the material properties ($f'_{c,r}$, $\varepsilon_{0,r}$ and $\varepsilon_{20c,r}$) in Concrete01 are based on the recommendations by Chang et al. (2006). Figure 3-8 shows the stress-strain curves of concrete with $f'_{c,0}$=40MPa at various temperatures, based on Chang concrete model and Concrete01. Significant difference exists in the initial elastic modulus of concrete between Concrete01 and the Chang concrete model, especially when the maximum

temperature is larger than 500°C. Thus, validation is required to ensure that the difference in the initial elastic modulus between the two concrete models does not significantly influence the numerical lateral load-drift behavior. Since Chang concrete model is not available in OpenSees, hysteretic material in OpenSees is used to approximate Chang concrete model. Wall specimen WR0 (Oh et al., 2002) was selected as an example to demonstrate this point. In the numerical analysis, specimen WR0 is subject to four-hour fire first (shown in Figure 3-9) and then subject to reversed-cyclic loads. The maximum temperature the fire-exposed side has experienced during the entire heating-cooling cycle is 897°C. Figure 3-10 shows the lateral load-drift behavior of the wall under monotonic lateral load based on Concrete01 and Hysteretic model which is set to approximate the Chang concrete model. The difference in the initial elastic modulus between Concrete01 and the Chang concrete model does not significantly influence the lateral load-drift behavior of WR0 under reversed-cyclic loads.

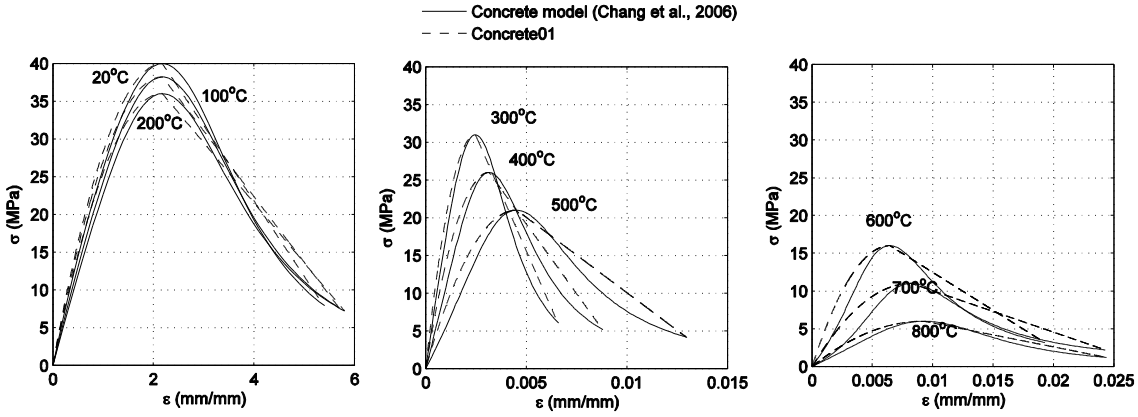

(a) 20°C, 100°C and 200°C (b) 300°C, 400°C and 500°C (c) 600°C, 700°C and 800°C

Figure 3-8 **Comparison of Chang concrete model and temperature-dependent Concrete01 model.**

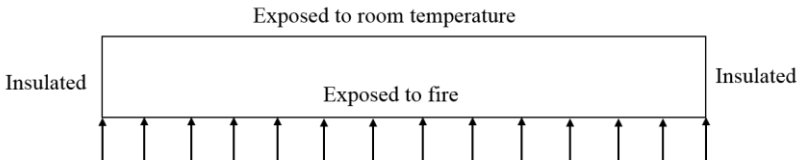

Figure 3-9 Thermal boundary conditions.

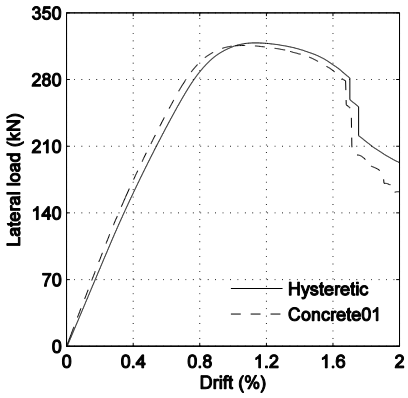

Figure 3-10 Post-fire lateral load-drift response of WR0 (Oh et al., 2002).

3.4.2. Confined Concrete Model for Fire-damaged Concrete

Confined concrete material properties are determined from the material properties and configuration of the confining reinforcement. Here, the Chang and Mander model (1994) is used, although a similar approach can be taken with any material model. The yield strength of the confining reinforcement determines the confined strength of the concrete, however, the temperature gradient results in different material properties at each location. Figure 3-11 shows the maximum temperature distribution of a wall section after a three-hour fire exposure. Since the lowest residual yield strength of the hoops controls the maximum confining effect, the lateral confining pressures are calculated based on the worst residual material properties of confining reinforcement. The transverse reinforcement in the boundary region is not modelled in SAFIR but should have similar temperature to the longitudinal reinforcing steel; thus the worst residual

material properties of the transverse reinforcement is determined by the highest maximum temperature of the longitudinal reinforcement fibers.

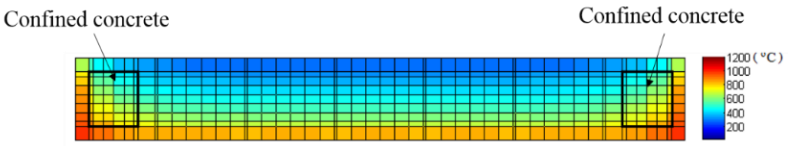

Figure 3-11 Temperature distribution of a wall section after three-hour fire exposure.

3.4.3. Material Regularization of Fire-damaged Materials

Material regularization is used to model cyclic response in OpenSees if the wall simulated has a softening section (Pugh et al., 2015) . For fire damaged walls, the variation of G_{fc} or G_{fcc} with maximum temperature and the variation of $\varepsilon_{u,exp}$ with maximum temperature are needed.

No direct experimental data are available for the fracture energy of fire-damaged concrete in compression. Instead, it was calculated using the tested stress-strain curves of fire-damaged concrete in compression. The definition of $G_{fc,r}/L_{IP}$ for fire-damaged concrete is shown in Figure 3-12. Based on the Chang concrete model, the stress-strain curves for the fire-damaged concrete can be determined and thus the values of $G_{fc,r}/L_{IP}$ at various maximum temperatures can be calculated. Once the values of $G_{fc,r}/L_{IP}$ at room temperature and other elevated temperatures are calculated, the variation of $G_{fc,r}$ with temperature can be determined. Figure 3-13 shows the variation of $G_{fc,r}$ with maximum temperature for concrete with undamaged compressive strength of 30 MPa, 40 MPa and 50 MPa. Since $G_{fcc,r}$=1.70 $G_{fc,r,}$, the variation of $G_{fc,r}$ with maximum temperature is the same as the variation of $G_{fcc,r}$ with maximum temperature. However, the large values between 400 and 800 degrees computed using this method may provide unrealistically large

crushing strains. In analysis of thicker wall sections, this may lead to the model predicting crushing of the concrete core while the cover concrete remains undamaged; such a physical behavior is unrealistic to expect in a wall. In the absense of experimental material tests to provide adequate models, a simpler approach is proposed in which:

$$G_{fc,r}=2f'_{c,r}\ (N/mm) \qquad \text{Eq. 3-4}$$

The variation of $G_{fc,r}$ with maximum temperature based on this assumption is the same as the variation of $f'_{c,r}$ with maximum temperature and is shown in Assumption 2 in Figure 3-13. This approach is considered to be conservative as it will predict crushing at smaller strains and may underpredict the true drift capacity of a wall.

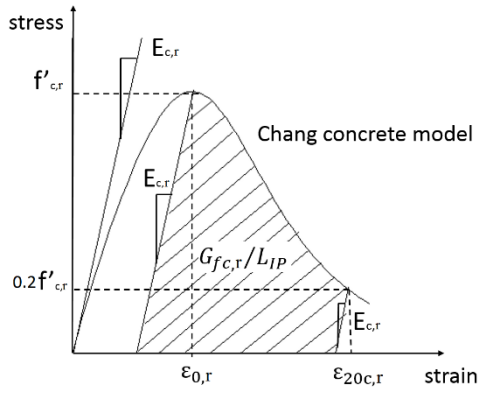

Figure 3-12 Calculation of $G_{fc,r}$ based on Chang concrete model.

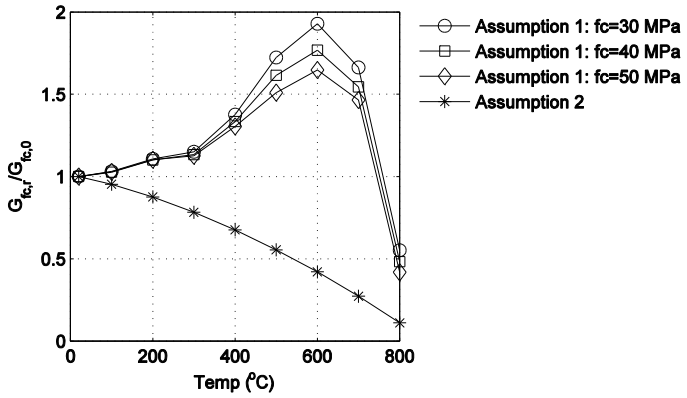

Figure 3-13 Variation of $G_{fc,r}$ with temperature.

In the simulation, it is assumed that the reinforcing steel ruptures when its tensile strain exceeds the rupture strain and that the reinforcing steel buckles when the crushing strain of the surrounding concrete is reached. The rupture strain and the buckling strain cannot be defined directly in Steel02, thus the MinMax command is used to define the rupture strain and the buckling strain. The material regularization of reinforcing steel modifies $\varepsilon_{u,exp,r}$ to $\varepsilon_{u,r}$ to define the maximum strain in OpenSees according to the integration point length L_{IP} (shown in Eq. 3-**3**). Models to define the variation of rupture strain with temperature are not available. The available experimental data about the rupture strain (maximum strain) of fire-damaged reinforcing steel are shown in Figure 3-14 (Topcu and Karakurt, 2008; Elghazouli et al., 2009; Felicetti et al., 2009). The data in Figure 3-14 are the test results of hot-rolled reinforcing steel cooled by air or cooled naturally and temperature at the horizontal axial is the maximum temperature a specimen has experienced during the heating-cooling cycle. While the data in Figure 3-14 suggest that rupture strain of fire-damaged reinforcing steel is a function of temperature, the data in Figure 3-14 were deemed to be insufficient to develop a predictive model. Here, it is assumed that the rupture strain of fire-damaged reinforcing steel does not change with the maximum temperature it has

experienced and is equal to the rupture strain at room temperature. The rupture of reinforcing steel is assumed to occur at tensile strain of 20% at the room temperature if the experimental data is unavailable. According to the rupture strain $\varepsilon_{u,r}$, ultimate strength $f_{u,r}$, yield strength $f_{y,r}$ and elastic modulus $E_{s,r}$ of reinforcing steel, the parameter b in Steel02 can be determined, shown in Figure 3-4b.

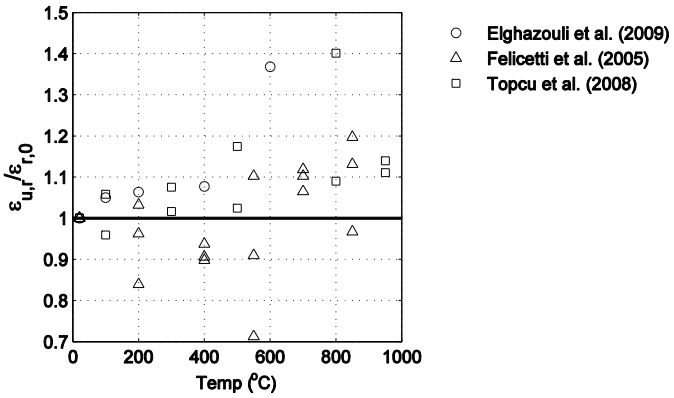

Figure 3-14 Variation of rupture strain $\varepsilon_{u,exp,r}$ with temperature.

3.5. Shear Model

The deformation of slender RC structural walls under lateral loads is primarily due to flexural deformation, although contributions from shear are also present. If it is assumed that the flexural deformation and the shear deformation is uncoupled, the flexural deformation of a RC structural wall can be simulated by the fiber-sections while a shear model can be aggregated to the fiber sections to simulate the shear deformation. The simplest shear model is the linear shear model:

$$V = \frac{G_{c,r} A_{cv}}{f_s} \gamma \qquad \text{Eq. 3-5}$$

where $G_{c,r}$ is the effective shear modulus of the concrete component; A_{cv} is the gross area bounded by the thickness of the web and the length of the wall section; γ is the shear strain; f_s is the shape factor for shear which accounts for non-uniform distribution of shear stress on the section (f_s=1.2 for a rectangular cross section).

The effective shear stiffness value for uncracked concrete components recommended by ACI 318-14 (2014) is shown in Eq. 3-6.

$$G_c A_{cv} = \frac{E_c}{2(1+v)} A_{cv} = 0.4 E_c A_{cv} \quad \text{Eq. 3-6}$$

However, due to the cracking of the concrete, the shear stiffness is often lower than $0.4E_cA_{cv}$. The effective shear stiffness at yield recommended by Birely (2012) is $0.15GA_{cv}$ ($0.06E_cA_{cv}$). This value was derived from the test results for four planar walls with axial load demands of approximately $0.1f'_{c,0}A_{cv}$. The derivation is based on Timoshenko beam theory and measurements.

The linear shear model is implemented in OpenSees using the Elastic material. For the simulation of shear deformation in a fire-damaged wall, $E_{c,r}$ which is the average elastic modulus of fire-damaged concrete will replace E_c in calculating the effective shear stiffness. Although linear elastic shear response is assumed in this paper, the shear model can be replaced by an alternative model is desired.

3.6. Validation of the Proposed Procedure

The proposed simulation procedure includes the thermal analysis of RC structural walls and the seismic analysis of fire-damaged RC structural walls. The two parts are validated in the following sections using the test data of fifteen RC structural walls tested by Liu (2010). These

walls are of a relatively low aspect ratio and made of normal-strength concrete. The thermal analysis in the proposed simulation procedure will be validated using the tested temperature data along wall thickness. The seismic analysis in the proposed simulation procedure will be validated using the tested load-drift behavior of these walls under reversed-cyclic loads.

3.6.1. Post-fire Seismic Tests of Walls

The fifteen walls tested by Liu (2010) are summarized in Table 3-2. Eleven walls were subject to the lateral reversed-cyclic loads after exposure to fires ranging in duration from 40 to 90 minutes, while four walls were subject to reversed-cyclic loads only. In the fire tests, walls were tested horizontally, with one surface exposed to fire, another surface exposed to room temperature and the two side surfaces along the wall thickness covered by asbestos. During the heating phase, walls had peak out-of-plane deflection ranging from 6mm to 16mm. Concrete spalling occurred in the fire test of N2T6, N4T6-D and N4T9-D. Walls were subjected to reversed-cyclic loading after five months, at which time most deformation had recovered. The lateral loading protocol consists of two stages: load-controlled up to yield and displacement-controlled after yield. All the walls failed in shear or shear-flexure mode. The fire-undamaged walls experienced one or several major diagonal cracks and also experienced concrete crushing and rebar buckling at wall toes. For fire-damaged walls, the major diagonal cracks are not as significant as those in the fire-undamaged walls, especially for walls which has been exposed to 90min fire.

Table 3-2 Summary of Liu wall tests used to validate modeling procedure (Liu, 2010).

	t(min)	P_f(kN)	P_L(kN)	$N/(f'_cLt_w)$(%)	ρ_h(%)	ρ_v(%)
N0T4	40	0	400	12	0.44	0.44
N0T6	48	0	400	12	0.44	0.44
N0T9	90	0	400	12	0.44	0.44
N2T0	0	200	200	6	0.44	0.44
N2T6	60	200	200	6	0.44	0.44
N2T9	90	200	200	6	0.44	0.44
N4T0	0	400	400	12	0.44	0.44
N4T6	60	400	400	12	0.44	0.44
N4T9	90	400	400	12	0.44	0.44
N6T0	0	600	600	18	0.44	0.44
N6T6	60	600	600	18	0.44	0.44
N6T9	90	600	600	18	0.44	0.44
N4T0-D	0	400	400	12	0.66	0.66
N4T6-D	60	400	400	12	0.66	0.66
N4T9-D	90	400	400	12	0.66	0.66

Note: f'_c is compressive strength of concrete; L is length of a wall section, 700 mm; $N/(f'_cLt_w)$ is axial load ratio; P_f is axial load during fire test; P_L is axial load during the reversed-cyclic loading test; t is fire duration; t_w is wall thickness, 100 mm; ρ_h is reinforcement ratio of the web horizontal rebar; ρ_v is reinforcement ratio of the web vertical rebar.

3.6.2. Description of Wall Models in SAFIR and OpenSees

The wall cross-sections, including thermal boundary conditions, are shown in

Figure 3-15. The thermal parameters ($\varepsilon_r=0.2$ and $h_c=25\ W/m^2K$ for the fire-exposed side and $h_c=9W/m^2K$ for the fire-unexposed side) were selected in such a manner that the calculated and the measured temperatures in concrete agreed as much as possible (Bratina et al., 2005). The fire curves input into SAFIR were those applied during the fire tests. SILICON_ETC and STEELEC2EN are selected as the concrete and steel models in SAFIR; Concrete01 and Steel02

are selected as the concrete and steel models in OpenSees. The material models were defined following the guidelines presented in Section 3.4.

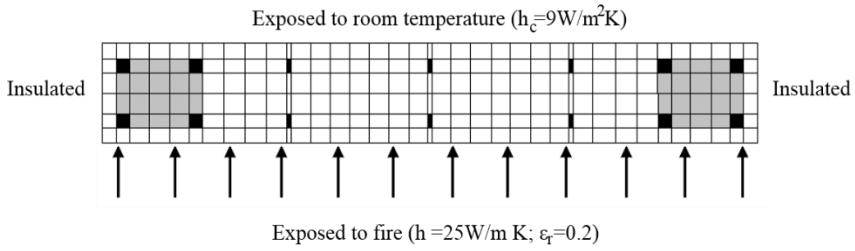

(a) Walls with ρ_h=0.44%

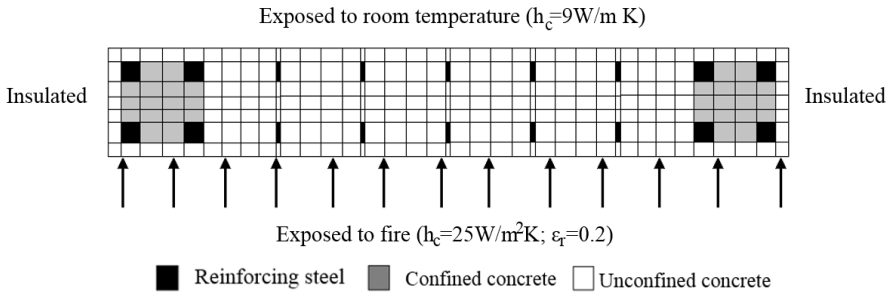

(b) Walls with ρ_h=0.66%

Figure 3-15 Thermal boundary conditions of walls in SAFIR.

3.6.3. Validation of Thermal-mechanical Analysis

Temperature data were only reported for N0T6, N2T6, N4T6, N4T9, N4T6D and N4T9D. The temperature history of concrete 5mm from the fire-exposed side and 5mm from the non-exposed side are shown in Figure 3-16. It shows that the SAFIR model can reasonably simulate the temperature history of concrete at 5mm from the fire-exposed side and from the non-exposed side, with the model predicting the peak temperature within 10% for most walls and the largest difference occurring for N2T6 in which the model predicated a higher temperature than measured. Table 3-3 compares the experimental and numerical peak temperatures at 5mm from the fire-

exposed side (gray circle and black circle respectively, shown in Figure 3-16f) , the experimental and numerical temperatures at the end of fire tests at 5mm from the fire-exposed side (gray square and black square respectively, shown in Figure 3-16f) and the experimental and numerical temperatures at the end of fire tests at 5mm from the fire-unexposed side (gray triangle and black triangle respectively, shown in Figure 3-16f). Results indicate that SAFIR can simulate the temperature of RC wall sections during both the heating and cooling phases. The peak temperatures at 5mm from the fire-unexposed side are not compared because they are very close to the temperature at the end of fire test at the same position.

Using the temperature-time history of the walls, SAFIR was then used to conduct a mechanical analysis to evaluate the ability of the model to capture the deformations and strains created by the thermal loads. While strain data were not presented by Liu, experimental deformations at the wall midpoint were compared to those from the model. Figure 3-17 shows this for wall N4T6. It should be noted that while these strains could be transferred to an OpenSees model to include in cyclic analysis, most of the experimental deformation had recovered prior to the cyclic test (Liu, 2010) and the impact of the strains on the cyclic response is sufficiently small that it can be neglected.

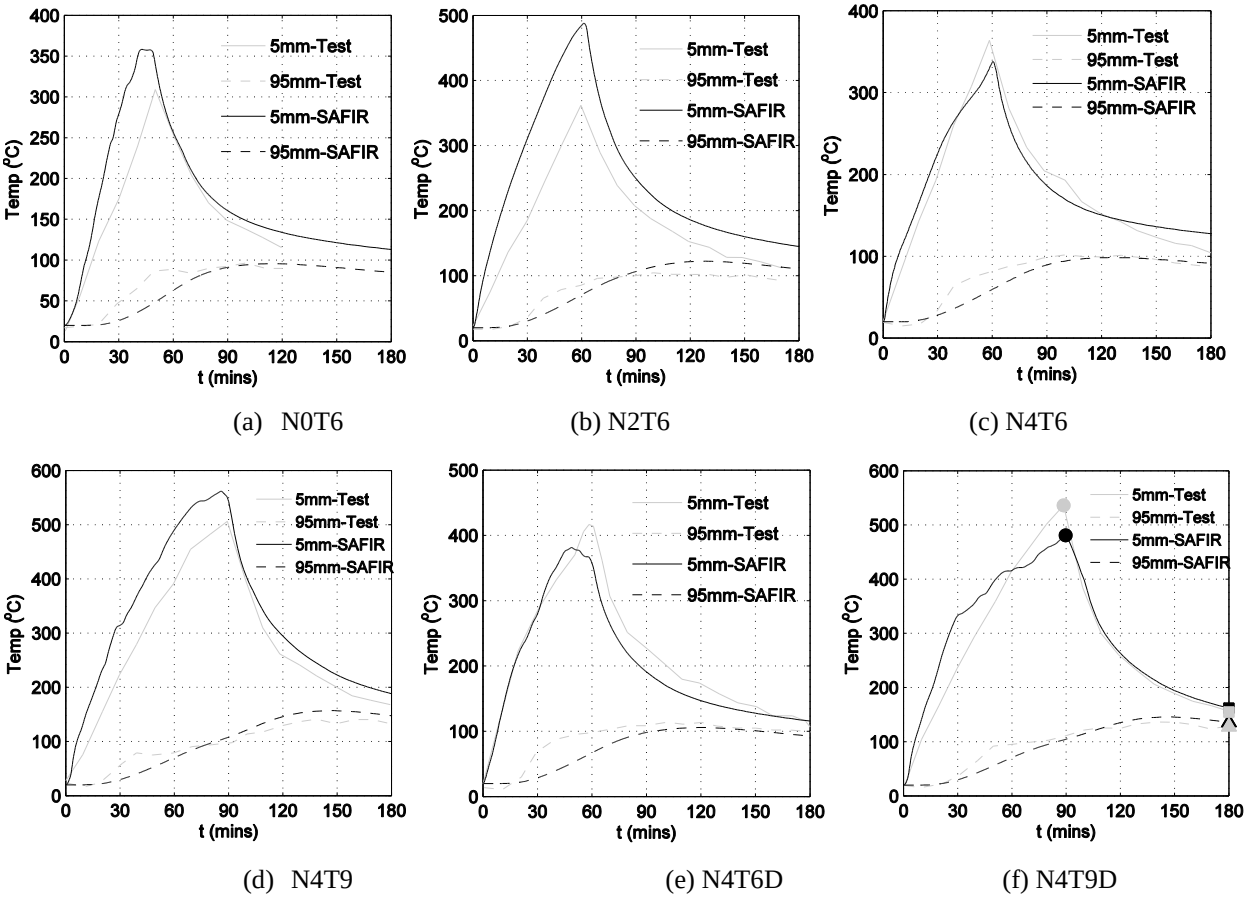

(a) N0T6 (b) N2T6 (c) N4T6

(d) N4T9 (e) N4T6D (f) N4T9D

Figure 3-16 **Experimental and numerical temperature history for concrete in Liu walls (Liu, 2010).**

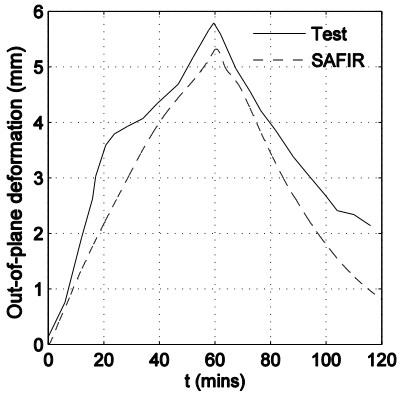

Figure 3-17 Experimental and numerical out-of-plane deformation for wall N4T6 under fire (Liu, 2010).

Table 3-3 Compare experimental and numerical temperatures of walls under fire (°C) (Liu, 2010).

	5mm-Peak			5mm-End			95mm-End		
	Test	SAFIR	Error	Test	SAFIR	Error	Test	SAFIR	Error
N0T6	309.0	357.4	15.7%	115.3	132.9	15.3%	89.8	95.3	6.1%
N2T6	361.9	488.1	34.9%	113.2	149.2	31.8%	92.4	113.7	23.0%
N4T6	363.2	337.9	7.0%	105.9	127.6	20.5%	87.0	91.4	5.1%
N4T9	506.0	561.3	10.9%	168.0	189.6	12.9%	132.0	148.2	12.3%
N4T6-D	416.7	381.5	8.4%	104.4	115.7	10.8%	98.9	92.9	6.1%
N4T9-D	536.2	479.4	10.6%	154.8	163.4	5.6%	127.7	135.5	6.1%
Mean			14.6%			16.1%			9.8%
Std. Dev.			10.4%			9.1%			7.0%

Note: 5mm-Peak means the peak temperature at 5mm from the fire-exposed side; 5mm-End means the temperature at the end of fire tests at 5mm from the fire-exposed side; 95mm-End means the temperature at the end of fire tests at 5mm from the unexposed side.

3.6.4. Validation of Cyclic Mechanical Analysis

With the maximum temperature distribution of wall sections, the post-fire seismic analysis of walls was conducted using the procedure outlined in Section 3 and using the properties discussed in Section 4. The response quantities investigated were: 1) V_{max}, the maximum lateral load a wall experiences before its lateral loading capacity begins to decrease; 2) K_{sec}, the secant stiffness at yield defined as the value of the lateral load at yield divided by the displacement at yield, and 3) Δ_{fail}/H, the drift capacity defined as the value of the failure displacement divided by the height of a wall and reported as a percentage.

3.6.4.1. Selection of Shear Model

The shear deformation of a RC structural wall is influenced by many factors, including cracking and yielding. It is reasonable to assume that a fire-damaged wall has seriously cracked

before subject to reversed-cyclic loads. Reasonable effective shear stiffness should be determined for the behavior of a fire-damaged wall under reversed-cyclic loads. The stiffness at yield K_{sec} of walls based different linear shear models (no shear model, $G_{c,r} = 0.4E_{c,r}$ and $G_{c,r} = 0.06E_{c,r}$) were determined. The numerical model errors are compared in Figure 3-18. The ability of the post-fire seismic analysis to predict the stiffness at yield is very dependent on the shear stiffness selected. For the Liu walls, both with and without fire damage, the effective shear stiffness of $0.06E_{c,r}$ provides the best prediction of wall stiffness at yield, with an average error 11.2%.

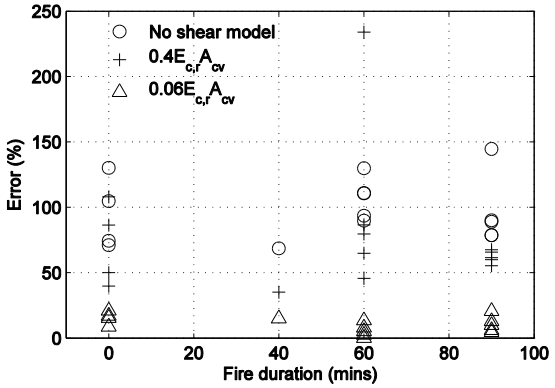

Figure 3-18 Error in simulated secant stiffness at yield as a function of fire duration.

3.6.4.2. Evaluation of Strength and Drift Capacity Prediction

The experimental and simulation post-fire lateral load-drift responses of walls based on the linear shear model with $G_{c,r}=0.06E_{c,r}$ are shown in Figure 3-19. Table 3-4 compares the experimental and numerical results of the fifteen walls. The numerical method described in Section 3 can predict the residual load-bearing capacity within an average error of 7.4%. Because the model can only capture flexural failure, it overestimates the drift capacity of those walls which were characterized by shear failure or shear-flexure failure in the tests. Despite this, these results

are useful in demonstrating the capabilities of the simulation procedure in capturing temperature distribution, stiffness at yield, and strength. Moreover, the proposed simulation procedure can finish all the simulation work above within half an hour, which is very efficient, compared to the time required by other software programs, such as Abaqus/Standard (2012) and VecTor2 (Wong et al., 2013).

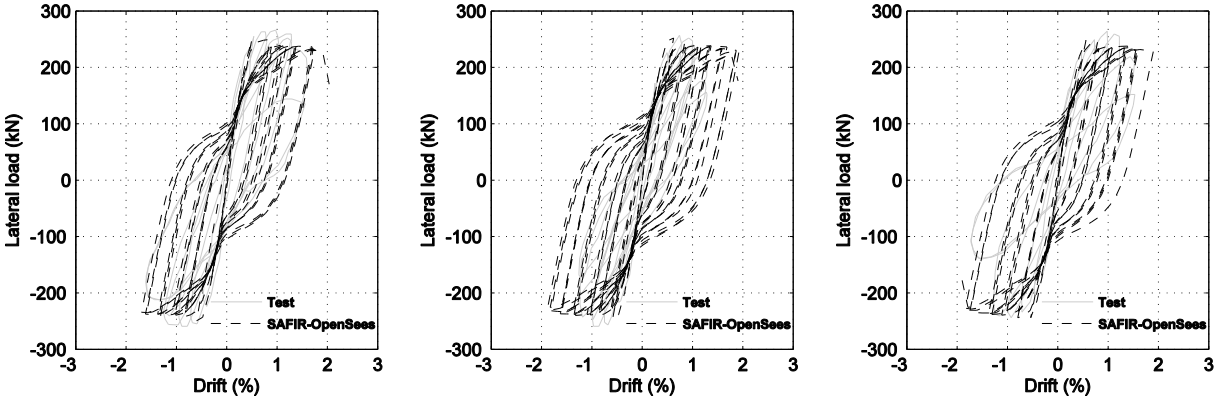

(a) N0T4 (b) N0T6 (c) N0T9

(d) N2T0 (e) N2T6 (f) N2T9

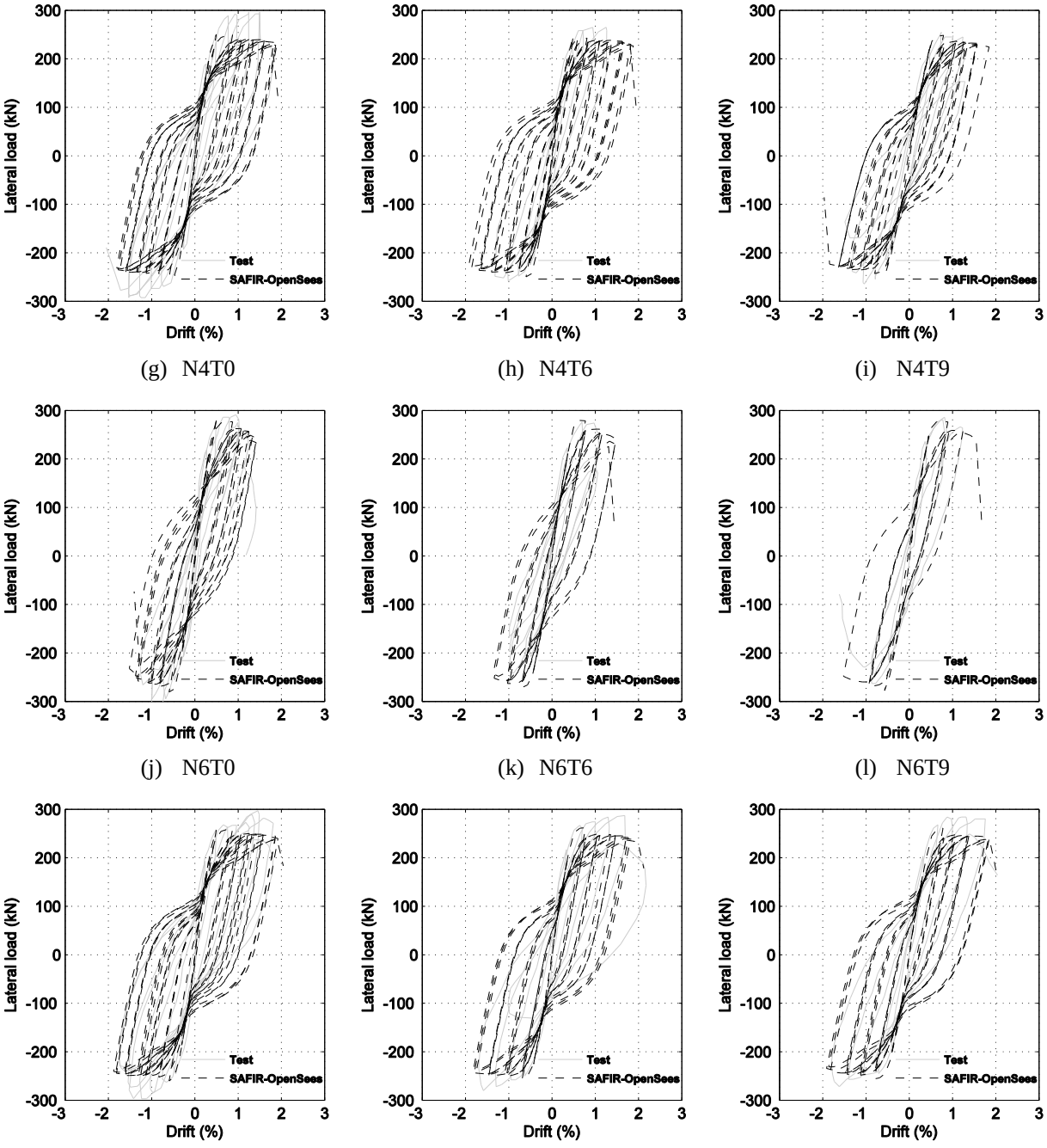

(g) N4T0 (h) N4T6 (i) N4T9

(j) N6T0 (k) N6T6 (l) N6T9

(m) N4T0-D (n) N4T6-D (o) N4T9-D

Figure 3-19 Experimental and numerical load-drift behavior of Liu walls under post-fire lateral load (Liu, 2010).

Table 3-4 Compare experimental and numerical response of walls under post-fire lateral loads.

	V_{max} (kN)			K_{sec} (kN/mm)			Δ_{fail}/H(%)		
	Test	SAFIR-OpenSees	Error	Test	SAFIR-OpenSees	Error	Test	SAFIR-OpenSees	Error
N0T4	266.0	249.7	6.1%	56.6	48.1	14.9%	1.6	2.0	24.2%
N0T6	259.0	252.1	2.7%	46.5	48.8	5.1%	1.3	1.9	50.6%
N0T9	264.0	250.1	5.3%	48.1	45.2	6.1%	1.5	1.9	28.3%
N2T0	240.0	218.5	8.9%	49.1	47.6	3.1%	2.1	2.8	32.0%
N2T6	226.0	214.6	5.0%	42.6	42.6	0.0%	1.8	2.7	51.4%
N2T9	234.0	214.0	8.6%	41.8	39.6	5.3%	1.4	2.7	89.8%
N4T0	296.5	250.7	15.4%	47.5	51.9	9.2%	1.9	1.8	2.7%
N4T6	265.0	249.5	5.8%	56.2	48.4	14.0%	1.3	1.9	45.8%
N4T9	264.6	248.3	6.1%	47.4	41.3	12.9%	1.3	1.9	44.5%
N6T0	325.0	280.7	13.6%	67.2	55.5	17.4%	1.2	1.5	22.0%
N6T6	276.0	279.4	1.2%	63.8	48.3	24.4%	1.1	1.5	36.9%
N6T9	286.0	277.6	2.9%	60.6	48.0	20.8%	1.3	1.6	25.3%
N4T0-D	297.0	260.3	12.4%	55.9	51.1	8.7%	1.8	2.0	9.6%
N4T6-D	287.0	262.1	8.7%	54.4	45.9	15.8%	1.7	2.0	19.4%
N4T9-D	284.0	260.9	8.2%	47.5	42.4	10.8%	1.8	1.9	7.0%
Mean Err			7.4%			11.2%			32.6%
Std. Dev.			4.1%			6.8%			22.0%

3.7. Discussions

3.7.1. Drawbacks

The simulation procedure discussed in this paper is proposed based on several assumptions and has several drawbacks. The first drawback is in regards to the material model for confined concrete. No test data are available for confined concrete sections with non-uniform strength distribution due to the non-uniform temperature increase. The model of confined concrete used in this paper is the extension of the Chang and Mander model. Test data are required to validate the application of the classical model to the confined concrete section with non-uniform strength distribution.

The second drawback is that the proposed simulation procedure can only predict flexural failure caused by the rupture of longitudinal reinforcing steel, buckling of longitudinal reinforcing steel or crushing of concrete. Shear failure modes, such as sliding shear failure, diagonal tension failure and diagonal compression failure, cannot be predicted. Therefore, the proposed simulation method is limited to modelling flexure-controlled RC walls. For the simulation of shear failure, a shear model with failure should be incorporated into the simulation procedure presented in this paper. However, more experimental data and numerical simulation studies are required to develop such a model.

The last drawback is that only material degradation due to fire exposure is considered in the simulation. Other damage, such as cracks and residual deformation due to fire exposure, are not considered. With regards to the residual deformations and stresses, these could be accounted for by extracting the stresses and strains from the thermal-mechanical analysis and including them as initial strains or stresses in the cyclic analysis. For the cyclic analysis of walls, the influence

will primarily be on the stiffness of the walls, with little impact on the strength and deformation capacity. For the Liu walls considered in this paper, the impact of the mechanical response on the cyclic analysis is negligible, as shown in Figure 3-20 for N4T6. For this wall, including seismic analysis with the residual strain due to thermal exposure changes the stiffness from 48.4 to 45.5 kN/mm; the numerical values for the strength and drift capacity are unaffected. If an analysis that includes the mechanical effects of the thermal loading is deemed necessary (i.e. stiffness is of primary concern or the residual strain/stress are expected to be of significant magnitude), the authors recommend the development of a specific material model for this purpose as the existing models are unable to use both initial strains/stresses and the maximum deformation limits that are needed to accurately capture the drift capacity of the walls.

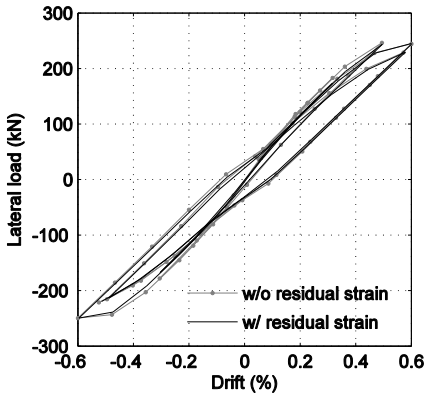

Figure 3-20 Effects of residual strain on the cyclic response of N4T6 (Liu, 2010) (only small displacement cycles shown for clarity).

3.7.2. Implementation for Study of Sequential Fire-earthquake Hazards

The proposed simulation procedure has been presented for the use of sequential fire-earthquake loading in which the fire is the initial event, but could also be used for earthquake-fire-earthquake analysis of RC structural walls. The damage due to the initial earthquake can be

determined by seismic analysis in OpenSees. The damage may include both residual strains and potential loss of concrete resulting in modified section thickness at some locations. This modified cross-section must be accounted for in the thermal analysis as the temperature distribution is likely to be significantly affected by the loss of cover. As discussed previously, if a wall is only exposed to fire before the seismic loads or if the damage from the initial earthquake is minor, the influence of residual strain due to fire exposure is negligible. However, if a main earthquake happens before the fire-earthquake sequential loads, the influence of residual strain may be significant, since both the main earthquake and the fire exposure would cause residual strain. To successfully conduct such an analysis would require the development of material models that could accurately account for the complex strain history of such a sequence of events, while at the same time accommodating a change in the stress-strain backbone curves due to thermal exposure.

3.8. Summary and Conclusions

This paper presents a simulation procedure for the post-fire seismic analysis of flexure-controlled RC structural walls. The simulation procedure combines thermal analysis in SAFIR with seismic analysis in OpenSees. The simulation method was verified by test data of RC walls under sequential fire-earthquake loads. The proposed simulation procedure can accurately predict the temperature history of wall sections under fire and the lateral load capacity and stiffness of fire-damaged walls under lateral reversed-cyclic loads. It is worth mentioning that the proposed simulation procedure could very efficiently simulate the post-fire seismic behavior of RC structural walls in both the thermal analysis and the seismic analysis. Although modeling of

reinforced concrete walls is the focus here, the method presented could be adapted for analysis of any lateral load resisting system.

Additional work is needed to develop models for the shear failure of fire-damaged RC structural walls. Additionally, more efforts should be made to make the concrete model in the simulation more accurate, such as experimentally validating the confining effect of transverse reinforcing steel on a concrete section with non-uniform strength distribution. These and other drawbacks are difficult to overcome in the presented simulation procedure, thus more advanced simulation procedure is required for the more accurate simulation of the post-fire seismic performance of RC structural walls and other RC structural members.

CHAPTER 4

POST-FIRE SEISMIC BEHAVIOR OF REINFORCED CONCRETE STRUCTURAL WALL*

A potential but infrequently studied hazard is the sequential occurrence of earthquakes and fires. Fire hazards following an earthquake can be significant due to increased likelihood of fires igniting, increased demands on firefighting resources, and potential obstacles to timely response. Increased ignitions and longer burn times can have significant structural impacts on reinforced concrete (RC) structures which are usually considered to have superior performance in a fire. The impact of this fire induced structural damage on the lateral load resistance of RC structures, particularly RC structural walls, is not well understood but may be critical in the event of aftershocks and/or future earthquakes. Given the severity of the consequences of reduced lateral load resistance, it is important for engineers to better understand fire-earthquake hazards in RC walls. This paper presents numerical studies to investigate the impact of fire damage on the lateral load resistance of flexure-control RC structural walls, including a parametric study to identify influential wall characteristics. Results indicate that fire damage decreases the load-bearing capacity and the stiffness of RC walls under reversed-cyclic loads. Curvature is shown to be a better indication of fire induced failure. At failure damage may shift to the web of a wall after fire exposure becomes more severe. Wall characteristics which significantly influence the residual wall response quantities were identified to be wall thickness, boundary element length, and axial load ratio.

---

* Ni., S. and Birely, A.C., Post-fire Seismic Behavior of Reinforced Concrete Structural Walls, Journal of Engineering Structures, 168 (2018) 163-178; reprinted with permission of publisher.

4.1. Introduction

To date, there are no documented failures of buildings due to fire-earthquake hazards, and in fact, the full or partial collapse of modern buildings during an earthquake is rare. However, fire following earthquakes have caused significant damage in modern earthquakes. Approximately 5000 buildings were damaged in the fire following the 1995 Kobe earthquake (Scawthorn, 1996), and numerous fires were reported following the Loma Prieta Earthquake (Levenson, 1992) in 1989 and Northridge earthquake (Trifunac and Todorovska, 1998) in 1994. Post-earthquake fire in urban regions has the potential to be particularly destructive as i) the breakage of utility lines increases the likelihood of fire ignition, ii) a strong earthquake may cause extensive damage to passive and active fire-defense systems in a structure, and iii) it may take considerably more time to control a fire due to blocked roads, hindered communication systems, disability of water supply system and limited available response teams. The increased ignitions and longer burn times may significantly degrade the material properties of a building such that the structural integrity is compromised. In such an event, buildings that may have been relatively undamaged following the original event may be at risk for significant damage or collapse in subsequent earthquakes. Post-fire earthquake scenarios may also arise in the event of a fire preceding an earthquake. Consequently, resilient design and evaluation of existing infrastructure necessitates an understanding of structural performance under such hazards.

A number of studies have been conducted on the influence of fire on the mechanical strength of reinforced concrete components. Post-fire material tests (Nassif, 2006; Chang et al., 2006; Harada and Daigaku, 1961) have shown that the mechanical properties of concrete degrade after fire exposure and do not fully recover after cooling. The mechanical properties of reinforcing

steel also degrade after exposure to elevated temperatures (Neves et al., 1996; Kirby et al.,1986) . Tests investigating the response of concrete components have been primarily focused on frame-elements. The impact of fire on the load bearing capacity and stiffness of columns has been investigated by Lie et al. (1989) and Chen et al. (2009). El-Hawary et al. (1996 and 1997) experimentally showed that the fire exposure time had a significant impact on the behavior of beams. Xiao et al. (2005) showed that fire exposure can transform the failure mode of a frame subjected to reverse-cyclic loads from strong-column-weak-beam to strong-beam-weak-column with poor cyclic performance. Xiao et al. (2004) and Liu (2010) tested reinforced concrete (RC) walls under reversed cyclic loading and found that fire decreased the stiffness and lateral load carrying capacity of walls; however, the low aspect ratios of the walls corresponded to shear failures and the drift capacity of walls with a flexural controlled response is unknown.

In this paper, the post-fire earthquake performance of reinforced concrete structural walls is investigated. RC structural walls are common in the design of multistory buildings subjected to ordinary and hazardous loads. For lateral loads such as wind and earthquakes, walls provide lateral stiffness and strength. Due to the non-combustibility and low thermal conductivity of concrete, RC walls are known for good fire performance, often working as fire walls to suppress the spread of fire in a building.

Although the post-fire earthquake performance of walls has been investigated in limited experimental studies (Xiao et al., 2004; Liu et al., 2010), it is important to better understand the behavior of flexural controlled walls, including the failure mechanisms and the influence of design parameters typically understood to impact the performance of walls under seismic loading, such as axial load ratio and boundary element confinement. Numerical simulations were conducted

using SAFIR and OpenSees to utilize the benefits of each for modeling fire and seismic demands, respectively. An overview of the simulation approach is presented in Section 4.2. Section 4.3 provides an in-depth analysis of a reference wall exposed to multiple fire scenarios to establish trends in the impact of fire on the seismic response. In Section 4.4, characteristics of the reference wall are altered to establish the influence of typical wall characteristics on the post-fire seismic response. A summary of results and recommendations for future research needs is presented in Section 4.5.

4.2. Description of Models

To simulate the post-fire seismic response of walls, it is necessary to utilize a methodology that can accurately account for both the thermal response of the structure during the fire loading and the mechanical response during seismic loading. In this study, a simulation procedure developed in previous work by the authors (Ni and Birely, 2018a) was utilized. Experimental tests (Liu, 2010) were used to validate the ability of the model to capture the temperature, stiffness, strength, and drift capacity of walls. Using from six walls with thermocouple data available, the temperature was simulated within 10-16% (std. dev. 7-10%) the experimental temperature at three points through the thickness of the wall. Using fifteen walls, the stiffness and strength was within 11% (std dev. 7%) and 7% (std. dev. 4%), respectively. The drift capacity was off by an average 33%, although this is a result of the tests failing in shear, a failure mechanism not captured in the modeling approach used (this study focuses on flexural-controlled walls only). As background, a brief overview of the model is presented here, with complete details of all material models provided in Reference by Ni and Birely (2018a).

For the thermal analysis, material properties must be defined to accurately simulate the temperature through the thickness of the wall as a function of time. Thermal boundary conditions define if each surface is exposed to fire, exposed to room temperature, or insulated. The material properties needed for thermal analysis are the conductivity, specific heat and density, as these impact the rate of heat transfer through the wall. The mechanical properties of the steel and concrete are affected by the temperatures; these modified material properties must then be accounted for in the subsequent mechanical analysis. A number of software programs are capable of conducting thermal analysis for reinforced concrete structures. For this study, SAFIR, which has been demonstrated extensively (Lopes et al., 2012; Dimia et al., 2011; Cachim and Franssen, 2009; Lim et al., 2004), was utilized for thermal analysis. OpenSees (Mazzoni et al., 2006) includes thermal analysis capabilities (Usmani et al., 2012) and can be used to provide a more efficient and seamless analysis for sequential fire-earthquake analysis. To ensure compatibility of the thermal and seismic models, the discretization of the cross-sections was the same and was governed by the needs of the seismic analysis. Thermal properties of the materials are defined based on EN 1992-1-2 (2004) using the SAFIR SILICON_ETC (Gernay and Franssen, 2012) and STEELEC2EN material models. The thermal boundary condition was defined for each face of the wall based on the desired analysis, with the fire exposed sides subjected to the ASTM E119 temperature-time curve (ASTM E119-18, 2018). At desired times, the maximum temperature of each fiber during the full heating-cooling cycle was determined using custom post-processing scripts. These scripts were then used to define the material properties for seismic analysis and generate the input files for seismic analysis.

For the mechanical analysis, it is necessary to accurately capture the stiffness, strength, hysteretic behavior, and drift capacity of the walls under seismic demands. While SAFIR is capable of conducting such an analysis, the post-peak strength, energy dissipation, and failure are not captured well. A better response can be obtained using OpenSees (Mazzoni, 2006), an open-source software developed for seismic analysis of structures. By utilizing OpenSees, materials that define the seismic response of walls are available, and the influence of confinement can be taken into account. Pugh et al. (2015) provide recommendations for modeling walls with force-based beam column elements, with the post-peak response of the material regularized to reduce mesh dependency of the fiber-section models. This modeling approach was utilized in this study, with the necessary adaptations made to account for the modified material properties due to the thermal analysis of the walls.

The built-in OpenSees material models of Concrete01 and Steel02 were used to define the mechanical response of the steel and concrete. As the temperature varied throughout the cross-section of the wall, unique material models are needed for each fiber. The maximum temperature during the full heating-cooling cycle was used to define the modified material properties. The backbone curve of the steel fibers were defined based on the recommendations by Tao et al. (2013), illustrated in Reference by Ni and Birely (2018a). The backbone curve of the concrete was defined based on recommendations by Chang et al. (2006), in which tests were carried out when residual strengths were lowest and recovery of strength had not recovered. Factors used to calculate the stress-stress curves for fire damaged concrete are shown in Reference by Ni and Birely (2018a). For confined regions, the backbone curve was further altered based on the Chang and Mander material model (Chang and Mander, 1994). Stress-strain curves were then regularized to eliminate

mesh dependency by adjusting the post-peak response based on the compressive facture energy and the length of the integration point; details are provided in Reference (Ni and Birely, 2018a).

The models used here were developed to provide a preliminary in-sight to the relationship between wall characteristics, loading, and fire duration on the seismic response of walls through enabling rapid analysis of many walls. Thus, there are a number of deficiencies that should be addressed in more refined models. These include the effect of fire on bond-slip between steel and concrete, and flexure-shear interaction, and mechanical damage induced by thermal loading. In the case of the latter, Ni and Birely (2018a) showed that the impact of residual strains had a limited impact on the seismic response.

4.3. Post-Fire Seismic Response of Reference Wall

A reference wall was designed to represent typical structural walls in seismic region and analyzed using the simulation procedure described in Section 4.2. Critical wall response quantities and damage patterns of the reference wall under sequential fire-lateral loads were determined and compared to indicate the influence of fire expose on the seismic performance of RC structural walls.

4.3.1. Description of Wall and Loading

A full-scale planar wall with boundary elements, shown in Figure 4-1 , was designed with characteristics representative of walls studied extensively in experimental test programs and summarized by Birely (2012). The wall has thickness (t_w) of 304.8 mm and length (l_w) of 3048 mm, providing a cross-sectional aspect ratio of 10. Figure 4-2 a shows the elevation of the wall.

The wall is 5 stories, with 3048 mm tall floors. The total wall height (not shown) is 15.24m, providing an aspect ratio, AR, of 5, and thus a flexure dominated response. Boundary elements are 15% of the total wall length with a 2.44% longitudinal reinforcement ratio and a 2.2% confining reinforcement ratio (#4 hoops and ties at 101.6 mm). Horizontal reinforcement spaced at 305 mm provides a 0.28% reinforcement ratio. The yield strength of reinforcing steel is 414 MPa. The peak compressive strength of concrete is 34 MPa.

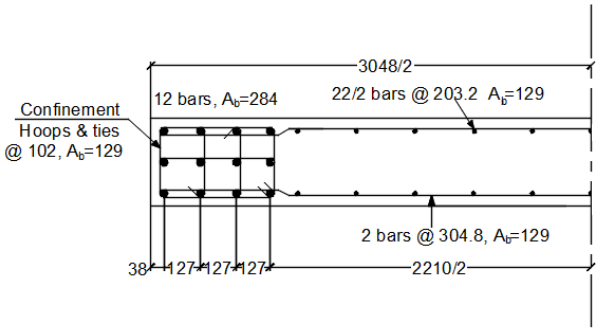

Figure 4-1 Cross section of the reference wall (unit: mm; A_b: cross-section area of each bar).

The first story of the reference wall was subjected to the four thermal boundary conditions shown in Figure 4-2 b: one-sided, two-sided, three-sided and four-sided fire. The fire-exposed sides of the wall were subject to radiation (emissivity coefficient ε_r, 0.7) and convection (film coefficient h_c , 25W/m^{2o}C) and the unexposed sides were subject to room temperature (film coefficient h_c, 9W/m^{2o}C) (EN 1992-1-2, 2004; EN 1991-1-2, 2002). The ASTM E119 fire curve (ASTM E119-18, 2018) with different durations were investigated, no fire, 0.5-hour fire, 1-hour fire, 2-hour fire, 3-hour fire and 4-hour fire. In this study, it was considered that the earthquake does not occur immediately following the fire, thus the materials will continue to increase in

temperature as the thermal effects penetrate through the thickness of the walls before eventually cooling off at a rate of 5 ^{o}C/min.

The base of the wall is fixed, with a lateral force applied at the top floor only. Reverse cyclic displacement cycles shown in Figure 4-3 were applied with an axial load of $0.1A_w f'_{c,0}$, where A_w is the area of wall section and $f'_{c,0}$ is the peak compressive strength of concrete at room temperature.

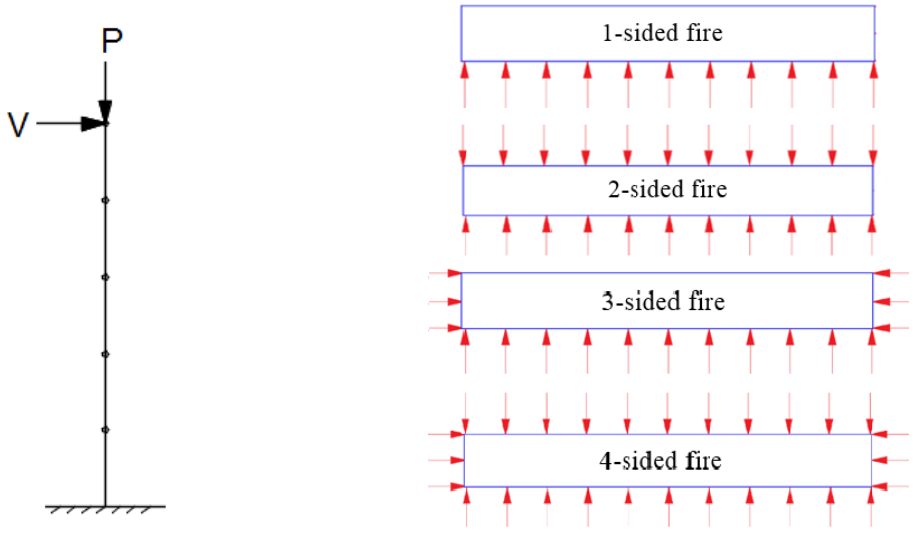

(a) Wall model elevation (b) thermal boundary condition

Figure 4-2 Boundary conditions, (a) mechanical boundary conditions for five story wall and (b) thermal boundary conditions applied to first floor of wall; arrows indicate heated sides and other sides are exposed to room temperature.

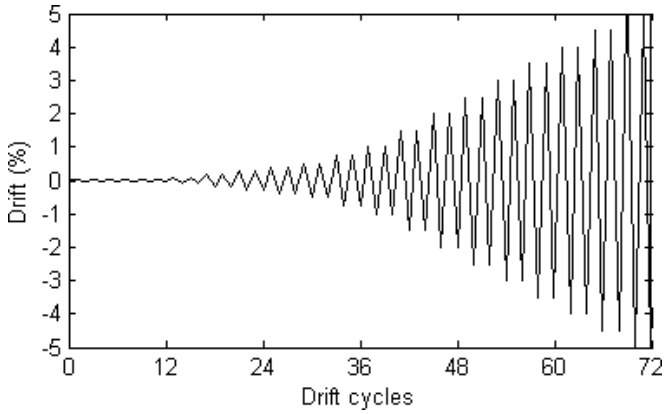

Figure 4-3 Applied drift history for seismic analysis of walls.

4.3.2. Seismic Response (No Fire)

Seismic response of reinforced concrete walls is typically described by the load-displacement hysteresis, shown in Figure4a for the reference wall with no fire. The wall has a maximum drift of 3% and losses lateral load capacity at approximately 2.5% during the first positive cyclic to 3.5%.

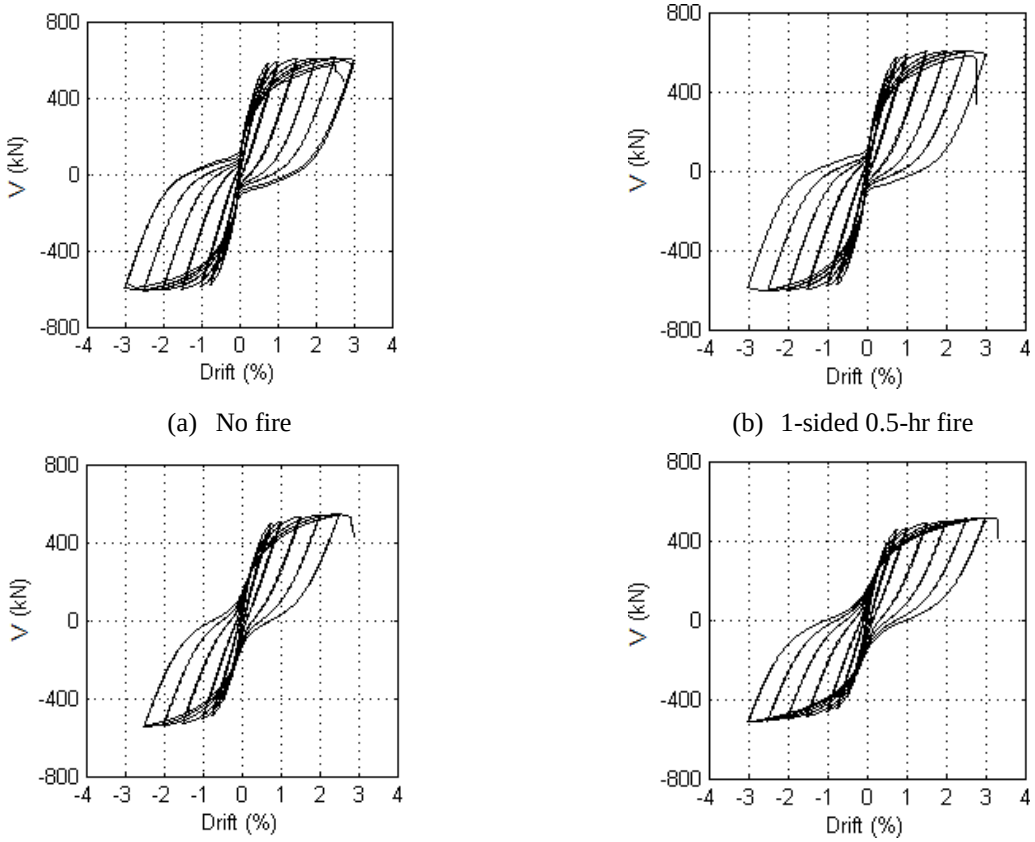

(a) No fire (b) 1-sided 0.5-hr fire

(c) 2-sided 3-hr fire (d) 4-sided 3-hr fire

Figure 4-4 Load-drift hysteresis curves of the reference wall.

In flexure-controlled RC walls, failure typically occurs due to concrete crushing and bar buckling in the boundary element under compressive loads. In this study, there was a need to show this graphically to study impact of fire on the failure mode of the wall. To accomplish this, a damage ratio was established for each concrete fiber in the lowest cross-section that indicates how far beyond the peak strength the fiber was loaded at the failure of the wall. The damage ratio is calculated as:

$$\text{Damage ratio} = (\varepsilon_{max} - \varepsilon_0)/(\varepsilon_c - \varepsilon_0) \quad \text{Eq. 4-1}$$

where ε_{max} is the maximum measured compressive strain in the concrete fiber, ε_0 is the strain at the peak stress, and ε_c is the strain at the assumed crushing point of concrete ($0.2f_c'$). This is illustrated graphically in Figure 4-5 .

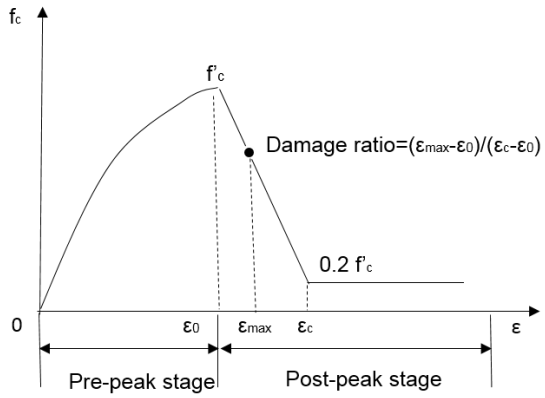

Figure 4-5 Definition of damage ratio of concrete fiber.

For the reference wall with no fire, the damage ratio for each fiber is shown on the cross-section in Figure 4-6. A value of 0 indicates the concrete fiber is in the pre-peak stage or just at the peak compressive strength. A value of 1 indicates the maximum compressive strain the concrete fiber has experienced is equal to or greater than the crushing strain. The damage ratio considers the demands that occurred during both pushing and pulling, resulting in the compression damage seen on both sides of the wall. The damage is concentrated in the boundary elements as expected, with higher ratios on the right side consistent with the failure of the wall occurring in the positive loading direction.

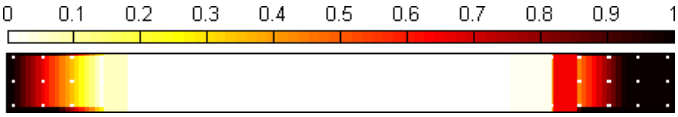

Figure 4-6 Damage-ratio distribution of the reference wall subjected to lateral loads only.

4.3.3. Impact of Fire on Mechanical Properties

Figure 4-7 shows the temperature distribution in the wall cross-section at the peak ambient temperature (left) and after the full heating-cooling cycle (right). At the peak fire temperature, the exposed surfaces have a significant increase in temperature, but the concrete and rebar in the center of the wall remains low. During cooling, the heat is able to penetrate further into the cross-section. The temperature distribution for 1- and 3-sided fire is similar, even after cooling, with only the fibers near the shorts ends affected; this region is the location of largest demands under seismic loading. Similarly, the temperature distribution for 2- and 4-sided fire are similar.

The maximum temperature in each fiber (right side of Figure 4-7) are used to identify residual material properties using the factors provided in Figure B-4 in Appendix B. The ratio of the residual strength and stiffness to the room temperature values are shown in Figure 4-8 . The concrete mechanical properties are severely degraded at the fire exposed sides, while the reduction in the center of the walls and in the rebar is considerably less.

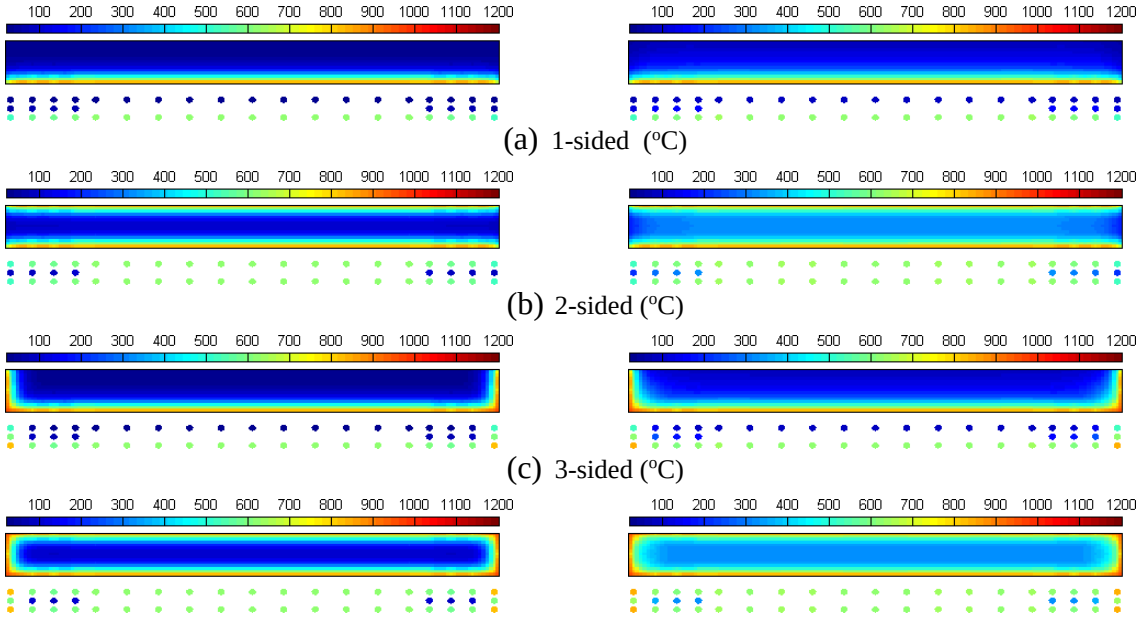

Figure 4-7 Temperature distribution of reference wall after 2-hour fire; left is at the end of the heating phase; right is maximum temperature during the full heating-cooling cycle; reinforcement temperature is shown below cross-section for clarity.

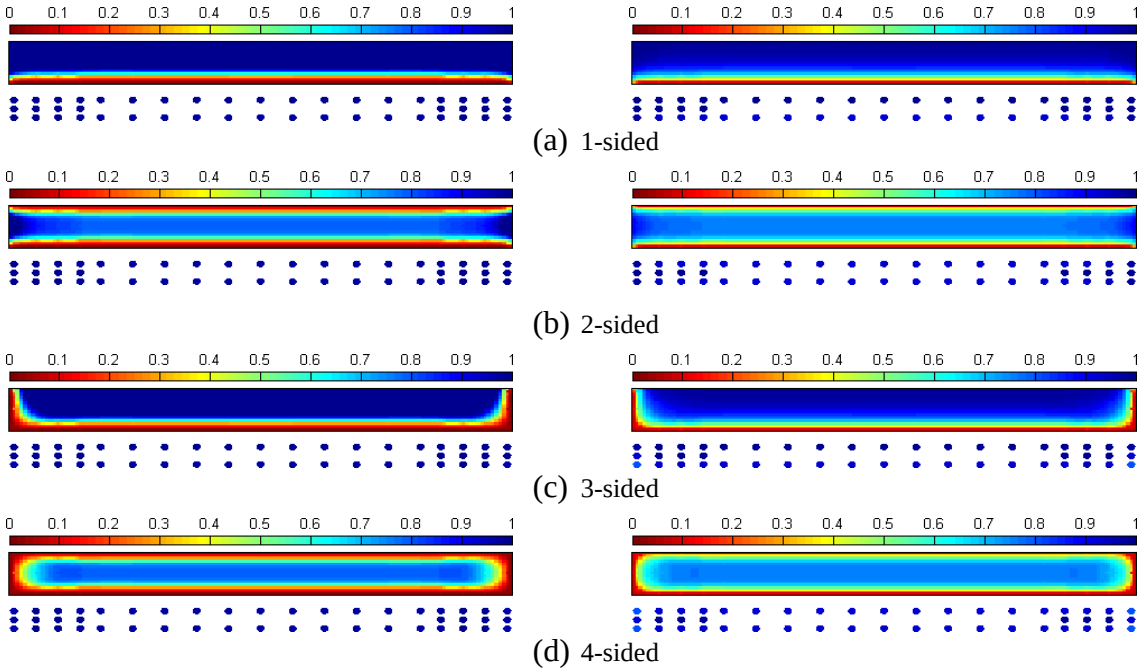

Figure 4-8 Residual material properties after 2-hour fire; left is the residual young's modulus ratio ($E_{c,fire}/E_{c,0}$ or $E_{s,fire}/E_{s,0}$) and right is the residual strength ratio ($f'_{c,fire}/f'_{c,0}$ or $f_{s,fire}/f_{s,0}$).

4.3.4. Impact of Fire on Seismic Response

The characteristic shapes of the hysteresis curves for the reference wall are similar to that of the reference wall without fire damage. Examples are shown in Figure 4-4.

From the cyclic response, the backbone curve and key response quantities, shown in Figure 4-9 , are extracted for comparison to walls with fire loading. Response quantities include maximum lateral load (V_{max}), secant stiffness (K) calculated at $0.75V_{max}$, failure drift (Δ_{fail}), and failure curvature (ϕ_{fail}). The failure drift is defined as the point when the load drops to $0.8V_{max}$ or the point before the lateral load decreases dramatically. Failure curvature is reported at this same point. Figure 4-10 shows backbone curves of the reference wall after exposure to all fire scenarios considered. The variation of key quantities with fire durations are shown in Figure 4-11 .

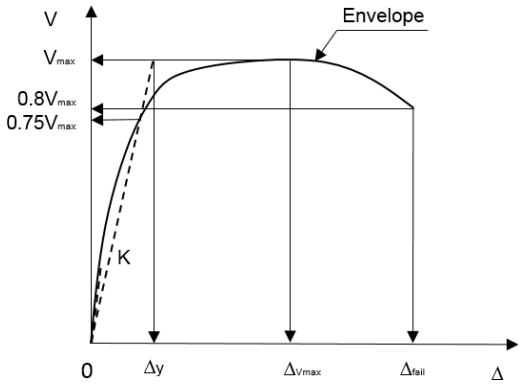

Figure 4-9 Definition of wall response quantities.

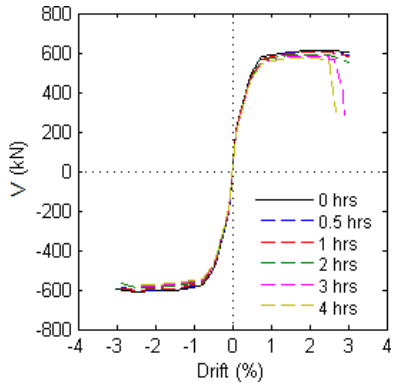

(a) After 1-sided fire

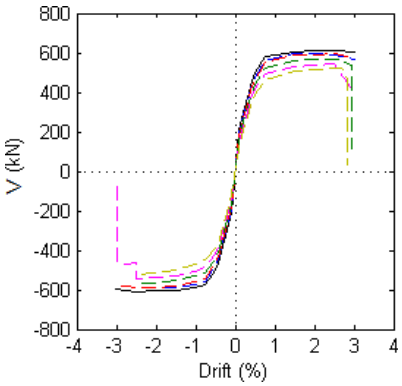

(b) After 2-sided fire

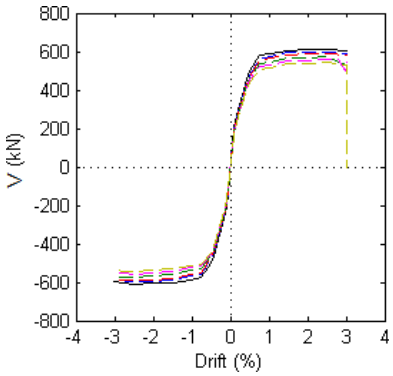

(c) After 3-sided fire

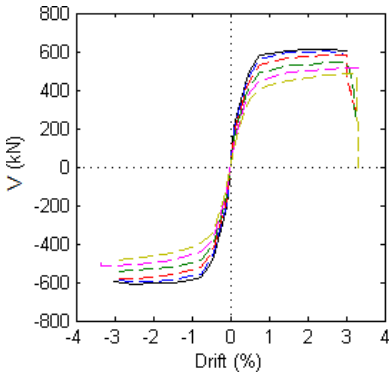

(d) After 4-sided fire

Figure 4-10 Backbone curves of the reference wall under reversed-cyclic loads.

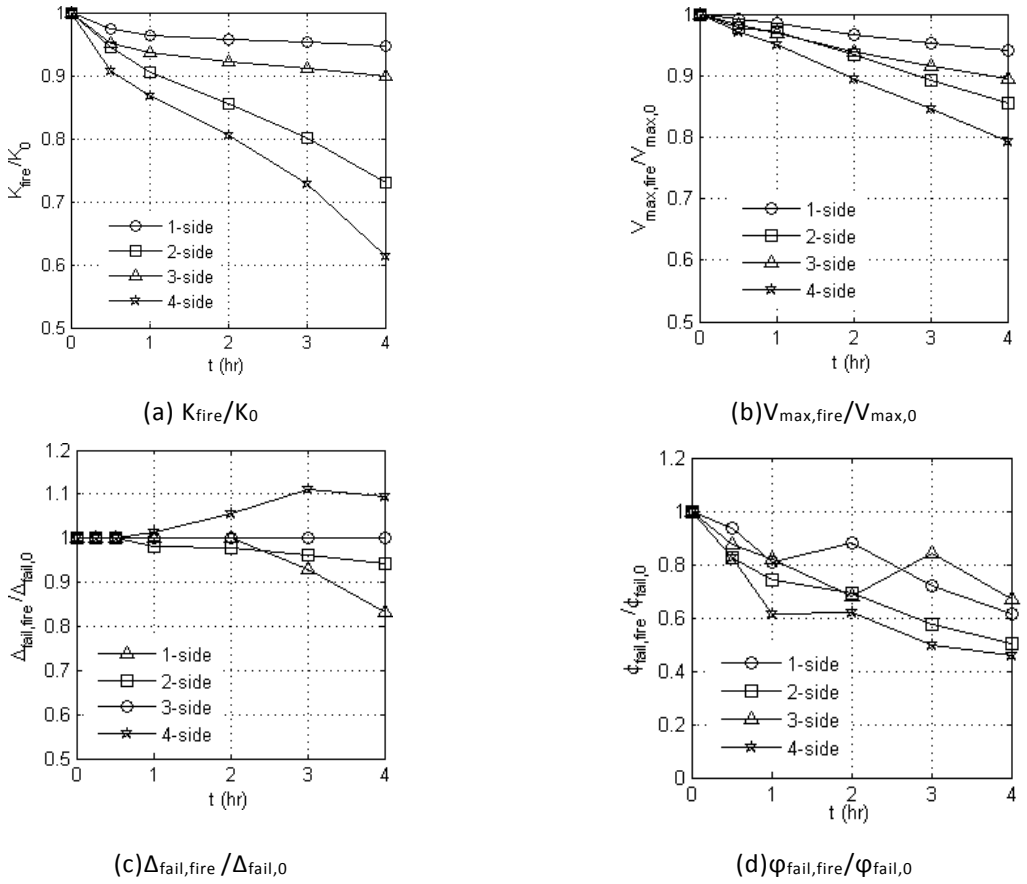

Figure 4-11 Variation of wall response ratios with fire durations.

4.3.4.1. Stiffness and Strength

Fire exposure decreases the lateral strength, V_{max}, of the wall regardless of thermal boundary conditions, with the magnitude of the decrease increasing with longer fire durations, shown in Figure 4-11 b. The rate of decrease is driven primarily by the sides exposed. For walls with one long side exposed (1- and 3-sided fire), the lateral strength decreases to no less than 90% of that of the reference wall. When both long sides of the wall are exposed (2- and 4-sided fire), the lateral strength decrease is more rapid, dropping as low as 80%. This is driven primarily by the increased temperature and therefore decreased material properties of a large region of the wall when both sides are exposed.

The effective stiffness of the walls is impacted with the same trends as that for the lateral strength, shown in Figure 4-11 a. After one long side is exposed (1- and 3-sided fire), the four-hour decrease is of the same magnitude as strength decrease, but the stiffness is affected more for shorter fires. For walls with both long sides exposed (2- and 4-sided fired), the magnitude of stiffness decrease is greater than the magnitude of the strength drop. The large stiffness decrease is driven by the magnitude of the decrease in the stiffness of the concrete, which drives the stiffness of the wall, while the strength of the steel, a major contributor to the strength, is not as large.

4.3.4.2. Shear and Axial Capacities

To ensure that the walls can be assumed to have a flexure-dominated response after the fire loading, the maximum strength (V_{max}) of the walls are compared to their nominal shear strength (V_n). The nominal shear strength is calculated by Equation 18.10.4.1 in ACI 318-14 (2014), with the average peak compressive strength of concrete and the average yield strength of horizontal rebar in a wall section used in place of $f_c^{'}$ and f_y to account for the fire damage. The average compressive strength was calculated as:

$$f'_{c,fire,avg} = \frac{\sum f'_{c,fire,i} A_i}{A_w - A_t} \quad \text{Eq. 4-2}$$

where A_i is the area of fiber i; $f^{'}_{c,fire,i}$ is the residual strength of concrete fiber I; A_w is the gross area of cross section; A_t is the total steel area.

The average horizontal reinforcement yield strength was calculated as:

$$f_{y,fire,avg} = \frac{\sum f_{y,fire,i} A_i}{A_t} \quad \text{Eq. 4-3}$$

where A_i is the area of the longitudinal reinforcing bar i; $f_{y,fire,i}$ is the residual strength of a longitudinal reinforcing bar i.

A ratio of V_{max}/V_n is shown in Figure 4-12. For all fire scenarios, the ratios are significantly less than 1, which is consistent with the assumption that walls investigated in this paper is controlled by flexural strength, rather than shear strength.

Walls with higher axial load ratio will have low capacities in energy dissipation and ductility. A potential influence on the response of the walls is the reduced material properties having the effect of the wall having a larger axial load ratio, referred to here as the effective axial load ratio. Here the effective axial load ratio is calculated using the applied axial load and the same average concrete compressive strength used for shear. This value is shown in Figure 4-13 for the reference wall. As a reference, an upper limit of 0.35 is shown, based on the ASCE/SEI 41-17 (2017) considers an axial load greater than 0.35 of the capacity be ineffective in resisting seismic forces.

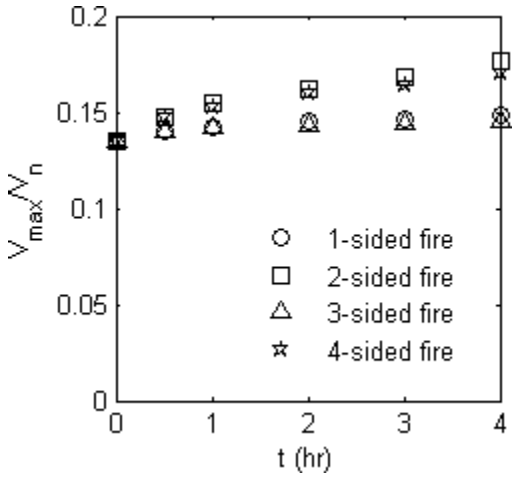

Figure 4-12 Ratios of max shear demand to nominal shear strength based on ACI 318-14 (Chapter 18).

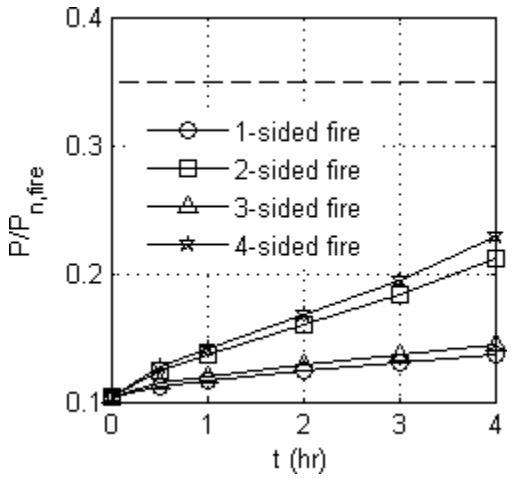

Figure 4-13 Variation of effective axial load ratio with fire duration.

4.3.4.3. Drift Capacity

The impact of fire on the strength and stiffness of the walls provides a clear trend that is easily related to the decreasing strength and stiffness of the material properties. The impact of fire on the drift capacity of the walls is more complex, as shown in Figure 4-11 c, with the drift capacity remaining unchanged for many walls and increasing for some. An examination of the hysteresis loops in Figure 4-4 offers insight.

The hysteresis for a 30 minute, one-side fire is shown in Figure 4-4b can be compared to the no-fire response in Figure 4-4a. While both walls reach a maximum drift of 3.0%, and fail at approximately 2.5% drift, the number of cycles sustained is different. The no-fire wall fails just prior to the third time to 3.0%, while the 30-minute fire wall fails during the second cycle to 3.0% and is foreshadowed by a significant decrease in strength and stiffness during that cycle. When there is more fire damage, as the 2-sided 3 hour fire in Figure 4-4c, a decrease in the drift capacity can be seen. When there is yet even more fire damage, it is possible to have an increase in the drift capacity of the wall, as shown in Figure 4-4d for a 4-sided 3 hour fire. This behavior has been

observed experimentally for reinforced concrete columns and walls (Xiao et al., 2004; Chen et al., 2009).

The question then arises of how many 3.0% drift cycles the wall in Figure 4d is be able to sustain. After 25 cycles to 3.0% drift, there is no failure of the wall. At each cycle, there is only minor degradation in the strength and stiffness of the wall. This is contrary to experimental observations and simulation results for walls with no fire, in which a more pronounced decrease in strength and stiffness is observed between the first and second cycles to the same drift. The lack of degradation in the global response is explained by the impact of the fire on the backbone curve of the concrete. The fire alters the stiffness of a sufficient number of fibers that many of them are still in the pre-peak stage at 3.0% drift and thus have essentially elastic behavior under unloading. It is not until drifts exceed 3.0% that there are a sufficient number of fibers with post-peak response that plastic strains impact the global response sufficiently to initiate a failure. It is reasonable to assume that the minor degradation in the material models used may not occur in a physical specimen, however, there is no available experimental results to provide clarity on this behavior. Thus, it is should be conservatively assumed that there is no change to the drift capacity at short fire durations and a decrease at durations exceeding an hour.

4.3.4.4. Failure Curvature

Deformation capacity of the walls can also be considered using curvature as a response quantity. The curvature at the lowest integration point curvature is directly reported by the OpenSees model. The impact of fire on the failure curvature, shown in Figure 4-11 d, has a more consistent trend than does the failure drift, although it is not as smooth as the trends for stiffness

and strength. The Curvature decreases more in 2- and 4-sided fires. In some cases less fire exposure results in a greater decrease in the curvature. This is a result of large increases in curvature right at failure and thus difficulty in defining the exact failure curvature; however, the trends observed are meaningful in assessing the general impact of fire on the failure curvature.

4.3.4.5. Damage at Failure

Cross-sections of the wall showing the damage ratio of each fiber were created for all walls, with the damage ratio defined using properties of the fire damaged concrete. In all fire scenarios, the wall failed by concrete crushing in the web or boundary elements, as the fire degrades the concrete more significantly than the steel. For example, after a 2-hour 2-sided fire exposure, average residual yield strength of steel bars at the boundary elements and web are 96% and 92% of the yield strength at room temperature, respectively. The average compressive strength of concrete at the boundary element and web is 63% and 59% of the compressive strength at room temperature. Moreover, research (Neves et al., 1996) has shown that the rupture strain of steel bars almost does not change after fire exposure, which decreases the possibilities of wall failure in tension. Therefore, it is reasonable to assume that if a wall fails in compression at the scenario without fire damage, the wall will fail in compression under the scenarios with fire damage. This assumption has been validated by the reference wall which fails in compression after all fire scenarios.

Examples of the damage prior to failure are shown in Figure 4-14 after 2-hour fires. At failure, many fibers crush and therefore it is difficult to identify the triggering mechanisms, thus, the figures shown are a few steps prior to failure and thus look less damaged than the wall with no

fire, shown in Figure 4-6. In all walls, the edge concrete has high damage ratios, indicating loss of cover concrete. A critical observation is regions in which there is a non-zero damage ratio (the concrete is in the post-peak range) and therefore potential failure location. For the no-fire wall, the region is limited to the boundary elements, consistent with response seen in experimental tests. With fire exposure, the web concrete adjacent to the boundary elements reach the post-peak range, indicating a potential shift in failure location from the web to the boundary element. The shift to the web is driven in part by the difference in confined (boundary element) and unconfined (web) post-peak response.

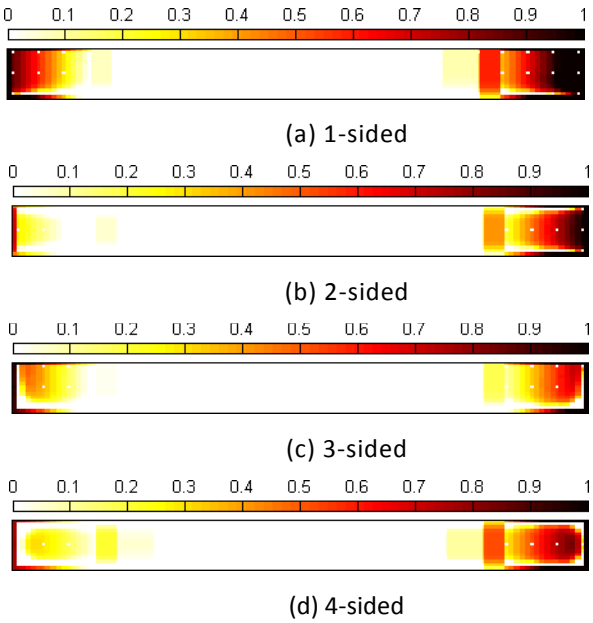

Figure 4-14 Damage of reference wall after 2 hour fires.

Within the boundary elements, the damage is greater in the unexposed region. This is explained by the Chang et al. (2006) model used to account for thermal damage to the concrete. Although fire exposure decreases the peak compressive strength and elastic modulus of concrete,

it increases the ductility of the material significantly. Figure 4-15 shows the concrete stress-strain curve for two fibers in the cross-section of Figure 4-14 d and the stress-strain curve at room temperature. The maximum temperature of the confined concrete at the corner of wall end is 694ºC while the maximum temperature of the confined concrete at the center of the boundary element is 224 ºC. The outside concrete is more ductile than that of the inside concrete. Compared to the residual properties of the inner concrete, the crushing strain of the outer concrete increased by 362%, although the peak compressive strength of the outside concrete decreased by 67%. This leads to the island of high damage ratio in Figure 4-14 d (excluding the black damage at the edges indicating. Practically speaking, a wall is unlikely to fail on the interior of the boundary element but not the exterior. In a physical wall the full thickness of the wall is likely to crush following a rapid progression of crushing once failure of part of the section initiates.

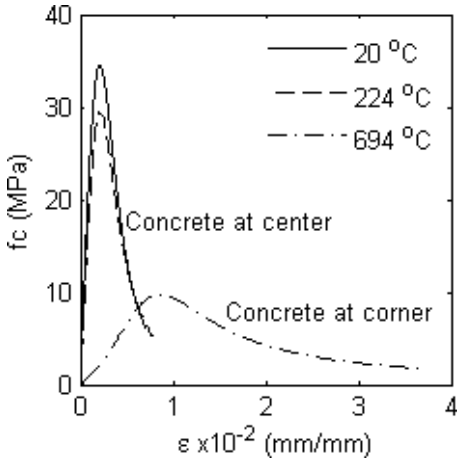

Figure 4-15 Stress-strain curves of fire-damaged concrete for reference wall with 4-hour 4-sided fire.

4.4. Influence of Wall Characteristics on Post-Fire Seismic Response

Having established the impact of fire on the response of a single wall design in the previous section, the impact of wall characteristics commonly considered to impact the seismic response of walls are considered under sequential fire-earthquake loading. All designs considered alter one characteristic of the reference wall to allow for a consistent baseline for discussions. Table 4-1 summarizes the wall designs considered. Highlighted cells indicate values different from the reference wall. For all walls, material properties are the same as the reference wall.

It is important to ensure walls do not fail in the fire resistance before the seismic analysis is conducted. Three criteria are used to define the fire resistance of a wall (EN 1991-1-2, 2002). Criterion R is satisfied where the load bearing function is maintained during the required time of fire exposure. Criterion I is satisfied if the average temperature rise over the whole non-exposed surface is limited to 140 K and the maximum temperature rise at any point of that surface does not exceed 180 K. Criterion E is satisfied if a separating element of building construction is able to prevent the passage through it of flames and hot gases and to prevent the occurrence of flames on the unexposed side. Here, Criterion I and Criterion R are considered. ACI 216.1-14 (2014) states, most of walls under fire are controlled by thermal insulation, instead of load-bearing capacity and walls with thickness greater than 8in. have a fire resistance larger than 4 hours. Therefore it is reasonable to assume that all walls considered here will not lose thermal-insulation capacity in the fire.

For simplicity, only 2-sided fires are considered in this section. The wall characteristics varied are grouped as wall geometry, reinforcement, or applied loads. The influence of wall characteristics is evaluated by comparing the variation of wall response ratios to those for the

reference wall (Figure 4-11). Solid markers are used to indicate walls with effective axial load ratios exceeding 0.35 and the reference wall is shown in black in all figures. In many cases, the general trends of changes to stiffness, strength, failure drift and failure curvature are the same as those for the reference walls, thus, discussion of wall characteristics are presented by discussing only changes in trends and the impact of wall characteristics on the magnitude of change of wall response quantities.

Table 4-1 Variation of wall characteristics.

Description	h_w	l_w	t_w	l_{be}/l_w	ρ_{be}	ρ_{web}	s	$P/A_w f'_{c,0}$
	(m)	(mm)	(mm)	(%)	(%)	(%)	(mm)	(%)
Reference wall	15.24	3048	304.8	15	2.44	0.44	102	0.1
t_w	15.24	3048	203.2	15	2.44	0.44	102	0.1
	15.24	3048	406.4	15	2.44	0.44	102	0.1
l_{be}/l_w	15.24	3048	304.8	10	2.44	0.44	102	0.1
	15.24	3048	304.8	20	2.44	0.44	102	0.1
CSAR	15.24	1524	304.8	15	2.44	0.44	102	0.1
	15.24	4572	304.8	15	2.44	0.44	102	0.1
ρ_{be}	15.24	3048	304.8	15	1.11	0.44	102	0.1
	15.24	3048	304.8	15	1.72	0.44	102	0.1
	15.24	3048	304.8	15	3.33	0.44	102	0.1
	15.24	3048	304.8	15	4.39	0.44	102	0.1
ρ_{web}	15.24	3048	304.8	15	2.44	0.24	102	0.1
	15.24	3048	304.8	15	2.44	0.68	102	0.1
	15.24	3048	304.8	15	2.44	0.97	102	0.1
s	15.24	3048	304.8	15	2.44	0.4	152	0.1
	15.24	3048	304.8	15	2.44	0.4	203	0.1
$P/A_w f'_{c,0}$	15.24	3048	304.8	15	2.44	0.4	102	0.02
	15.24	3048	304.8	15	2.44	0.4	102	0.05
	15.24	3048	304.8	15	2.44	0.4	102	0.15
	15.24	3048	304.8	15	2.44	0.4	102	0.2
	15.24	3048	304.8	15	2.44	0.4	102	0.25

4.4.1. Wall Geometry

Design parameters for wall size investigated in the parametric studies includes wall thickness (t_w), length of boundary element (l_{be}/l_w), and cross-section aspect ratio (CSAR). Figure 4-16 shows the results based on the thickness of the walls. Walls thinner and thicker than the reference wall were considered. The thinner the wall, the greater the decrease in response quantities. This is expected based on the increased transmission of the heat to the center of the wall thickness. For the thinnest wall (203 mm), there is increase in failure drift at fire durations 1-hour or longer, but a decrease in the failure curvature. After a four hour failure, the wall has an effective axial load exceeding 0.35 (shown as solid marker). An examination of the response indicates that these walls have response largely dominated by the steel; the hysteresis is shown in Figure 4-17 a. The thinnest walls also have a shift in the failure mode. Figure 4-17 b shows the damage after a three hour fire, in which more severe post-peak response occurs in the web than in the boundary element, similar to the reference wall after significant fire exposure in Figure 4-14 d. After a four-hour fire, the thin walls has post-peak response nearly exclusively in the web and only the cover of the boundary element. This shift of in location of post-peak behavior is an indication of a potential shift if failure mode from boundary element crushing to web crushing. Web crushing is commonly considered as behavior that occurs in shear dominated walls, but can be seen in walls with a uniform distribution of reinforcement (Lowes et al., 2012) and in flexure-controlled walls with barbell cross-sections.

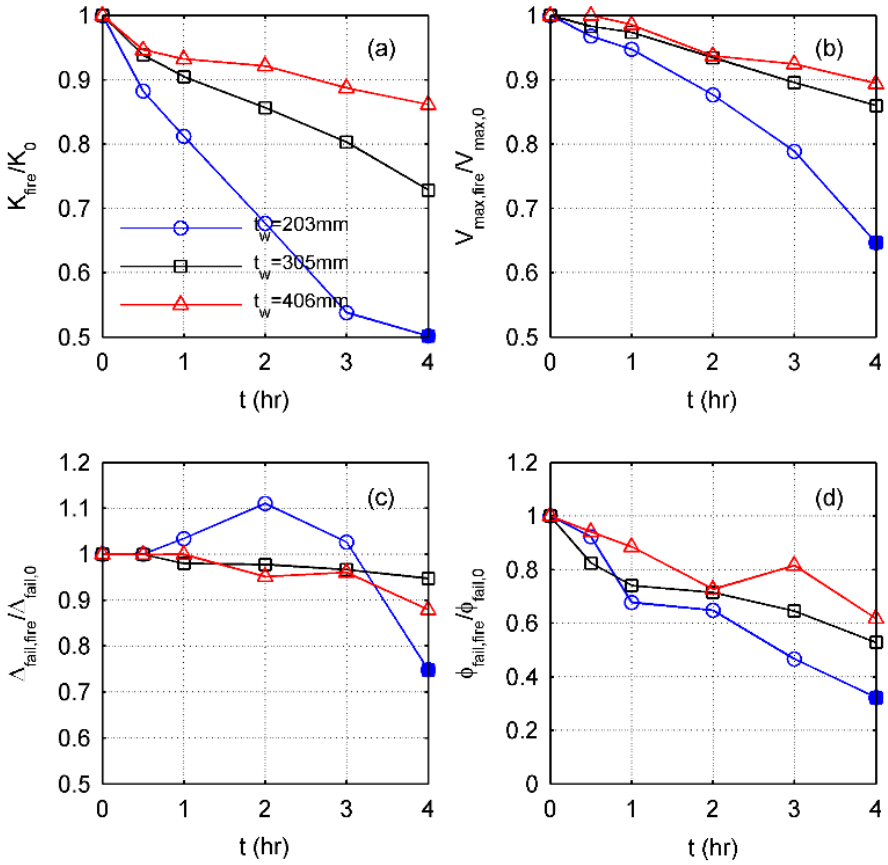

Figure 4-16 Impact of wall thickness (t_w) on post-fire seismic response.

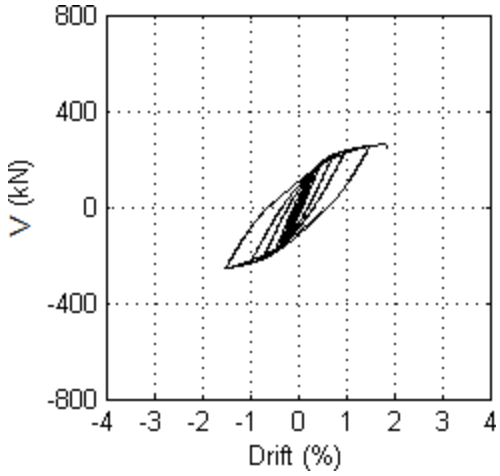

(a) 4-hour fire load-drift response

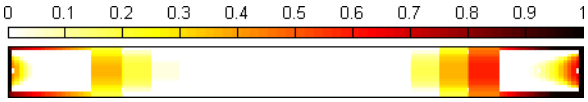

(b) 3-hour fire damage pattern

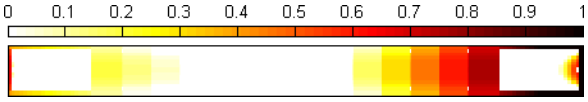

(c) 4-hour fire damage pattern

Figure 4-17 Response of thin wall (203 mm) to 2-sided fire.

Both longer and shorter boundary elements were considered in the parameter study, with results shown in Figure 4-18 . There is only a minor influence on the ratio of the stiffness and strength, but a clear impact on the failure drift and curvature. In the reference walls and the wall with a longer boundary element, the fire results in no more than a 5% reduction in failure drift, while the shorter boundary element has a significant decrease in the failure drift.

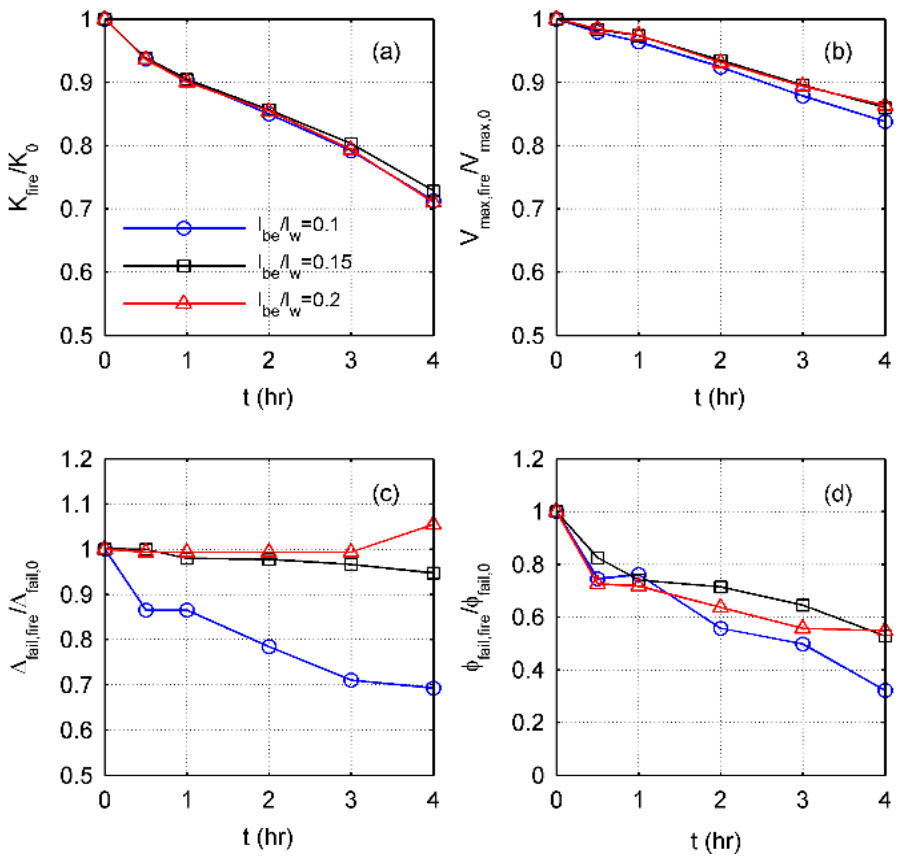

Figure 4-18 Impact of boundary element length ratio (l_{be}/l_w) on post-fire seismic response.

The cross-sectional aspect ratio (CSAR) is the ratio of the length to thickness and characterizes the cross-sectional slenderness. The smaller the CSAR, the more column-like the wall becomes, with values less than or equal to 4 generally considered to be rectangular columns. It has been shown that increasing CSAR may decrease the drift capacity of a wall (Birely, 2012). The results for the three CSAR considered are shown in Figure 4-19 . Larger CSAR values have a greater decrease in stiffness loss but no impact on the strength. Failure drift is affected for the smallest CSAR, but the failure curvature decreases with increasing fire duration for all walls. Damage patterns were the same for all CSAR, switching from crushing in the boundary element to crushing in the boundary element and web as the fire duration increased.

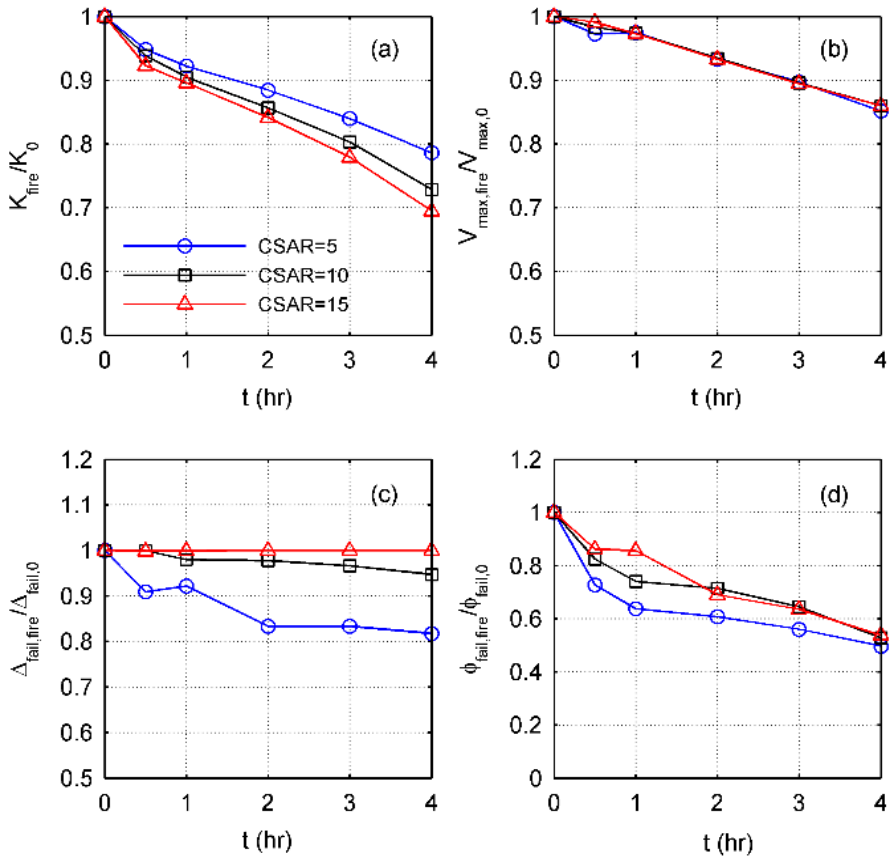

Figure 4-19 Impact of cross-sectional aspect ratio (CSAR) on post-fire seismic response.

4.4.2. Wall Reinforcement

Design parameters for reinforcement investigated in the parametric studies includes boundary longitudinal reinforcement ratio (ρ_{be}), web longitudinal reinforcement ratio (ρ_{web}) and spacing of the confining reinforcement (s).

Results for the boundary reinforcement ratio are shown in Figure 4-20 . The fire-induced decrease in stiffness is greater in walls with smaller reinforcement ratios, but the amount of strength loss is affected only by the lowest reinforcement ratio considered, and then even only a minor amount. The effect on failure drift is scattered, but there is generally a more rapid decrease in failure curvature loss due to fire for walls with larger boundary element reinforcement ratios.

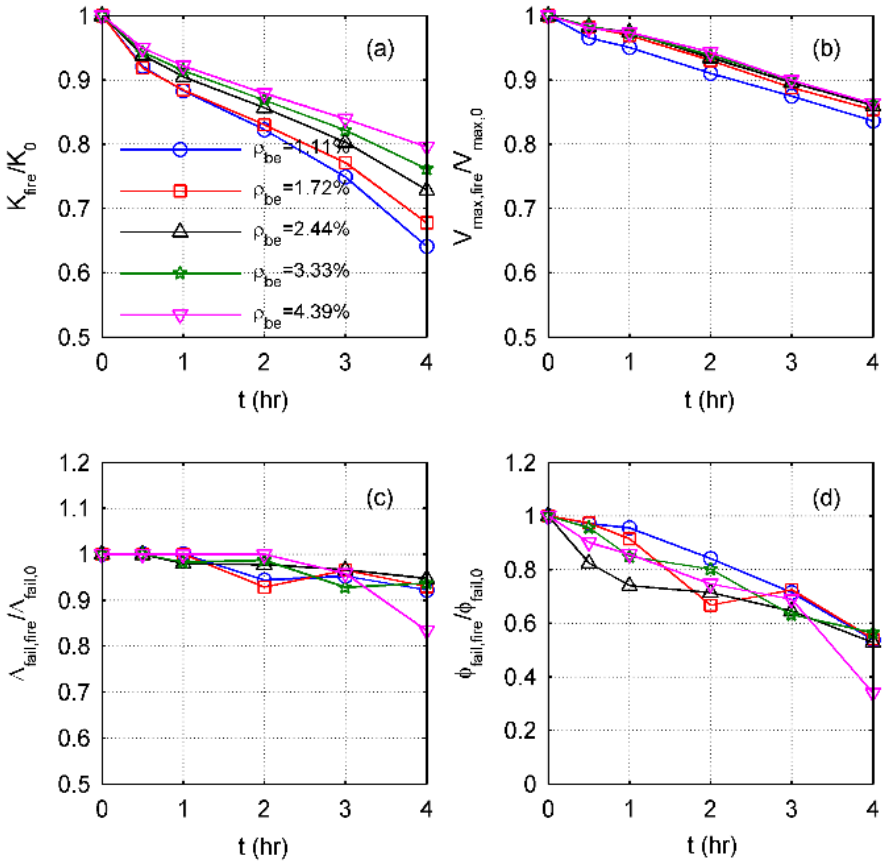

Figure 4-20 Impact of boundary element reinforcement ratio (ρ_{be}) on post-fire seismic response.

Figure 4-21 shows the results for walls with different web reinforcement ratios. The stiffness is unaffected and there is a minor effect of larger ratios decreasing the strength, failure drift, and failure curvature as the fire duration increase. Such a result may seem counter-intuitive, but in walls with more reinforcement, there is a greater contribution of the web steel to the strength with no fire and upon heating, this strength contribution decreases.

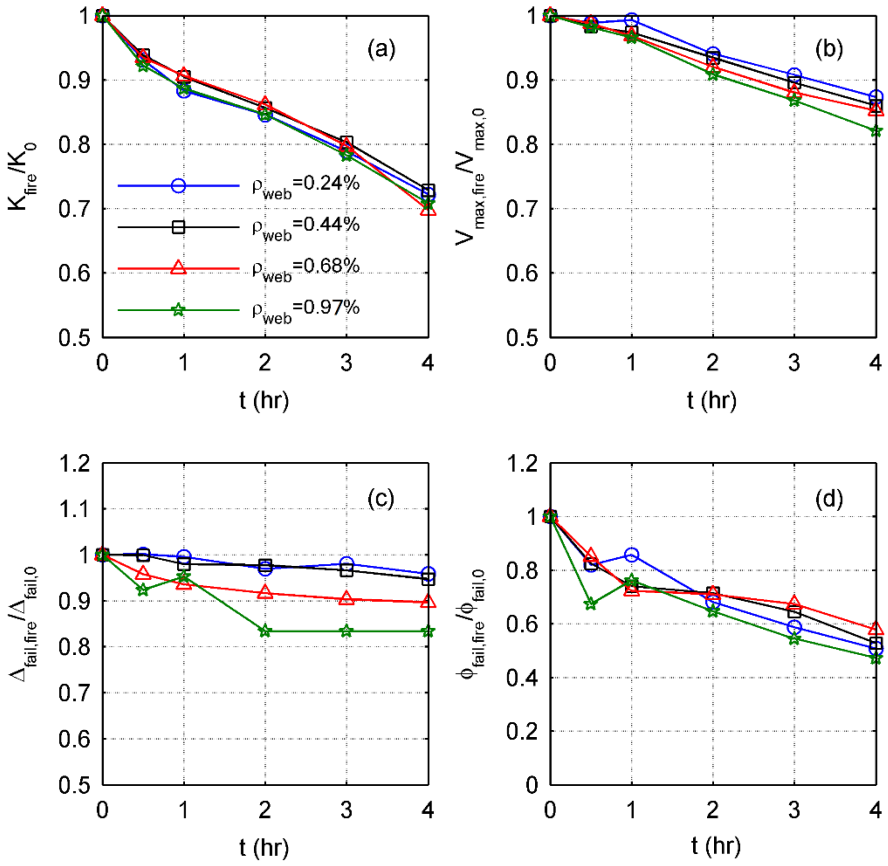

Figure 4-21 Impact **of web reinforcement ratio (ρ_{web}) on post-fire seismic response.**

The impact of confinement is considered by altering the spacing of the confining reinforcement in the boundary element. Results are presented in Figure 4-22 . The confinement does not significantly influence the loss of stiffness, strength, or failure drift, but more confinement negatively influences the failure curvature.

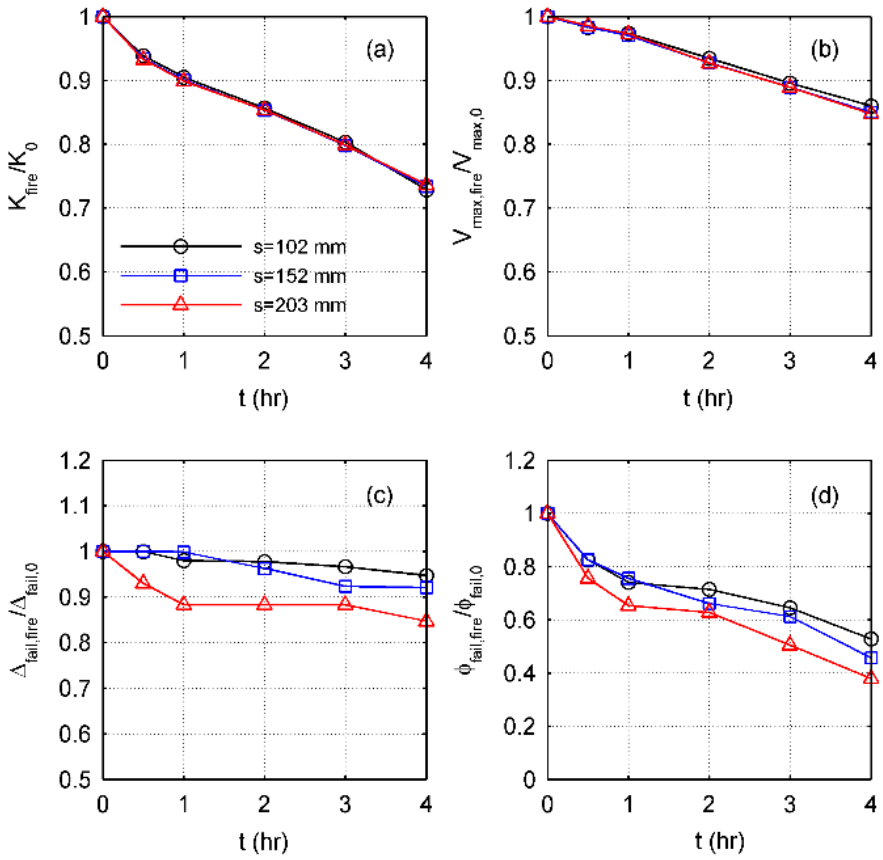

Figure 4-22 Impact of confining reinforcement spacing (s) on post-fire seismic response.

4.4.3. Axial Load Ratio

The impact of the axial load ratio is shown in Figure 4-23 . Higher axial loads result in a more rapid decrease in the stiffness and strength after a fire. At short fire durations, the failure drift decreases but the magnitude of the decrease levels off after about 1 hour. This is not seen for the failure curvature. For walls with low axial load ratios (2% and 5%), there is an increase in failure curvature. This is explained by the failure with and without fire damage fail due to fracture of the boundary element reinforcing bars in tension. In walls with axial load ratios greater than 15% at long fire durations, the effective axial load ratio exceeds 0.35 and thus the ability of the wall to resist lateral loads should be disregarded per ASCE 41.

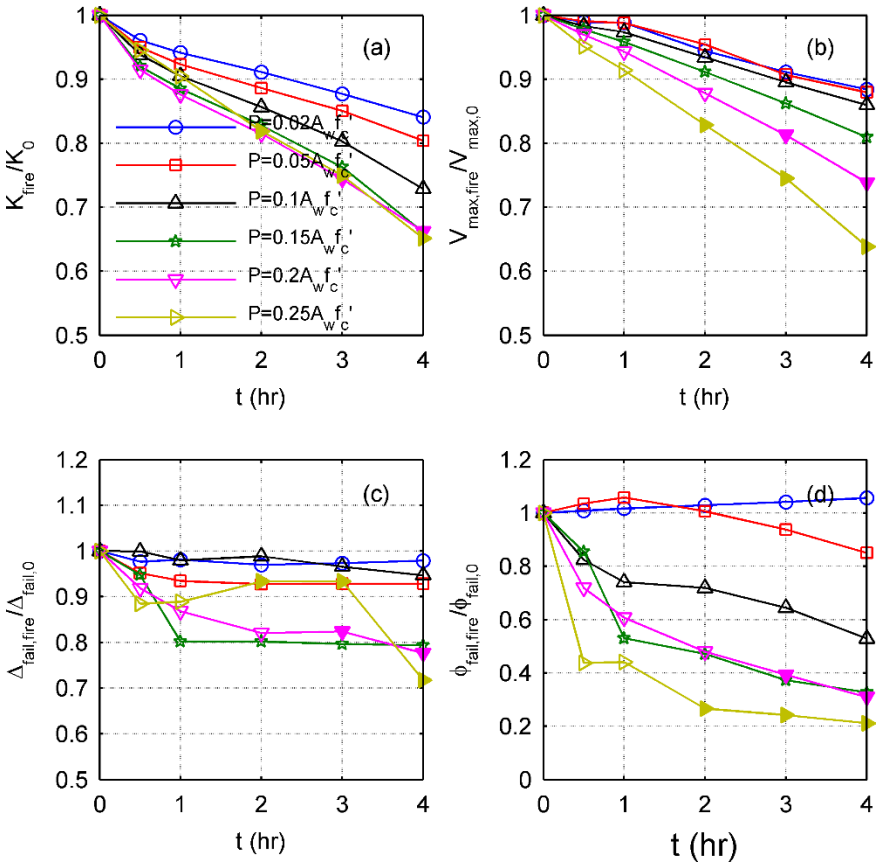

Figure 4-23 Impact of axial load ratio ($P/A_w f'_{c,0}$) on post-fire seismic response.

4.5. Summary and Conclusions

The post-fire earthquake (PEF) response of flexure-controlled reinforced concrete walls was studied using simulations that utilized the strengths of SAFIR for thermal analysis and OpenSees for mechanical analysis under reverse-cyclic demands. A planar wall representative of those commonly tested to understand seismic behavior was subjected four thermal boundary conditions and fire durations up to 4 hours. A parametric study was conducted to investigate the impact of key wall characteristics on the PFE response. The following observations were made:

1) The characteristic shape of the hysteretic load-drift response of the wall changes following severe fire loads in thin walls. In such walls or in walls with high applied axial loads, the

fire damage to the concrete is so large that the effective axial load ratio exceeds upper limits for consideration of walls to provide lateral load resistance. In analyzing structures for PFE responses, it is crucial to assess this effective axial load ratio.

2) Fire decreases both the strength and stiffness of a wall, with the magnitude of decrease in strength and stiffness are greatest in walls with both long sides exposed; when one long side is exposed, the decrease is substantially less and would be expected to have a minor impact on the response of a structure subjected to PFE. The magnitude of the decrease of the strength and stiffness is affected primarily by the wall thickness and axial load, with minor impact by confining reinforcement.
3) Short fires often had no effect on the failure drift or in some instances, increased it slightly. This is potentially a by-product of the simulation assumptions, and conservatively no increase in drift capacity should be assumed in analyzing the PFE response of a structure. For fires more severe in length and number of exposed sides, the failure drift decreased. Curvature at failure was shown to have a more consistent trend, with the curvature decreasing as the fire duration increased. All parameters considered had an impact of the amount of the reduction in the failure curvature, with the most noticeable effects due to axial load, wall thickness and boundary element length.
4) For walls with axial load ratio greater than 0.05, the walls have a flexure-compression failure, although the location and size of the damaged region was impacted by the fire characteristics. Fire damage can increase the post-peak damage in the wall webs, and in the case of long fires in thin walls, the failure may be exclusively due to web crushing. The failure modes were similar for most variations of the wall parameters, although the

boundary element length led to a shift in compressive damage from the boundary element to the web adjacent to the boundary element.

Some of these observed behaviors, particularly failure mode and drift capacity, are contrary to the expected results. The simulated behavior may be representative of what would occur in a fire-earthquake loading scenario or may be the results of assumptions made in establishing the material properties used. These assumptions include the impact of fire damage on the cyclic response of concrete and on the compressive fracture energy. Experimental testing of these material properties and of flexural controlled walls are needed to validate assumptions used and to support further development of the models to better assess post-fire seismic response of RC walls.

CHAPTER 5

A SIMPLIFIED MODEL FOR THE POST-FIRE EARTHQUAKE FLEXURAL RESPONSE OF REINFORCED CONCRETE WALLS WITH BOUNDARY ELEMENTS*

A potential multi-hazard scenario for buildings is the sequential occurrence of fire and earthquakes, with such a scenario possible if a fire is triggered by an initial seismic event and a subsequent aftershock occurs. With fire negatively influencing the stiffness, strength, and deformation capacity of structural components, the building may be at risk for local or global collapse. The key role of reinforced concrete (RC) walls as lateral load resisting components make them of particular importance in considering the post-fire earthquake performance of buildings. Since the risk of fire-earthquake hazards is low, simplified models are needed to efficiently evaluate building performance. In this paper, a framework for simplified nonlinear modeling of RC walls is presented. The models are defined by modification factors that account for the change in wall response relative to that of a wall without fire damage. Modification factors, established from the results of a parameter study of walls using a verified simulation method, are a function of fire damage indices that account for the effect of fire on the material properties of steel and concrete. The dependence of wall response on most wall characteristics is eliminated by use of the damage indices, with the recommended modification factors dependent on the fire damage index and axial load alone.

---

*Ni, S. and Birely, A.C., A Simplified Model for the Post-Fire Earthquake Flexural Response of Reinforced Concrete Walls with Boundary Elements, submitted to Journal of Engineering Structures in May 2018.

5.1. Introduction

The evaluation and design of structures subjected to multi-hazards has been a topic of increased study in recent years (Bruneau et al., 2017). Multi-hazard consideration for fire and earthquake is generally considered to be a sequential hazard, with an earthquake creating an increased likelihood of fire ignition (Sekizawa et al., 2003). At the same time, fire duration and severity are expected to increase due to damage to fire protection systems and to firefighter access restricted by damaged/blocked roads and bridges, as well as firefighter priorities shifting to other emergency response operations (Mousavi et al., 2008). In such events, seismic damage may significantly impact the load-bearing fire resistance of structural components (Wen et al., 2016; Shah et al., 2017; Behnam et al., 2013). For structural components with no or minimal seismic damage, post-earthquake fire may significantly compromise the structural integrity and therefore have a significant impact on the performance in subsequent aftershocks (Lie and Woollerton, 1988; Chen et al., 2009; EI-Hawary et al., 1996 & 1997; Xiao and Meng, 2005; Xiao et al., 2004; Liu, 2010; Xie et al., 2018). Reinforced concrete (RC) structural walls are particularly important in the context of post-fire earthquake (PFE) events as they serve key functions for the resistance of both hazards (lateral load resistance for earthquake; physical barriers and load-bearing capacity for fire).

Frameworks for assessment and design of buildings have been developed for multihazards in general (Bruneau et al., 2017; Zaghi et al., 2016) and more specifically for post-earthquake fire (Meacham, 2016) and mainshock-aftershock earthquake sequences, generally with a focus on how to account for probability of occurrence and how to link to building and/or structural component performance. However, utilization of such frameworks requires the ability to accurately account for the structural response of building components. With large numbers of potential combinations

of fire and seismic hazards, the ability to assess them via detailed analysis becomes challenging. Simplified analysis methods are needed that fit within the framework of how buildings are modeled for seismic hazards, are able to capture the effects of fire on the mechanical resistance to loads, and are able to simulate the seismic behavior accurately. Simplified modeling methods exist for both fire and earthquake loading and should be utilized in assessing post-fire seismic performance.

Simplified methods of accounting for fire effects on RC structural members can be achieved through methods and design aids provided by design codes and guidelines (e.g. EN 1992-1-2 (2004) or ACI 216.1-14 (2014)). These simplified methods allow users to identify the temperature at a particular distance from a heated surface via a suite of temperature vs fire duration curves. This in turn is used to identify modified material strengths used to calculate revised strengths. Further modifications from current fire analysis methods needed for post-fire earthquake are the changes to stiffness and deformation capacity.

A number of simplified methods are available for seismic analysis of walls. Linear elastic models utilize stiffness modifiers to account for the flexibility of the structure and may be used to assess deformation capacity following the requirements of ASCE 7 (2016) or to conduct preliminary assessment of existing buildings following the guidelines of ASCE 41 (2017). Backbone curves are provided by ASCE 41 to define the nonlinear response, including deformation capacity, to allow engineers to quickly define response characteristics for use in nonlinear models; backbone curves are provided for both shear- and flexure-controlled walls, with flexure-controlled walls having aspect ratios (height over length) greater than or equal to 2.0.

This paper presents recommendations for modifying backbone curves for flexure-controlled RC walls to account for the effects of fire damage. The simplified models are recommended as an alternative option to calculate the stiffness, strength, and deformation capacity directly. Recommendations are developed using the results of detailed simulation for both the thermal and mechanical loading on the walls. The recommended simplified analysis method utilizes modification factors to account for the reduction in stiffness, strength, and drift capacity. Modification factors are defined based on fire-damage indices that account for the effect of fire on the mechanical response at the material level.

5.2. Fire Impact on Seismic Resistance of RC Walls

The simplified modeling approach for the post-fire seismic performance of flexure-controlled RC walls presented in this paper is based on findings of a parameter study of planar walls with confined boundary elements (Ni and Birely, 2018b). Details of the simulation procedure and in-depth analysis of the impact of fire damage on the stiffness, strength, and failure are documented by Ni and Birely (2018a and 2018b). Here, a brief overview of the models and findings are presented to support the development of the simplified modeling approach.

A wall representative of planar wall characteristics in mid-rise buildings on the West Coast of the United States was used as the reference wall. Twenty additional walls investigated the impact of parameters that have the potential to affect the seismic performance of walls. Parameters included the axial load ratio ($p = P/A_w f'_{c,0}$), thickness (t_w), cross-section aspect ratio (CSAR = l_w/t_w), boundary element length (l_{be}), boundary element reinforcement ratio (ρ_{be}), web reinforcement ratio (ρ_{web}), and spacing of boundary element confining reinforcement (s).

Figure 5-1 shows the generalized cross-section of the wall and Table 5-1 provides the range of values for each wall characteristic considered; full details of the wall cross-sections are provided by Appendix B.

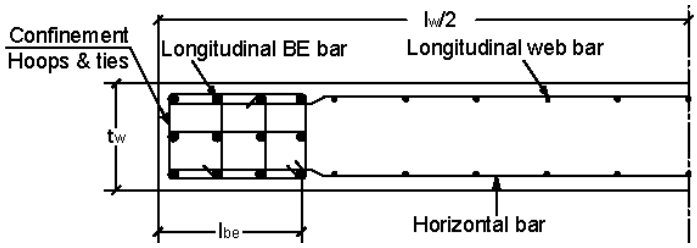

Figure 5-1 Generalized planar wall characteristics.

Table 5-1 Summary of wall characteristics considered in model development.

Parameter	#	Min.	Max.
$p = P/A_w f'_{c,0}$	9	0.02	0.25
t_w (mm)	3	203	406
l_{be}/l_w	3	10	20
CSAR = l_w/t_w	3	5	15
ρ_{be} (%)	5	1.11	4.39
ρ_{web} (%)	4	0.24	0.97
s (mm)	3	102	203

Walls were subjected to five thermal boundary conditions: no fire, 1-side fire (long side exposed), 2-sided (both long sides exposed), 3-sided (one long side and both end exposed), and 4-sided. Fire-exposed sides were subject to radiation (emissivity coefficient 0.7) and convection (film coefficient 25W/m^{2o}C). Unexposed side thermal boundary conditions were room temperature with film coefficient 9W/m^{2o}C. The ASTM E119 fire curve (ASTM E119-18, 2018) with durations of 0.25, 0.5, 1, 2, 3, and 4 hours, followed by cooling at a rate of 5°C/min, was applied to the first floor only. Heat transfer analysis was conducted using SAFIR (Franssen, 2011) with thermal properties defined based on EN1992-1-2 (2004). The lower limit of thermal

conductivity for concrete is used. Post-processing used custom scripts to determine the maximum historic temperature (taken from the full heating-cooling cycle) in each steel and concrete fiber to define the post-fire residual material properties, which considers the effect of cooling phase. These properties were used to define cross-sections of force-based beam column elements with five integration points in OpenSees (Mazzoni et al., 2006). The post-fire residual concrete properties are based on the recommendation by Chang et al., (2008). The post-fire residual concrete model is defined as functions of the maximum historic temperature concrete has experienced, including accounting for the cooling phase. The post-fire residual steel properties are based on the recommendation by Tao et al. (20013). Reinforcing steel which has exposed to temperature higher than 500^{o}C will not fully recover ambient strength after cooling to room temperature (Tao et al., 2013).

Seismic loads were applied with a reversed cyclic displacement history, consisting of two cycles to drifts of increasing magnitude. Lateral load is applied as a single force at the top of the wall. Parameter study results (Ni and Birely, 2018b) were reported as base shear forces; here base moment, equal to the base shear times the wall height, is used. Residual strains and stresses were not considered, but the impact on response has been shown to have minor impact, primarily on the wall stiffness (Ni and Birely, 2018a). Out-of-plane deformation has been shown to recover following fire (Liu, 2010), although may contribute to a premature out-of-plane local buckling failure of the wall. Axial loads were defined as a percentage of $A_w f_{c,0}^{'}$, where A_w is the area of the wall cross-section, and $f'_{c,0}$ is the peak compressive strength of the concrete at room temperature. In order to ensure that the walls can be assumed to have a flexure-dominated response after the fire loading, the maximum shear (V_{max}) of the walls are compared to their nominal shear strength

(V_n) (Equation 18.10.4.1 in ACI 318-14). The ratios of V_{max} to V_n are significantly less than 1, which is consistent with the assumption that all the analyzed walls are flexure-controlled (Ni and Birely, 2018b).

Figure 5-2a shows the load-drift envelopes for a wall with no fire, 0.5 hr 4-sided fire, and 2 hr 4-sided fire, illustrating the effect the fire has on the stiffness, strength, and drift capacity of the wall, where drift (Δ) is defined as the displacement at the top of the wall divided by the wall height. To quantify the response for a wider range of fire and wall characteristics, key response characteristics are extracted from the load-drift envelopes (Figure 5-2b) and the load-curvature envelopes (Figure 5-2c), where curvature is recorded at the lowest integration point. The stiffness (K) is defined as the secant stiffness at 75% of the maximum capacity (M_{max}). The drift capacity (Δ) and curvature capacity (ϕ) is defined as the point when the load decreases to 80% of the maximum capacity, or if not reached, the point immediately prior to a sudden decrease in the lateral load carrying capacity.

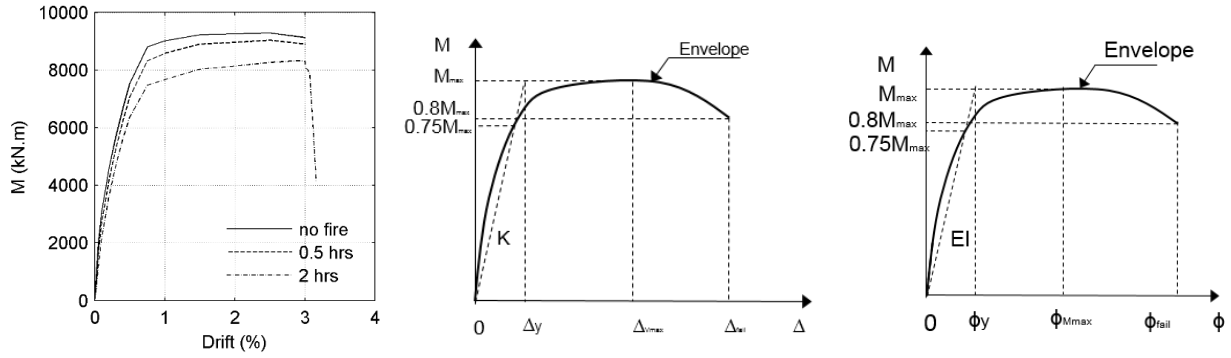

(a) (b) (c)

Figure 5-2 Summary of characterization of impact of fire on wall response, (a) moment-drift envelope for wall with no fire and 4-sided fires of durations of 0.5 and 2 hr, (b) definition of response quantities based on moment-drift backbone curve, and c) definition of response quantities based on moment-curvature backbone curve.

To characterize the effect of fire on the wall response, the stiffness, strength, and deformation quantities for fire damage, denoted by the subscript $_f$, are normalized by the same quantity for the wall without fire damage, denoted by a subscript $_0$. Figure 5-3 shows a sample of the response of walls with different thickness subjected to four-sided fire of increasing durations. For all walls, the stiffness, strength, and curvature capacity decrease with increasing fire duration, however, the rate of decrease is greater in thinner walls. Figure 5-4 shows the same information for walls with varied cross-section aspect ratio, indicating that the impact of fire is largely unaffected by this particular wall characteristic. Evaluation of similar graphs for all wall characteristics and thermal boundary conditions considered indicates that 1) the degree of fire damage on stiffness and strength is primarily affected by the wall thickness and axial load, with minor influence of cross-section aspect ratio and confining reinforcement, and 2) the deformation capacity is primarily affected by the axial load, wall thickness, and boundary element length.

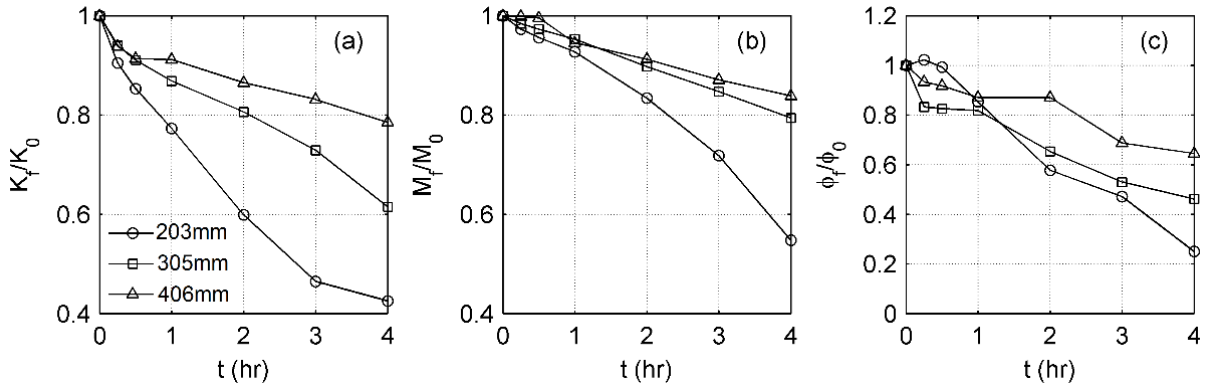

Figure 5-3 Ratio of fire-damaged response to no fire response ((a) stiffness, (b) strength, and (c) curvature) as a function of time for walls with different thicknesses (t_w) subjected to four side fires of increasing duration.

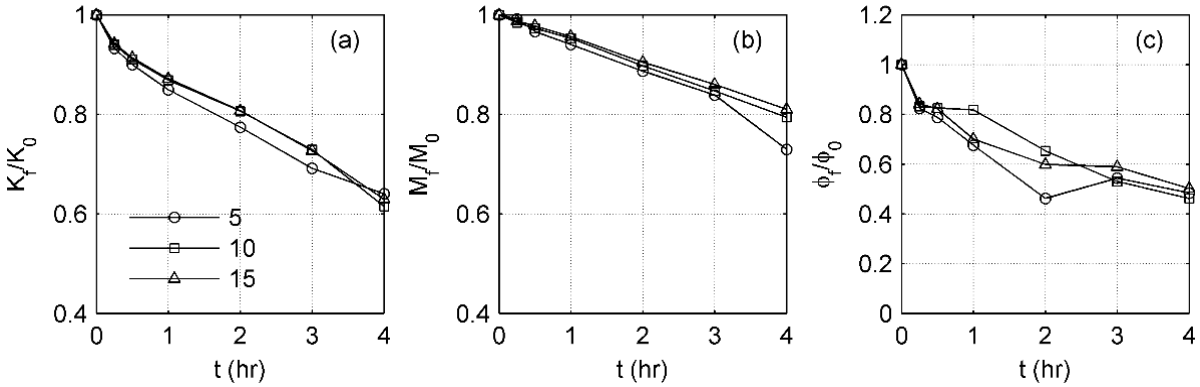

Figure 5-4 Ratio of fire-damaged response to no fire response ((a) stiffness, (b) strength, and (c) curvature) as a function of time for walls with different cross-section aspect ratios (CSAR = l_w/t_w) subjected to four side fires of increasing duration.

5.3. Framework for Simplified Analysis

While the SAFIR-OpenSees simulations used to assess the impact of PFE are able to capture the impact of fire damage and replicate the seismic response, implementation for assessment of new or existing buildings is not practical on a large-scale or for engineers assessing impact of fire on a limited basis. Thus, it is necessary to develop modeling tools that can assist engineers in capturing the effects of fire within the context of models and software commonly used for seismic analysis. Herein, the use of a backbone curve, such as that defined by ASCE 41 (2017), is considered.

As shown in the previous section, the effects of fire damage can be quantified as a ratio of the fire-damaged to non-fire damaged response of the wall. It follows that the wall stiffness can be modified to account for fire damage through introduction of a modification factor:

$$EI_f = \alpha_K EI_0 \qquad \text{Eq.5-1}$$

where EI_0 is the flexural stiffness used for analysis for seismic demands, EI_f is the flexural stiffness used for analysis of seismic demands following a fire, and α_K is a unitless modification factor to account for the reduced stiffness.

Similarly, the reduction in strength can be defined by:

$$M_f = \alpha_S M_0 \qquad \text{Eq.5-2}$$

where M_0 is the flexural strength of the wall, M_f is the fire damaged flexural strength, and α_S is a unitless modification factor to account for the reduced strength.

The impact of fire on the drift at failure may be evaluated on the basis of drift capacity or curvature capacity. Here, the curvature capacity is considered as it provides the clearest relationship between fire exposure and deformation capacity (Ni and Birely, 2018b). The fire damaged curvature capacity is defined as

$$\phi_f = \alpha_\phi \phi_0 \qquad \text{Eq.5-3}$$

where φ_0 is the curvature capacity at room temperature, φ_f is the fire damaged curvature capacity, and α_φ is a unitless modification factor to account for the reduced capacity.

Figure 5-5a shows a modified backbone curve for a flexure-controlled wall that accounts for the fire damage effect on strength, stiffness, and curvature capacity. Definition of the α factors could be established for the relationships in graphs such as those in Figure 5-4, however, the development of equations or design aids to account for the many possible combinations of thermal boundary conditions, fire durations, and wall characteristics would lead to a complex set of equations. To streamline the definition of α values, an alternative definition is needed to account for the impact of the fire damage independent of the thermal boundary conditions and fire duration, and ideally, independent of wall characteristics. Ni and Birely (2017) demonstrated through

preliminary analysis that it is practical to define the α factors for stiffness and strength as a function of the fire-reduced material properties of the steel and concrete.

The proposed framework for simplified analysis defines α as

$$\alpha = f(FDI) \qquad \text{Eq.5-4}$$

where FDI is the fire-damage index that quantifies the effect of the fire on the mechanical properties of the steel and concrete.

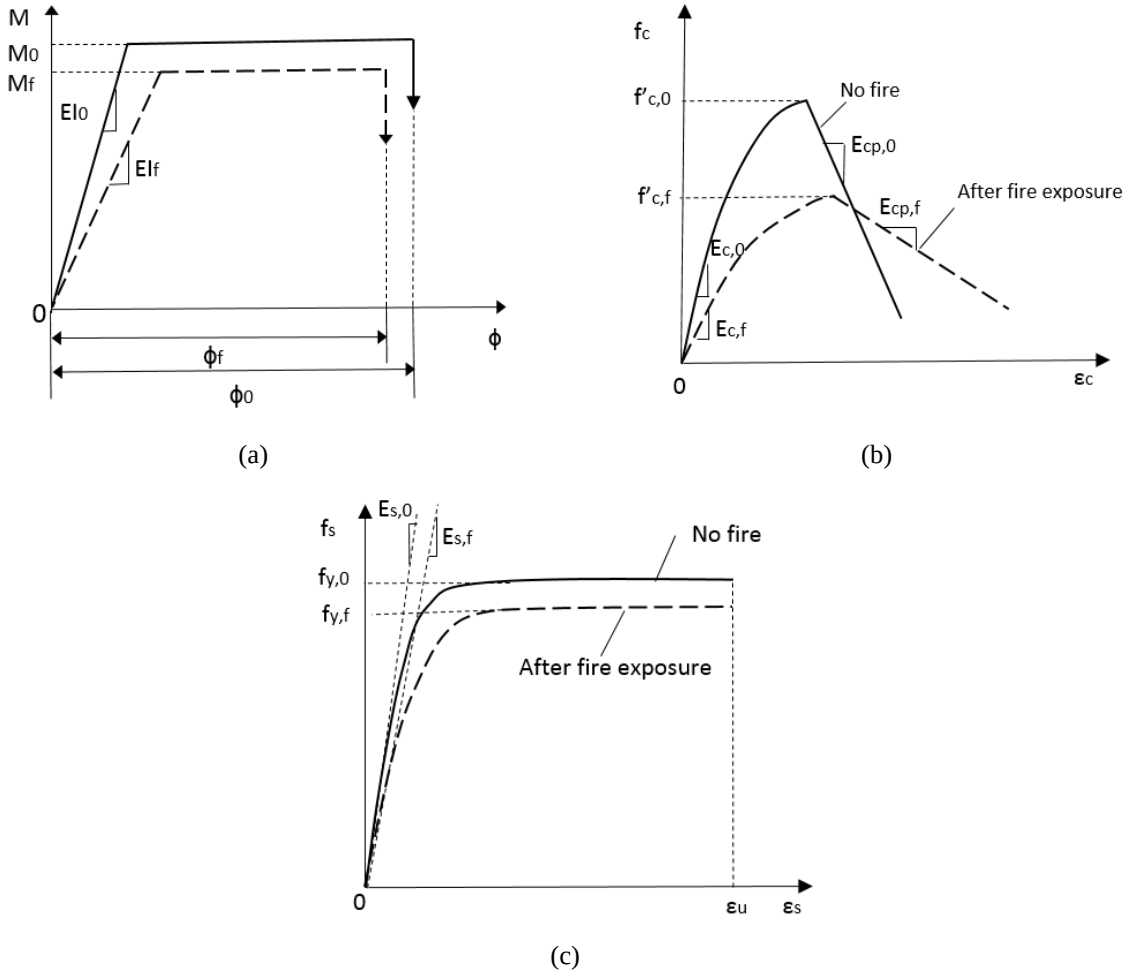

Figure 5-5 Overview of wall cross-section and material response at room temperature and with heat damage, (a) M-ϕ backbone curve, (b) concrete stress-strain and (c) steel stress-strain.

5.4. Fire-Damage Index Definitions

In defining a fire-damage index (FDI) for walls, the objectives are to 1) minimize the effort needed to calculate the FDI, 2) permit simple equations for α that are a function of few, if any, wall characteristics, and 3) are effective in characterizing the effects of fire on the wall response.

FDI is defined as one minus the ratio of the fire-damaged properties of the wall to the room temperature properties of the wall, while accounting for the relative area of each material. From this, a FDI will be equal to zero if no fire damage is present, with increasing values indicating more severe fire damage. Figure 5-5b and Figure 5-5c show the concrete and steel stress-strain curves for no fire and fire-damaged materials, along with notation used to indicate stiffness and strength values. The variation of the residual material properties with maximum historic temperature is based on the recommendations by Chang et al. (2006) and Tao et al. (2013). Any other similar residual material models can be used in the calculation of the fire damage indices.

Since the boundary elements have the largest influence on the wall response, only the boundary elements are considered. Preliminary exploration of damage indices (Ni and Birely, 2017) demonstrated that the use of confined properties had a negligible impact on the accuracy of the FDI in predicting response, thus, only unconfined properties are considered here.

Two sets of definitions, indicated by the superscript *j* and summarized in Figure 5-6, were considered, with each definition utilizing a different portion of the cross-section. The first set (j = 1), uses the temperature at a single steel/concrete point in the center of the boundary element and the full area of the steel/concrete in the boundary element. This definition is ideal as it minimizes the need for wall temperature but can actively capture the relative area of steel and concrete. Recognizing that it may be more appropriate to account for changes in residual material properties

throughout the boundary element, a second definition (j = 2) is defined, in which each fiber in the boundary element was considered.

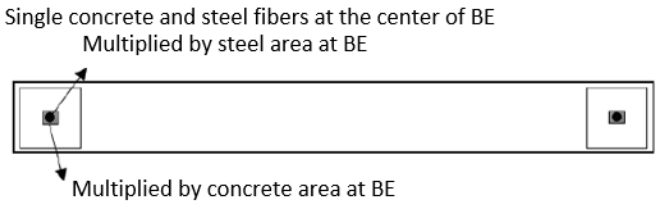

(a) FDI_1

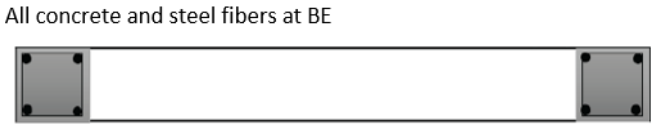

(b) FDI_2

Figure 5-6 Definition of fire damage index (FDI) considered.

FDI based on material stiffness are defined as:

$$FDI_K^j = 1 - \frac{\Sigma_{i=1}^{n_{c,j}} E_{c,f} A_c + \Sigma_{i=1}^{n_{s,j}} E_{s,f} A_s}{\Sigma_{i=1}^{n_{c,j}} E_{c,0} A_c + \Sigma_{i=1}^{n_{s,j}} E_{s,0} A_s} \quad \text{Eq.5-5}$$

where j is the definition number; $n_{c,j}$ and $n_{s,j}$ are the number of concrete and steel fibers for definition j; A_c and A_s are the concrete and steel areas; $E_{c,0}$ and $E_{c,f}$ are concrete elastic modulus at room temperature and after fire exposure, respectively; $E_{s,0}$ and $E_{s,f}$ are steel elastic modulus at room temperature and after fire exposure, respectively.

FDI based on material strength are defined as:

$$FDI_S^j = 1 - \frac{\Sigma_{i=1}^{n_{c,j}} f_{c,f}^{'} A_c + \Sigma_{i=1}^{n_{s,j}} f_{y,f} A_s}{\Sigma_{i=1}^{n_{c,j}} f_{c,0}^{'} A_c + \Sigma_{i=1}^{n_{s,j}} f_{y,0} A_s} \quad \text{Eq.5-6}$$

where $f'_{c,0}$ and $f'_{c,f}$ are the peak concrete compressive strength at room temperature and after fire exposure, respectively; $f_{y,0}$ and $f_{y,f}$ are the steel yield strength at room temperature and after fire exposure, respectively.

While damage to wall stiffness and strength can be easily related to the damage to the material stiffness and strength, accounting for effects on the deformation capacity cannot be accomplished as directly. Deformation capacity is affected in part by the post-peak response of the concrete, including the slope and the strain capacity. Fire damage affects the stress and strain values at both the peak strength and point of crushing, thus, a deformation FDI is defined based on the post-peak stiffness of the original and fire damaged material properties:

$$FDI_{\phi}^{j} = 1 - \frac{\sum_{i=1}^{n_{c,j}} E_{cp,f} A_c}{\sum_{i=1}^{n_{c,j}} E_{cp,0} A_c} \quad \text{Eq.5-7}$$

where $E_{cp,0}$ and $E_{cp,f}$ are the post-peak concrete stiffness at room temperature and after fire exposure, respectively.

5.5. Evaluation of FDI

Fire damage index values were calculated for all walls in the parameter study by Ni and Birely (2018b). Figure 5-7 summarizes the results for axial load ratio, wall thickness, and cross-section aspect ratio, based on FDI^1. The range of fire-damage index values was 0-0.9 for stiffness (FDI_K), 0-0.6 for strength (FDI_S), and 0-0.95 for deformation capacity (FDI_φ). FDI is larger in walls that are thinner or shorter; FDI is larger in walls with more sides heated and longer fires. FDI is unaffected by axial load.

In the following sections, the FDI data is evaluated to assess the effectiveness in predicting the response of the walls, with the objective of identifying the appropriate FDI to use and the wall characteristics on which α should depend.

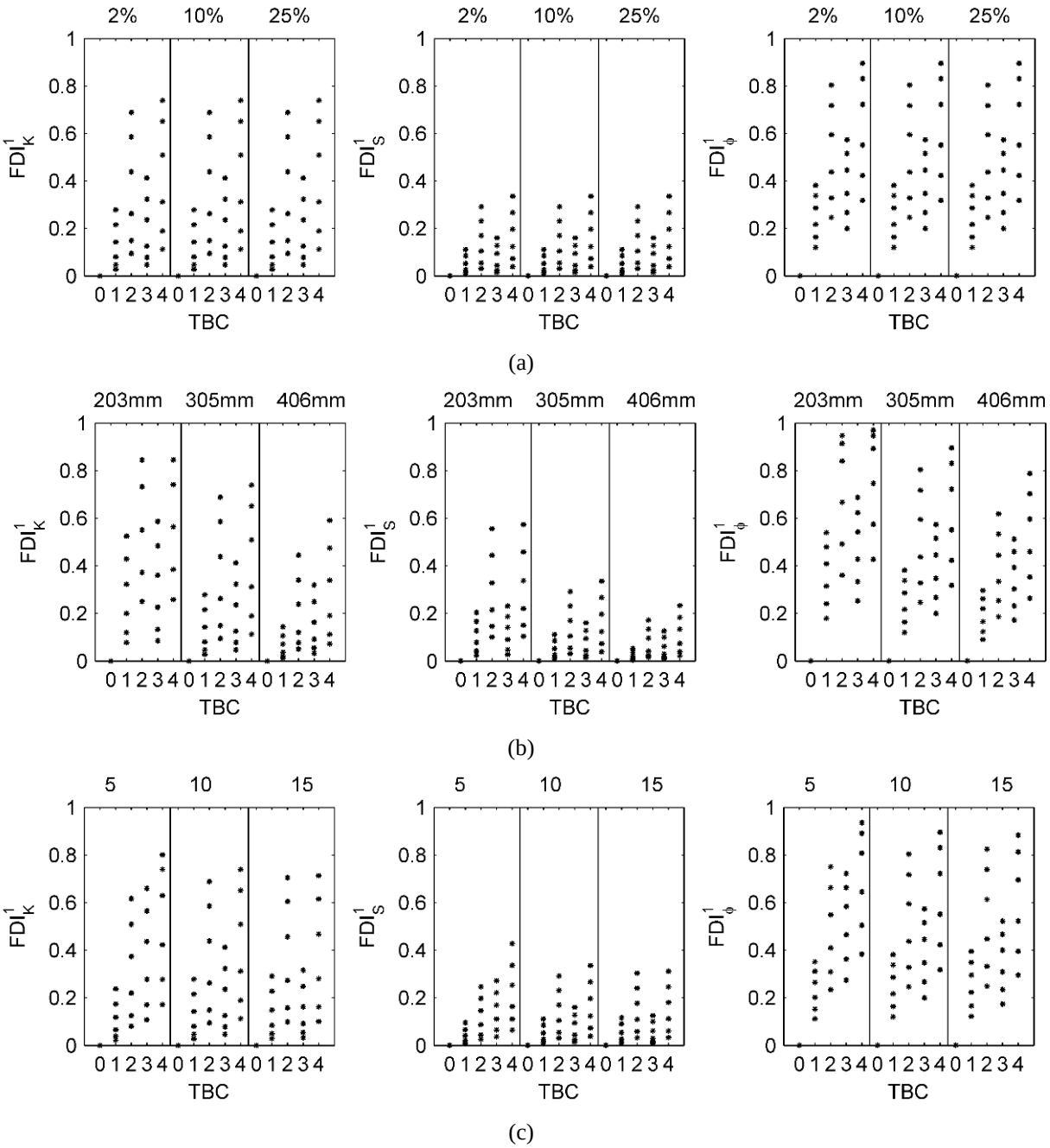

Figure 5-7 Range of simulated fire-damaged index for each thermal boundary condition (TBC: 0, no fire; 1, 1-sided fire; 2, 2-sided fire; 3, 3-sided fire; 4, 4-sided fire) for (a) axial load ratio, (b) wall thickness, and (c) cross-section aspect ratio.

5.5.1. Stiffness and Strength

Figure 5-8 shows the relationship between FDI^1 and the α values for stiffness (α_K) and strength (α_S) for walls with varied thickness (left column) and axial load ratio (right column); FDI_K^1 is used for stiffness and FDI_S^1 for strength. For wall thickness, there is a distinct relationship between α and FDI, with limited scatter of the data. For axial load ratio, a clear trend is observed for α and FDI, but there is significantly more scatter than for wall thickness. These observations are quantified in Table 5-2 by Spearman's rank correlation coefficient (Spearman, 1904), in which the magnitude of the coefficient is smaller for axial load than for thickness (-0.90 vs -0.93 for stiffness, based on FDI_K^1; -0.91 vs -0.93 for strength, based on FDI_S^1). Evaluating the correlation coefficient for other variables indicates that their influence on α is similar to that of wall thickness. A key observation from this is that the FDI is effective in accounting for the influence of thickness and boundary element reinforcement that was noted by Ni and Birely (2018b), but is unable to capture the influence of axial load. To further assess the dependence of α on the axial load, Table 3 provides correlation coefficients for each axial load evaluated, with larger correlation than when all axial loads are grouped. Figure 5-9 shows data for four of these axial load ratios. It is concluded that expressions for prediction of α should be dependent on the FDI and the axial load ratio.

The above discussion provides an evaluation of the first FDI definition, in which material properties are determined for a single point and assumed constant throughout the boundary element. The second set of FDI definitions, FDI^2, considers a more detailed quantification of material properties throughout the boundary element. Correlation coefficients for FDI^2 are presented in the last column of Table 5-2 and Table 5-3. As expected, the magnitude of the

coefficient is larger than for FDI^1, indicating a better relationship between FDI and α, however, the increase in magnitude relative to that for FDI^1 is minimal. Given the greater efforts to calculate FDI^2, it is concluded that the use of FDI^1 is most appropriate for achieving the target outcome of a simple method of accounting for post-fire seismic response.

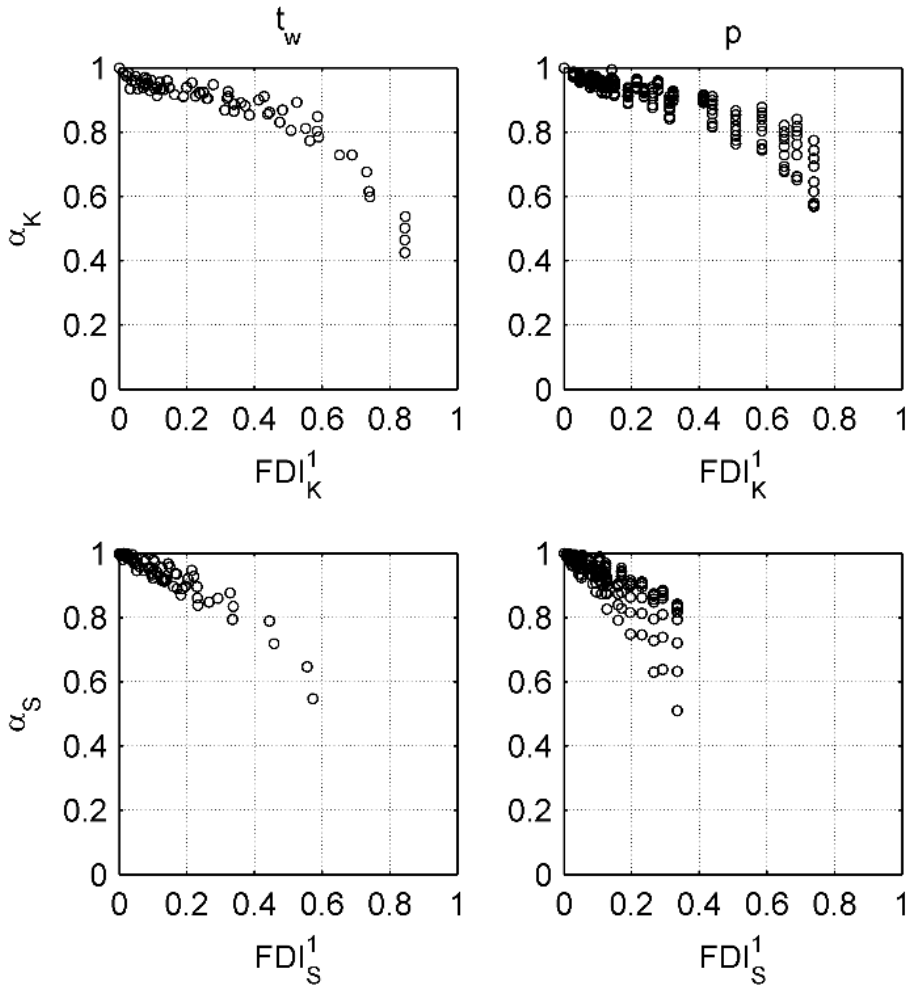

Figure 5-8 Relationship between FDI^1 and wall response for walls with varied thickness (left column) and varied axial load (right column).

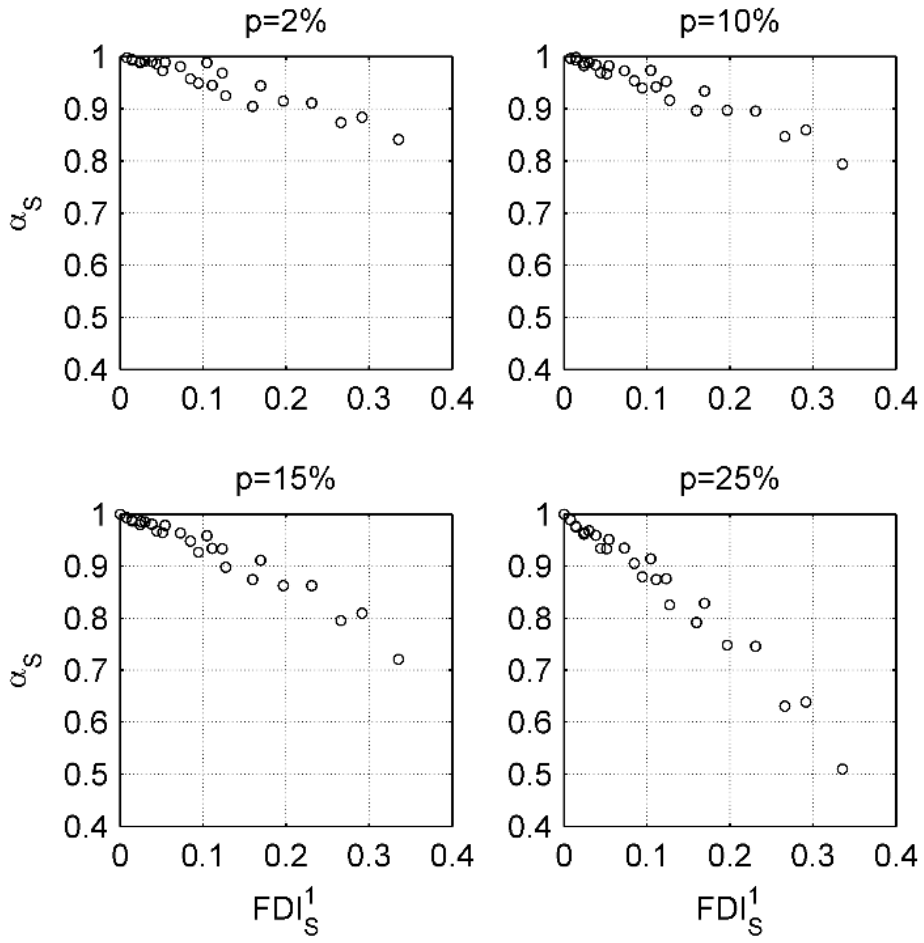

Figure 5-9 Relationship between FDI^1_S and wall response for walls with different axial load ratios.

Table 5-2 Summary of Spearman's rank correlation coefficient for different wall characteristics.

	Parameter	FDI^1	FDI^2
α_K	p	-0.90	-0.93
	t_w	-0.93	-0.97
	CSAR	-0.93	-0.97
	l_{be}/l_w	-0.93	-0.96
	ρ_{be}	-0.93	-0.97
	ρ_{web}	-0.93	-0.96
	s	-0.94	-0.97
α_S	p	-0.91	-0.91
	t_w	-0.93	-0.95
	l_w	-0.95	-0.96
	l_{be}/l_w	-0.97	-0.98
	ρ_{be}	-0.95	-0.96
	ρ_{web}	-0.94	-0.96
	s	-0.96	-0.97

Table 5-3 Summary of Spearman's rank correlation coefficients for different axial load ratios.

	p	FDI^1	FDI^2
α_K	2%	-0.94	-0.99
	5%	-0.93	-0.97
	10%	-0.94	-0.98
	15%	-0.94	-0.97
	20%	-0.94	-0.97
	25%	-0.88	-0.93
α_S	2%	-0.96	-0.97
	5%	-0.92	-0.93
	10%	-0.96	-0.97
	15%	-0.98	-0.99
	20%	-0.98	-0.99
	25%	-0.98	-0.99

5.5.2. Curvature

Figure 5-10 shows the relationship between α_φ and FDI^1_φ for walls with varied thickness (left column) and axial load (right column). Correlation coefficients for all wall characteristics and each axial load are provided in Table 5-4.

Overall, the relationship between FDI^1 and α_φ is not as strong as that for α_K and α_S, however, the same general observations hold in that a) the relationship is the weakest for all axial loads considered together, but increases to values similar to those of other parameters when adjusting for the axial load, and b) the increased effort to calculate FDI^2 produces minimal benefit for prediction of α.

In the case of walls with low axial load ratios ($\leq 5\%$), there is the potential for α_φ values near or greater than one ($\alpha_\varphi > 1$ indicates an increase in failure curvature due to fire). As discussed by Ni and Birely (2018b), these include walls that fail due to rebar fracture rather than boundary element crushing, and that while the curvature may increase, the impact on drift capacity is minimal. As a result of these α_φ values near or greater than 1 at small FDI^1 values, the correlation coefficients are positive or small for low axial load ratios. From this, it was determined that the equations for α_φ should have an upper limit of 1.0, and the dataset was expanded to have more data for walls with axial load ratios less than 10%. These data are included in Figure 5-8 and Figure 5-10.

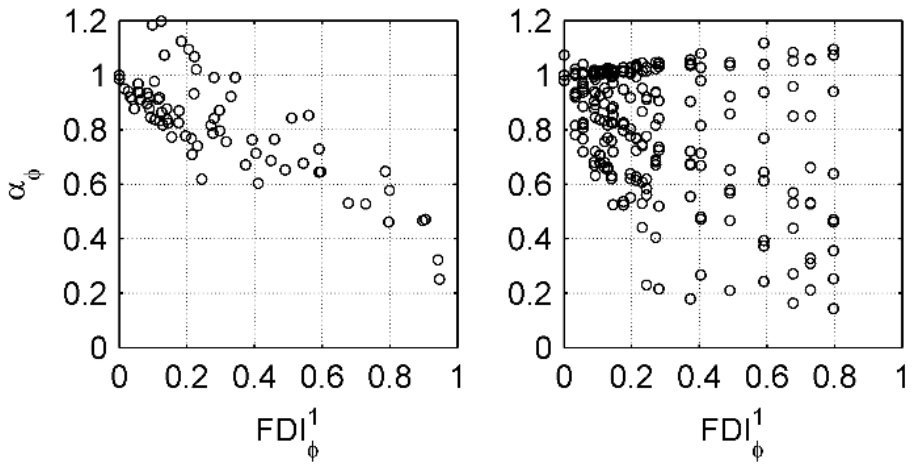

Figure 5-10 Relationship between FDI^1 and wall response for walls with varied thickness (left column) and axial load (right column) varied.

Table 5-4 Summary of Spearman's rank correlation coefficient for curvature.

Parameter	FDI^1	FDI^2
p	-0.37	-0.35
t_w	-0.74	-0.76
CSAR	-0.85	-0.84
l_{be}/l_w	-0.83	-0.83
ρ_{be}	-0.86	-0.86
ρ_{web}	-0.83	-0.83
s	-0.82	-0.82
p = 2%	0.97	0.97
p = 5%	-0.42	-0.36
p = 10%	-0.92	-0.91
p = 15%	-0.87	-0.84
p = 20%	-0.92	-0.89
p = 25%	-0.96	-0.93

5.6. Proposed Equations

Based on the evaluations of the previous section, equations were developed to predict α values for stiffness, strength, and curvature capacity. For stiffness and strength, a linear fit curve was established. For curvature, a linear fit was appropriate for low axial loads only. All relationships are dependent on the axial load ratio (p), thus only the set of walls with different axial load ratio were used to develop the proposed equations.

The fire-damaged stiffness is expressed as:

$$EI_f = \alpha_K EI_0 \quad \text{Eq.5-8}$$

$$\alpha_K = 1 - c_k FDI_K \quad \text{Eq.5-9}$$

$$c_K = 1.8p + 0.2 \leq 0.45 \quad \text{Eq.5-10}$$

$$FDI_K = 1 - \frac{E_{c,f}A_{c,BE} + E_{s,f}A_{s,BE}}{E_{c,0}A_{c,BE} + E_{s,0}A_{s,BE}} \quad \text{Eq.5-11}$$

where $A_{c,BE}$ is the area of concrete in the boundary element; $A_{s,BE}$ is the area of steel in the boundary element; $p = P/A_W f'_{c,0}$ is the axial load ratio using room temperature material properties; and c_K is a dimensionless coefficient used to define the relationship between stiffness-based fire damage index FDI_K and the stiffness modifier α_K.

The fire-damaged strength is expressed as:

$$M_f = \alpha_S M_0 \quad \text{Eq.5-12}$$

$$\alpha_S = 1 - c_S FDI_S \quad \text{Eq.5-13}$$

$$c_S = 4.9p \geq 0.46 \quad \text{Eq.5-14}$$

$$FDI_S = 1 - \frac{f'_{c,f}A_{c,BE} + f_{s,f}A_{s,BE}}{f'_{c,0}A_{c,BE} + f_{s,0}A_{s,BE}} \quad \text{Eq.5-15}$$

where c_S is a dimensionless coefficient used to define the relationship between the strength-based fire damage index FDI_S and the strength modifier α_S.

The fire-damaged curvature capacity is expressed as:

$$\phi_f = \alpha_\phi \phi_0 \quad \text{Eq.5-16}$$

$$\alpha_\phi = 1 - c_\phi FDI_\phi \text{ for } p \leq 0.06 \quad \text{Eq.5-17}$$

$$\alpha_\phi = \frac{c_\phi}{c_\phi + FDI_\phi} \leq 1.0 \text{ for } p > 0.06 \quad \text{Eq.5-18}$$

$$c_\phi = 24.3p - 1.1 \text{ for } p \leq 0.06 \quad \text{Eq.5-19}$$

$$c_\phi = -3.4p + 1 \text{ for } p > 0.06 \quad \text{Eq.5-20}$$

$$FDI_\phi = 1 - \frac{E_{cp,f}}{E_{cp,f}} \quad \text{Eq.5-21}$$

where c_ϕ is a dimensionless coefficient used to define the relationship between the fire damage index FDI_ϕ and the curvature capacity modifier α_ϕ.

5.6.1. Evaluation

Figure 5-11 shows the predicted α values versus the simulated α values for walls used to develop Equations (1)-(12). A point falling on the diagonal line indicates that the model predicts the simulated response exactly. A point above the diagonal line indicates that the predicted value is larger than the simulated response, thus providing an underestimation (unconservative) of the effects of fire damage on the seismic response of the walls. The results demonstrate that the models are effective in efficiently predicting the impact of fire damage on the stiffness, strength, and deformation (curvature) capacity of the walls.

While the modeling recommendations were developed with a limited set of walls in the author's parameter study (Ni and Birely, 2018b), they should be applicable to all walls considered. Figure 5-12 expands the data in Figure 5-11 for all walls in the parameter study. For stiffness and strength, the predicated results are unconservative at low α values, which typically correspond to walls with long durations and four sides exposed, and agree well with the simulated results at larger α values. For curvature, α values exceeded 1.0 in the simulations, but are capped at 1.0 in the model, resulting in more conservative results at larger α values.

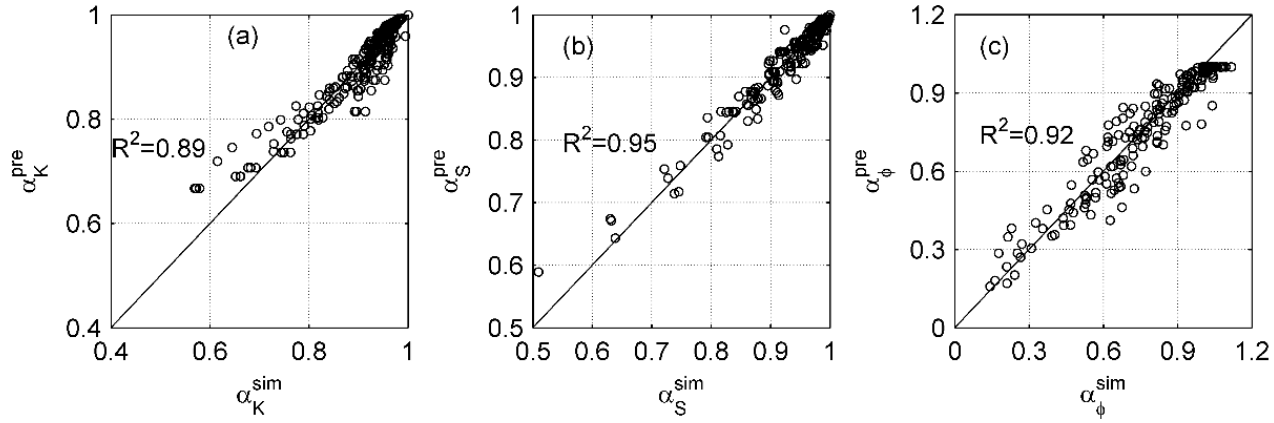

Figure 5-11 Evaluation of proposed model for walls used to develop the model.

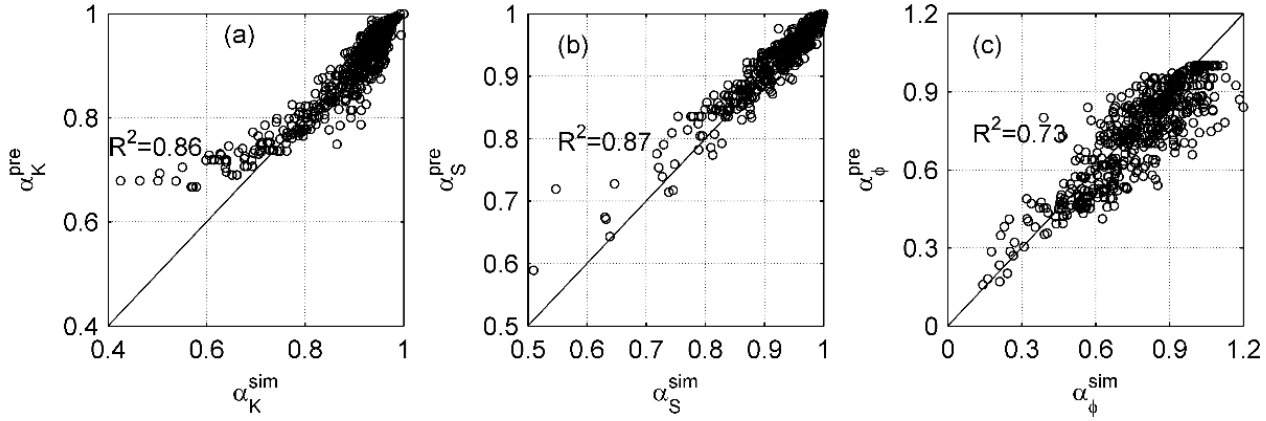

Figure 5-12 Evaluation of proposed model all walls in the parameter study by Ni and Birely (2018b).

5.7. Implementation

For simplified modeling of flexure-controlled reinforced concrete walls with boundary elements, the recommended models can be implemented using the following steps:

1. Identify fire hazard of interest in design.
2. For the fire hazard identified in Step 1, establish the temperature at the center of the boundary element. The engineer may select the appropriate sophistication of the heat transfer analysis and fire characteristics. At the low end, the design aids provided by ACI 216.1-14 (2014) may be used. At the high end, finite element models with exact thermal boundary conditions and material characteristics (conductivity, water content, etc.) may be defined. Fire characteristics may be standard fire curves (e.g. ASTM E119 (ASTM E119-18, 2018)) or may represent natural fires. The rate and duration of cooling, if any, may be specified as needed.
3. Using the temperature identified in Step 2, the residual mechanical properties can be defined by any material model appropriate for the wall considered. As an example, the reduction factors used in the parameter study by the authors (Ni and Birely, 2018b) are based on recommendations by Tao et al. (2013) for steel and Chang et al. (2006) for concrete, both with consideration for cooling.
4. Using the residual properties found in Step 3, the fire damage indices for strength and stiffness are calculated using Equations (4), (8), and (12).
5. Calculate the residual backbone curve for the analysis using Equations (1)-(3), (5)-(7), and (9)-(11).

The proposed simplified model is developed for the flexure response of planar RC structural walls with confined boundary elements and axial load ratios no greater than 25%; applicability for walls without boundary elements, with flexure-shear interaction, or with expected shear failure models has not been investigated.

5.8. Conclusions

To enable simulation of the post-fire seismic response of flexure-controlled reinforced concrete (RC) structural walls with boundary elements, a simplified modeling approach was developed that defines modification factors to alter the stiffness, strength, and curvature of moment-curvature backbone curves. Modification factors are a function of the fire-damaged material properties in the wall boundary element and the axial load ratio of the wall.

Modification factors were developed from data generated by a parameter study by the authors using a detailed simulation model. Wall characteristics varied in the parameter study are summarized in Table 5-1 and resulted in fire-damage index (FDI) values summarized in Figure 5-7. Caution should be used in extrapolating the results beyond this range of wall characteristics and FDI, as applicability is not clear. While the models are generally more conservative than unconservative for individual walls, the models overpredict the stiffness, strength and curvature at small values.

By decoupling thermal and mechanical aspects, the model is independent of thermal boundary conditions and material fire-damage reduction factors, allowing a greater flexibility in application. A comparison of the simulated and predicted stiffness modifiers indicated that the model was generally able to predict the response.

In selecting FDI values and in developing the proposed equations for response modifiers, the simplest were chosen, but refinement can be achieved using a more detailed quantification of fire damage in the boundary region. Such an application may be useful if a limited thermal boundary condition (e.g. one-sided fire), with alternative equations for modification factors desired; to enable such development, the data used to develop the models presented in this paper are available in raw form Reference (Ni and Birely, 2018c) and in processed form (Ni and Birely, 2018d).

CHAPTER 6

SUMMARIES AND CONCLUSIONS

The central concern during the design of an RC structure is to ensure the life safety of its occupants. In the event of extreme loads, e.g. fire or earthquake, the design is intended to provide adequate time for the evacuation of the occupants and to ensure the life safety of any emergence-services personnel. Most previous research was limited to the behavior of structures under individual extreme loads over the past few decades. Less research has focused on the behavior of structures under multiple hazards. The work presented in this dissertation focused on the behavior of flexure-controlled RC walls under sequential fire-earthquake loads (both post-earthquake fire (PEF) and post-fire earthquake (PFE)).

To evaluate the performance of RC walls under sequential fire-earthquake loads, the following tasks has been completed: i) development and validation of the numerical modelling approaches for the PFE and PEF performance of RC structural walls (presented in Chapter 2 and Chapter 3), ii) analysis of the PEF performance of a full-scaled RC structural wall with different seismic damage states and lateral restraint (presented in Chapter 2), iii) a parametric study on the PFE performance of RC structural walls, including twenty-one full-scale walls with different wall geometries, reinforcement ratios and axial load ratios (presented in Chapter 4), and iv) development of a simplified model to assist engineers in capturing the effects of fire within the context of models and software commonly used for seismic analysis (presented in Chapter 5). A summary of findings is provided in the following sections.

6.1. Post-earthquake Fire Performance of RC Walls

The impact of physical seismic damage on the fire resistance of RC walls was investigated using uncoupled thermal-mechanical analysis in Abaqus/Standard. Models were validated using published experimental data of fifteen RC walls tested under fire. A wall with characteristics representative of typical construction in seismic regions was utilized as the basis of the analysis. The behavior of the undamaged full wall with non-uniform layout of reinforcement was assessed relative to the behavior of wall segments with reinforcement layout representative of the boundary region and web region of the full wall. Individual damage states, representative of damage observed following earthquakes and in laboratory tests, were introduced to the wall to assess the impact on fire resistance. The fire resistance of a wall was discussed based on the thermal-insulation criterion and the load-bearing criterion. The effect of lateral restraint on the post-earthquake fire performance of RC walls was also considered. From this investigation, the following conclusions were drawn:

1. The full wall with a non-uniform layout of reinforcement was shown to provide a more complex deformed shape than wall segments with a uniform distribution of reinforcement.

2. Cracking does not influence the fundamental characteristics of the axial deformation or the out-of-plane deformation under fire. The decrease of load-bearing capacity due to cracks is very limited.

3. When seismic damage consists of cover loss, the decrease of load-bearing fire resistance is more significant with increasing dimension of cover loss along wall length. The load-bearing fire resistance of the wall with full B.E. cover loss decreases to less than half the fire resistance of the undamaged wall. The location of cover loss has a significant impact on the deformed shape of

a wall and its load-bearing fire resistance. The loss of concrete cover at the web decreases the rotational stiffness at the damaged region, making the behavior of that region similar to a hinge under fire.

4. Although the presence of core crushing at the boundary element decreases the load-bearing resistance relative to that for cover loss, the amount of the decreases is limited.

5. The impact of earthquake damage on the load-bearing fire resistance of RC walls can be minimized by sufficient out-of-plane restraint.

6. Although load-bearing fire resistance of the earthquake damaged wall studied in this dissertation decreases, it is still acceptable even under the ASTM E119 fire curve which represents maximal values of temperature during fire that may occur in buildings. Therefore, no further research is needed for the load-bearing fire resistance of walls with thickness equal to or greater than 8 inches. Their fire resistance is controlled by insulation criterion, rather than load-bearing criterion. Cover loss decreases the insulation fire resistance below the requirement in ACI/TMS 216.1-14.

6.2. Post-fire Earthquake Performance of RC Walls

A simulation was proposed for the effective and efficient post-fire seismic analysis of RC walls. The simulation procedure combines thermal analysis in SAFIR with seismic analysis in OpenSees. The procedure was used to investigate the behavior of walls with characteristics of walls at seismic regions. From this investigation, the following conclusions were drawn:

1. The proposed simulation procedure can accurately predict the temperature history of wall sections under fire and the lateral load capacity and stiffness of fire-damaged walls under

reversed-cyclic lateral loads. Moreover, this simulation is efficient in analysis and data processing. Although modeling of RC walls is the focus in this dissertation, the simulation procedure could be adapted for the analysis of any other RC structural components or systems.

2. Fire damage decreases both the strength and stiffness of a wall, with the magnitude of decrease in strength and stiffness greatest in walls with both long sides exposed; when only one long side is exposed, the decrease is substantially less and would be expected to have a minor impact on the response of a structure subjected to PFE.

3. Short fires often have no effect on the deformation capacity or in some instances, increase it slightly. This is potentially a by-product of the simulation assumptions, and conservatively no increase in drift capacity should be assumed in analyzing the PFE response of a structure. For fires more severe in duration and number of exposed sides, the failure drift decreases. Curvature at failure usually has a more consistent trend, with the curvature decreasing as the fire duration increases in most cases.

4. With the exception of walls with lower axial load ratio, deformation capacity is characterized by flexure-compression failure, although the location and size of damaged region is impacted by fire characteristics and wall characteristics. Concrete crushing typically concentrates at the region of the boundary element with less fire exposure. However, the boundary element length may lead to a shift in compressive damage from the boundary element to the adjacent web. The failure of thinner walls exposed to long fire duration is triggered by web crushing.

5. The magnitude of stiffness decrease is primarily affected by the wall thickness, boundary longitudinal reinforcement ratio and axial load ratio. The magnitude of the decrease of strength is mainly affected by wall thickness and axial load ratio. The magnitude of the variation of failure

drift is mainly affected by length of boundary element. The magnitude of the variation of failure drift is sensitive to wall thickness, cross-section aspect ratio, and axial load ratio although the impact of those parameters is not as significant as that of boundary element length. The magnitude of the decrease of failure curvature is mainly affected by wall thickness, length of boundary element, boundary element longitudinal reinforcement ratio and axial load ratio. Similar to failure drift, the other parameters also have some influence on the decrease of failure curvature of fired-damaged walls.

6. In thin walls and in walls with high applied axial loads under severe fire exposure, the fire damage to the concrete is so large that the effective axial load ratio exceeds upper limits for consideration of walls to provide lateral load resistance. In analyzing structures for PFE responses, it is crucial to assess this effective axial load ratio.

Based on the data from the parametric studies, a framework for simplified nonlinear modelling of RC walls was proposed. The models are defined by modification factors that account for the change in response relative to that of a wall without fire damage. The modification factors are a function of fire damage indices that account for the effect of fire on the material properties of steel and concrete. Those following conclusions were drawn:

1. The fire damage indices minimize the effort for calculation and permit the development of a simple prediction model for the modification factors which are only dependent on the fire damage indices and axial load ratios.

2. A comparison of the simulated and predicted modifiers indicates that the proposed framework is generally able to predict the response of a wall after exposed to a fire. While the modification factors calculated by the proposed frame are generally more conservative than

unconservative for individual walls, the models overpredict the stiffness, strength and curvature at small modification factors.

6.3. Future Research Needs

This dissertation studied the post-earthquake fire (PEF) and post-fire earthquake (PFE) performance of flexure-controlled RC structural walls. Additional research is needed to refine the work of this dissertation and to further advance the understanding of the behavior of RC structures under sequential fire-earthquake loads.

For the post-earthquake fire performance of RC structural walls, the analysis in the dissertation was limited to an eight inch thick wall with selected seismic damage states and two idealized lateral restraint. The following future research is needed:

1. The study considers only the physical seismic damage. The load-bearing fire resistance may be further impacted by residual deformations and mechanical damage of materials caused by an earthquake. More work is required to analyze walls with earthquake-related residual deformation and material degradation.

2. Additional studies are needed to establish wall characteristics for which the load bearing criterion may control; this may occur in thinner walls, walls with larger axial load ratios, walls with different boundary element lengths and reinforcement ratios, and/or walls with several damage states. For earthquake-damaged walls potentially controlled by loading-bearing fire resistance, research about those walls under more realistic fire curves is necessary.

3. Given the significant impact of lateral restraint on the load bearing fire resistance, there is a need for modeling realistic full or partial building models with slabs to better understand the

performance of a structure exactly, as these are likely to increase the load bearing capacity and affect out-of-plane and axial deformations.

In addition, more fundamental research about the effect of cracks on the heat propagation of RC sections is required. Some research has already focused on the effect of cracks on the heat propagation in concrete section or RC structural components. However, those research focused on the interface cracks between aggregates and mortar or focused on cracks at the surface of structural components parallel to the direction of heat propagation, which are not the cracks studied in this dissertation. Efforts should be made in the future to develop the relationship between the crack characteristics (crack width, crack density, crack location and the relative angle between heat propagation and cracks) and the increase/decrease of heat propagation.

Studies on the post-fire earthquake performance of RC walls in this dissertation includes development of a simulation procedure, a parameter study, and development of a simplified modelling approach. The proposed simulation procedure should be improved and expanded; more parameters should be considered in the parameter study; and the simplified modelling approach should be refined to predict the seismic response of a fire-damaged RC wall in a more accurate way without losing its advantage in easy calculation.

The simulation procedure discussed in this dissertation is proposed based on several assumptions and has several drawbacks. More work is required to address those drawbacks:

1. The first drawback is in regards to the material model for fire-damaged concrete. Test data are required to validate: 1) the application of the classical model to the confined concrete section with non-uniform strength distribution; 2) the current assumption of concrete fracture

energy under temperature; 3) the application of the current cyclic response of undamaged concrete to the analysis of fire-damaged RC structures.

2. The proposed simulation method is limited to modelling flexure-controlled RC walls. For the simulation of shear failure, a shear model with failure should be incorporated into the simulation procedure. However, more experimental data and numerical studies are required to develop such a model.

3. Only material degradation due to fire exposure is considered in the simulation. Other damage, such as cracks and residual deformation due to fire exposure, are not considered. In order to do this, thermal-mechanical analysis (instead of only the heat transfer analysis) should be incorporated into the simulation procedure. The development of a specific material model to use both initial strains/stresses is necessary.

4. The application of the simulation procedure is currently limited, focusing only on planar walls. More development is required to make the simulation procedure easy to analyze flanged walls and other structural components.

5. This simulation procedure can also be adjusted for the analysis of RC structural components under earthquake-fire-earthquake. More work can be done to make the heat transfer analysis in the simulation procedure easy for the earthquake-damaged RC sections, such as a wall section with part of cover spalled under the seismic loads. Moreover, the thermal-mechanical analysis instead of the heat transfer analysis in SAFIR should be incorporated into the simulation procedure with abilities to consider the impact of the residual stress/strain from the main earthquake.

The post-fire seismic parametric studies based on the validated simulation procedure only considered design parameters related to wall dimensions, reinforcement ratios and axial load ratio. More research about other parameters is required

1. Some preliminary studies have shown that the cooling rate will significantly influence the post-fire seismic performance of a RC wall. More parametric studies are required in the future about cooling rates and other characteristics of fire curves.

2. The impact of fire damage on the seismic performance of RC walls was incorporated to the analysis by considering the fire damage to concrete and reinforcing steel, which makes a parametric study about the material properties necessary in the future.

3. The parametric study only focused on the planar walls; research is required for the post-fire seismic performance of flanged walls.

The simplified modeling framework is proposed based on the data from the parametric studies. In selecting FDI values and in developing the proposed equations for response modifiers, the simplest were chosen in this dissertation. More research is required in the future to refine and validate the proposed framework:

1. The refinement of the framework can be achieved using a more detailed quantification of fire damage in the boundary region.

2. The application of the modeling framework to the followings should be demonstrated: i) a fire-damaged planar wall with characteristics beyond the wall range studied in this dissertation; ii) fire-damaged flanged walls and iii) the analysis of buildings.

REFERENCES

ACI Committee 318: Building code requirements for structural concrete and commentary (ACI 318-14), American Concrete Institute, Farmington Hills, MI, U.S., 2014.

AS1530.4: Methods for fire tests on building materials, components and structures: Part 4 - Fire resistance tests of elements of building construction, Standards Association of Australia, Sydney, NSW, AU, 1997.

ACI 216.1-14: Code requirements for determining fire resistance of concrete and masonry construction assemblies, ACI/TMS Committee 216, Farmington Hills, MI, US, 2014.

ASTM E119-18: Standard test methods for fire tests of building construction and materials, ASTM International, West Conshohocken, PA, US, 2018.

ASCE 41-17: Seismic evaluation and retrofit of existing buildings, 2017 edition, American Society of Civil Engineers, Reston, VA, US, 2017.

Bénichou, N., Mostafaei, H., Green, M.F. and Hollingshead, K., The impact of fire on seismic resistance of fiber reinforced polymer strengthened concrete structural systems, Canadian Journal of Civil Engineering, 40 (11) (2013) 1044-1049.

Birely, A.C., Seismic performance of slender reinforced concrete structural walls, Dissertation, Department and Civil and Environmental Engineering, University of Washington, Seattle, WA, US, 2012.

Behnam, B. and Ronagh, H.R., Investigating the effect of prior damage on the post-earthquake fire resistance of reinforced concrete portal frames, International Journal of Concrete Structures and Materials, 6 (4) (2012) 209-220.

Behnam, B., Ronagh, H.R. and Baji, H., Methodology for investigating the behavior of reinforced concrete structures subjected to post earthquake fire, Advances in Concrete Construction, 1 (1) (2013) 29-44.

Behnam, B. and Ronagh, H., Performance of reinforced concrete structures subjected to fire following earthquake, European Journal of Environmental and Civil Engineering, 17 (4) (2013) 270-292.

Behnam, B. and Ronagh, H. R., A study on the effect of sequential post-earthquake fire on the performance of reinforced **c**oncrete structures, International Journal of Structural Integrity, 5 (2) (2014) 141-166.

Berg, G.V. and Stratta, J.L., Anchorage and the Alaska earthquake of March 27, 1964. Technical report, American Iron and Steel Institute, New York, US, 1964.

Bergman, T.L., Incorporate, F.P., Dewitt, D.P. and Lavine, A.S., Fundamentals of heat and mass transfer (7th Edition), John Wiley & Sons, Inc. Hoboken, NJ, 2011.

Ba, G., Miao, J., Zhang, W. and Liu, C., Influence of cracking on heat propagation in reinforced concrete structures, Journal of Structural Engineering, 142 (7) (2016) 04016035.

Bruneau, M., Barbato, M., Padgett, J.E., Zaghi, A.E., Mitrani-Reiser, J., and Li, Y., State of the art of multihazard design, Journal of Structural Engineering, 143 (10) (2017) 0311702

Chang, Y.F., Chen, Y.H., Sheu, M.S. and Yao, G.C., Residual stress–strain relationship for concrete after exposure to high temperatures, Journal of Cement and Concrete Research, 36 (2006) 1999-2005.

Crozier, D.A. and Sanjayan, J.G., Tests of load-bearing slender reinforced concrete walls in fire, ACI Structural Journal, 97 (2) (2000) 243-252.

Chen, Y.H., Chang, Y.F., Yao, G.C. and Sheu, M.S., Experimental research on post-fire behavior of reinforced concrete column, Fire Safety Journal, 44 (5) (2009) 741-748.

Chen, M., Pantoli, E., Wang, X., Astroza, R., Ebrahimian, H., Mintz, S., Hutchinson, T.C., Conte, J.P. and Restrepo, J., BNCS, Report #4: Full-scale structural and nonstructural building system performance during earthquakes and post-earthquake fire – construction details and technical specifications of specific subsystems, Report No. SSRP-13/12, BNCS Report #4, Department of Structural Engineering, University of California, San Diego, La Jolla, CA, US, 2013.

Chen, M., Pantoli, E., Wang, X., Astroza, R., Ebrahimian, H., Hutchinson, T.C., Conte, J.P., Restrepo, J.I., Marin, C., Walsh, K.D., Bachman, R.E., Hoehler, M.S., Englekirk, R. and Faghihi, M., Full-scale structural and nonstructural building system performance during earthquakes: Part I - Specimen description, test protocol and structural response, Earthquake Spectra, 32 (2) (2016) 737-770.

Chang, G.A. and Mander, J.B., Seismic energy based fatigue damage analysis of bridge columns: Part I – Evaluation of seismic capacity, NCEER Technical Report No. NCEER-94-0006, State University of New York, Buffalo, NY, US, 1994.

Cachim, P. B. and Franssen, J. M., Numerical modelling of timber connections under fire loading using a component model, Fire Safety Journal, 44 (6) (2009) 840-853.

Dazio, A., Beyer, K. and Bachmann, H., Quasi-static cyclic tests and plastic hinge analysis of RC structural walls, Engineering Structures, 31 (2009) 1556-1571.

Doğangűn, Performance of reinforced concrete buildings during the May 1, 2003 Bingől Earthquake in Turkey, Journal of Engineering Structures, 26 (6) (2004) 841-856.

Dimia, M. S., Guenfoud, M., Gernay, T. and Franssen, J. M., Collapse of concrete columns during and after the cooling phase of a fire, Journal of Fire Protection Engineering, 21 (4) (2011) 245-263.

Dassault Systèmes Simulia Corp, Abaqus analysis user's manual, Version 6.12, Providence, RI, US, 2012.

EI-Hawary, M.M., Ragab, A.M., EI-Azim, A.A. and Elibiari, S., Effect of fire on flexural behavior of RC beams, Construction and Building Materials, 10 (2) (1996) 147-150.

EI-Hawary, M.M., Ragab, A.M., EI-Azim, A.A. and Elibiari, S., Effect of fire on shear behavior of RC beams, Journal of Computer & Structures, 65 (2) (1997) 281-287.

EN 1992-1-2: Eurocode 2: Design of concrete structures - Part 1-2: General rules—structural fire design, European Committee for Standardization, Brussels, Belgium, 2004.

Ervine, A., Damaged reinforced concrete structures in fire, Dissertation, Department of Civil Engineering, University of Edinburgh, Edinburgh, UK, 2012.

Elghazouli, A.Y., Cashell, K.A. and Izzuddin, B.A., Experimental evaluation of the mechanical properties of steel reinforcement at elevated temperature, Fire Safety Journal, 44 (6) (2009) 909-919.

Franssen, J.M. and Kodur, V., Residual load bearing capacity of structures exposed to fire, In Proceedings of the 2001 Structures Congress and Exposition, Washington, D.C., US, May 21-23, 2001

Felicetti, R., Gambarova, P.G. and Meda, A., Residual behavior of steel bars and R/C sections after fire, Construction and Building Materials, 23 (12) (2009) 3546-3555.

Fradkin, P., The great earthquake and firestorms of 1906: How San Francisco nearly destroyed itself, University of California Press, Berkeley, CA, US, 2005.

fib Model Code 2010: fib model code for concrete structures 2010, International Federation for Structural Concrete, John Wiley & Sons, Inc., 2013.

Gernay, T., Effect of transient creep strain model on the behavior of concrete columns subjected to heating and cooling, Fire Technology, 48 (2) (2012) 313-329.

Gernay, T. and Franssen, J.M., A formulation of the Eurocode 2 concrete model at elevated temperature that includes an explicit term for transient creep. Fire Safety Journal, 51 (2012) 1-9.

Harda, T., Research on fire proof of concrete and reinforced concrete construction, Dissertation, Tokyo Institute of Technology, Tokyo, JP, 1961.

Hertz, K.D., Limits of spalling of fire-exposed concrete, Fire safety journal, 38 (2) (2003) 103–116

Hutchinson, T.C. and Wang, T., Gas flow rate through damaged low aspect ratio shearwalls, Earthquake Spectra, 26 (3) (2010) 685-708.

ISO 834-12, Fire resistance tests - Elements of building construction – Part1: General requirements, International Organization for Standardization, Geneva, Switzerland 2012.

Kumar, P. and Kodur, V.K.R., Modeling the behavior of load bearing concrete walls under fire exposure, Construction and Building Materials,154 (2017) 993-1003.

Kirby, B. R., Lapwood, D. G. and Thomson, G., The reinstatement of fire damaged steel and iron framed structures, ISBN 0 900206 46 2, B.S.C., Swinden Laboratories, 1986.

Kam, W.Y. and Pampanin, S., The seismic performance of RC buildings in the 22 February 2011 Christchurch earthquake. Structural Concrete, 12 (2011) 223-233.

Lie, T.T. and Woollerton, J.L., Fire resistance of reinforced concrete columns – Test results, National Research Council Canada, Internal Report No. 569, Ottawa, CA, 1988.

Lie, T.T., Rowe, T.J. and Lin, T.D., Residual strength of fire-exposed reinforced concrete columns, American Concrete Institute, ACI SP92-9, 1986, 153-174.

Liu, G., Experimental study on fire resistance and post-fire earthquake behavior of concrete shear wall, Dissertation, Dalian University of Technology, Dalian, CN, 2010.

Lee, J., Xi, Y. and Willam, K., Properties of concrete after high temperature heating and cooling, ACI Material Journal, 105 (4) (2008) 334-341.

Lim, L., Buchanan, A., Moss, P. and Franssen, J. M., Numerical modelling of two-way reinforced concrete slabs in fire, Engineering Structures, 26 (8) (2004) 1081-1091.

Lee, S.W. and Davidson, R.A., Physics-based simulation model of post-earthquake fire spread, Journal of Earthquake Engineering 14 (5) (2010) 670-687.

Lee, S., Davidson, R., Ohnishi, N. and Scawthorn, C., Fire following earthquake - Reviewing the state-of-the-art of modeling, Journal of Earthquake Spectra, 24 (4) (2008) 933-967.

Lee, S. and Lee, C., Fire resistance of reinforced concrete bearing walls subjected to all-sided fire exposure, Materials and Structures 46 (6) (2013) 943-957.

Lowes, L.N., Lehman, D.E., Birely, A.C., Daniel, A.K. Marley, K.P. and Hart, C.R., Earthquake response of slender planar concrete walls with modern detailing, Journal of Engineering Structures, 43 (2012) 31-47.

Lopes, N., Real, P.V., Silva, L. S. and Franssen, J. M., Numerical analysis of stainless steel beam-columns in case of fire, Fire Safety Journal, 50 (2012) 35-50.

Levenson, L.M., Residential water heater damage and fires following the Loma Prieta and Big Bear Lake Earthquakes. Earthquake Spectra, 8 (1992) 595-603.

Lew, H.S., Leyendecker, E.V. and Dikkers, R.D., Engineering aspects of the 1971 San Fernado Earthquake, National Bureau of Standards (US), NBS building science series 40, 1971.

Matlab R2013a, [Computer software]. MathWorks, Inc., Natick, Massachusetts, United States.

Mostafaei, H., Vecchio, F.J. and Benichou, N., Seismic resistance of fire-damaged reinforced concrete columns, In Goodno, B. (Ed.), Proceedings of the ATC&SEI 2009 Conference on Improving the Seismic Performance of Existing Buildings and Other Structures, American Society of Civil Engineers, 2010, 1396-1407.

Mostafaei, H. and Kabeyasawa, T., Performance of a six-story reinforced concrete structure in post-earthquake fire, In Proceedings of the 9th US National and 10th Canadian Conference on Earthquake Engineering, Toronto, Ont., CA, 2010

Mo, Y.L., Hwang, C. and Wang, J., Seismic response of fire-damaged reinforced concrete buildings, Advances in Structural Engineering, 7 (1) (2004) 95-109.

Mueller, K.A., Kurama, Y.C. and McGinnies, M.J., Out-of-plane behavior of two RC bearing walls under fire, In Teng, J.G. (Ed.), Proceedings of 1st International Conference on Performance-based and Life-cycle Structural Engineering, Faculty of Construction and Environment & Research Institute for Sustainable Urban Development, Hong Kong Polytechnic University, Hong Kong, CN, 2012

Mueller, K. A., Kurama, Y.C. and McGinnis, M.J., Out-of-plane behavior of two reinforced concrete bearing walls under fire: A full-scale experimental investigation, ACI Structural Journal, 111 (5) (2014) 1101-1110.

Mueller, K.A. and Kurama, Y.C., Out-of-plane behavior and stability of five planar reinforced concrete bearing wall specimens under fire, ACI Structural Journal, 112 (06) (2015) 701-712.

Mueller, K. A. and Kurama, Y., Out-of-plane behavior of reinforced concrete bearing walls after one-sided fire. ACI Structural Journal, 114 (1) (2017), 149-160.

Mostafaei, H., Vecchio, F.J. and Bénichou, N., Seismic resistance of fire-damaged reinforced concrete columns, ATC & SEI 2009 Conference on Improving the Seismic Performance of Existing Builds and Other Structures, 2009, 1396-1407.

Mousavi, S., Bagchi, A. and Kodur, V.K.R., Review of post-earthquake fire hazard to building structures, Canadian Journal of Civil Engineering, 35 (7) (2008) 689-698.

Meacham, B.J., Post-earthquake fire performance of buildings: Summary of a large-scale experiment and conceptual framework for integrated performance-based seismic and fire design, Fire Technology, 52 (4) (2016) 1133-1157.

Nassif, A., Postfire full Stress-strain Response of Fire-damaged Concrete, Journal of Fire and Materials, 30 (2006) 323-332.

Ni, S. and Birely, A.C., Fire resistance of earthquake damaged reinforced concrete walls, In Proceedings of the 10th U.S. National Conference on Earthquake Engineering Anchorage, AK, US, 2014, Paper No. 179.

Ni, S. and Birely, A.C., Damage indices for load-bearing capacity and stiffness of fire-damaged walls, In Proceedings of the 16th World Conference on Earthquake Engineering, Santiago, CL, Jan, 2017, Paper No. 2973.

Ni, S. and Birely, A.C., Simulation procedure for the post-fire seismic analysis of reinforced concrete structural walls, Fire Safety Journal, 95 (2018a) 101-112.

Ni, S. and Birely, A.C., Post-fire seismic behavior of reinforced concrete structural walls, Engineering Structures, 168 (2018b) 163-178.

Ni, S. and Birely, A.C., Simulation of post-fire seismic response of planar reinforced concrete walls, DesignSafe-CI, Dataset (2018c), doi: 10.17603/DS22T12.

Ni, S. and Birely, A.C., Local and global response data from post-fire earthquake simulations of RC structural walls, Data in Brief, accepted, 2018d.

Neves, I. C., Rodrigues, J.P.C and Loureiro, A.P., Mechanical properties of reinforcing and prestressing steels after heating, Journal of Materials in Civil Engineering, 8 (4) (1996) 189-194.

Ngo, T., Fragomeni, S., Mendis, P. and Ta, B., Testing of normal- and high-strength concrete walls subjected to both standard and hydrocarbon fires, ACI Structural Journal, 110 (3) (2013) 503-510.

Oh, Y., Han, S. and Lee, L., Effect of boundary element details on the seismic deformation capacity of structural walls, Earthquake Engineering & Structural Dynamics, 31 (2002) 1583-1602.

Pugh, J.S., Numerical Simulation of walls and seismic design recommendations for walled buildings, Dissertation, Department and Civil and Environmental Engineering, University of Washington, Seattle, WA, US, 2012.

Ronagh, H.R. and Behnam, B., Investigating the effect of prior damage on the post-earthquake fire resistance of reinforced concrete portal frames, International Journal of Concrete Structures and Materials, 6 (4) (2012) 209-220.

Sharma, U.K., Kumar, V., Singh, B., Bahargava, P., Singh, Y., Kamath, P., Usmani, A., Torero, J., Gillie, M. and Pankaj, P., Testings of full-scale frame under simulated fire following earthquake, In Fontana, M., Frangi, A. and Knobloch, M. (Ed.), Proceedings of the 7th International Conference on Structures in Fires, ETH Zurich, Zurich, CH, 2012, 719-728.

Scawthorn, C., Fire following earthquake, Fire Safety Science, 1 (4) (1986) 971-979.

Scawthorn, C., Fire following the Northridge and Kobe earthquakes, Thirteen Meeting of the UJNR Panel on Fire Research and Safety, NIST Report NISTIR 6030, Gaithersburg, MD, US, March, 1996, 325-335.

Sekizawa, A. and Sasaki, K., Study on fires following the 2011 Great East-Japan earthquake based on the questionnaire survey to fire departments in affected areas, In Nilsson, D. and Hees, P.V. (Ed.), Fire Safety Science – Proceedings of the 11th International Symposium, Lund University, Lund, Sweden, 2014, 691-703.

Shah, A.H., Kamath, P. and Sharma, U. K., Influence of ductility on the behavior of RC frames in post-earthquake fire, In Li, G., Jiang, S. and Chen, S., Proceedings of the 8th International Conference on Structures in Fire, Tongji University, Shanghai, CN, 2014, 279-286.

Shah, A.H., Sharma, U.K. and Bhargava, P., Outcomes of a major research on full scale testing of RC frames in post earthquake fire, Construction and Building Materials, 155 (2017) 1224-1241.

Shah, A.H., Sharma, U.K., Kamath, P., Bhargava, P., Reddy, G.R. and Singh, T., Fire performance of earthquake-damaged reinforced-concrete structures, Materials and Structures, 49 (7) (2016) 2971-2989.

Shen, L., Ren, Q., Zhang, L., Han, Y. and Cusatis, G., Experimental and numerical study of effective thermal conductivity of cracked concrete, Construction and Building Materials, 153 (2017) 55-68.

Sekizawa, A., Ebihara, M., and Notake, H., Development of seismic-induced fire risk assessment method for a building, In Evans, D.D. (Ed.), Fire Safety Science – Proceedings of the 7th international symposium, International Association for Fire Safety Science, Gaithersburg, MD, US, 12002, 309-320.

Spearman, C., The proof and measurement of association between two things, American Journal of Psychology, 15 (1904) 72–101.

Topçu, I. B. and Karakurt, C., Properties of reinforced concrete steel rebars exposed to high temperatures, Research Letters in Materials Science, 2008 (2008) 1-4.

Tao, Z., Wang, X. and Uy, B., Stress-strain curves of structural and reinforcing steels after exposure to elevated temperatures, Journal of Materials in Civil Engineering, 25 (2013) 1306-1316.

Trifunac, M.D. and Todorovska, M.I., The Northridge, California, Earthquake of 1994: Fire ignition by strong shaking, Journal of Soil Dynamics and Earthquake Engineering, 17 (1998) 165-75.

Todd, D., Carino, N., Chung, R.M., Lew, H.S., Taylor, A.W. and Walton, W.D., 1994 Northridge Earthquake: Performance of structures, lifelines and fire protection systems, National Institute of Standards and Technology, NSTIR 5396, 1994.

Vejmelková, E., Padevět, P. and Černý, R., Effect of cracks on hygric and thermal characteristics of concrete, Bauphysik, 30 (6) (2008) 438-444.

Wen, B., Wu, B. and Niu, D., Post-earthquake fire performance of reinforced concrete columns, Structure and Infrastructure Engineering, 12 (9) (2016) 1106-1126.

Wong, P. S., Vecchio, F. J. and Trommels, H., Vector2 & formworks user's manual, 2nd edition, Department of Civil Engineering, University of Toronto, Toronto, Ont., CA, 2013.

Wilkinson, S., Grant, D., Williams, E., Paganoni, S., Fraser, S., Boon, D., Mason, A. and Free, M., Observations and Implications of Damage From the Magnitude 6.3 Christchurch, New Zealand Earthquake of 22 February 2011, Bulletin of Earthquake Engineering, 11 (2013) 107-140.

Xiao, J., Li, J. and Jiang, F., Research on the seismic behavior of HPC shear walls after fire, Journal of Materials and Structures, 37 (2004) 506-512.

Xie, Q., Xiao, J., Xie, W. and Gao, W. Cyclic tests on composite plate shear walls-concrete encased before and after fire exposure, Advances in Structural Engineering, June, 2018, 1-15.

Zaghi, A.E., Padgett, J.E., Bruneau, M., Barbato, M., Li, Y., Mitrani-Reiser, J., McBride, A. and McBride, A., Establishing common nomenclature, characterizing the problem, and identifying future opportunities in multihazard design, Journal of Structural Engineering, 142(12) (2016) H2516001-7.

APPENDIX A

WALL SECTION DETAILING FOR THE PFE PARAMETRIC STUDY

Twenty-one unique reinforced concrete planar walls were modeled for the parametric studies in Chapter 4. Table B-1 provides wall reinforcement with boundary and web reinforcement information. Wall 1 is the reference wall, with all other walls varying a single characteristic from the reference wall (geometry, reinforcement, or axial load). Boundary and web reinforcement detailing are shown in Figure A-1 and Figure A-2, respectively.

Table A-1 Wall reinforcement detailing.

	Wall ID	BE[1]	Web[2]	A_{sb}	A_{sw}	A_{conf}	s
				(mm^2)	(mm^2)	(mm^2)	mm
Reference wall	1	1	1	284	129	129	102
t_w	2	2	2	252	135	102	102
	3	3	3	302	135	135	102
l_{be}/l_w	4	4	1	252	135	117	102
	5	5	1	252	135	121	102
CSAR	6	6	4	284	118	120	102
	7	7	1	283	133	132	102
ρ_{be}	8	1	1	129	129	129	102
	9	1	1	200	129	129	102
	10	1	1	387	129	129	102
	11	1	1	509	129	129	102
ρ_{web}	12	1	1	284	71	129	102
	13	1	1	284	200	129	102
	14	1	1	284	284	129	102
s	15	1	1	284	129	129	152
	16	1	1	284	129	129	203
$P/A_w f'_{c,0}$	17	1	1	284	129	129	102
	18	1	1	284	129	129	102
	19	1	1	284	129	129	102
	20	1	1	284	129	129	102
	21	1	1	284	129	129	102

Note: 1. See Figure A-1; 2. See Figure A-2

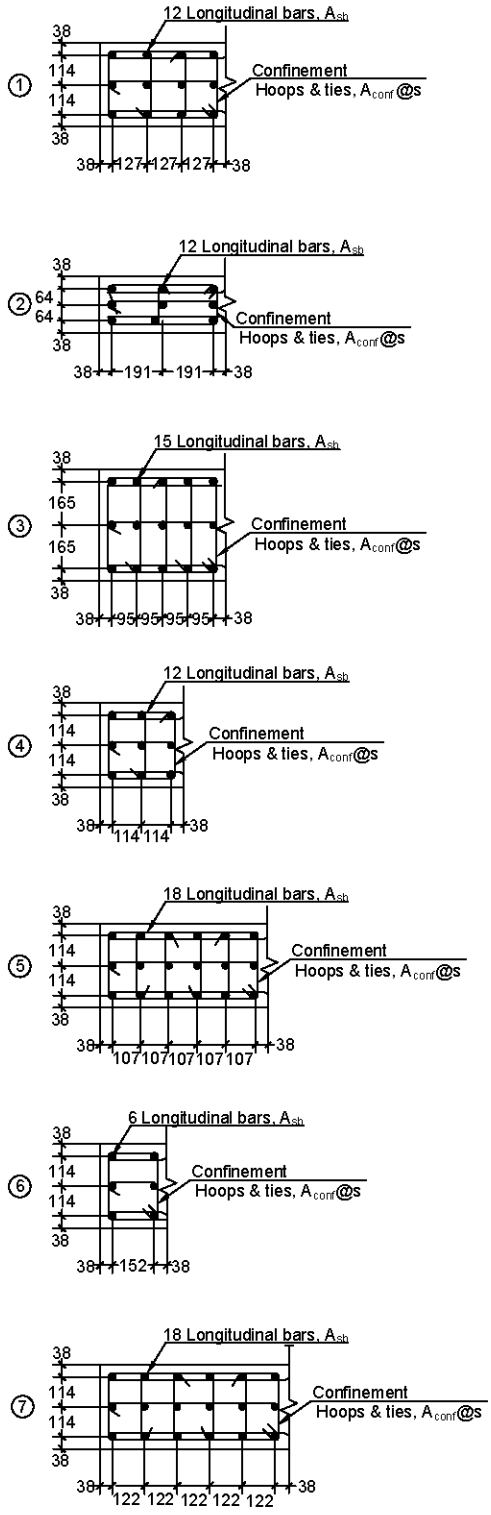

Figure A-1 Boundary element reinforcement configurations.

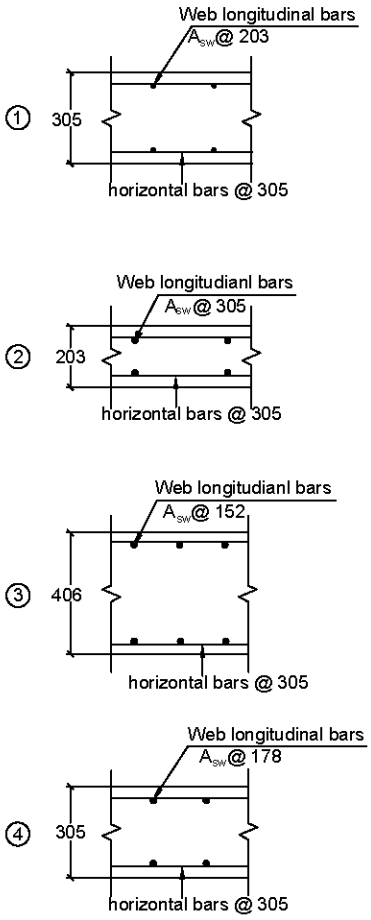

Figure A-2 Web reinforcement configurations.